

ENVIRONMENTAL PROCESSES AFFECTING THE TEMPORAL
AND SPATIAL VARIABILITIES OF SNOWMELT
IN THE BEN LOMOND SKI FIELD AREA, TASMANIA

Stuart. by

Peter S. Faulkner, B.Ed., Dip.T.

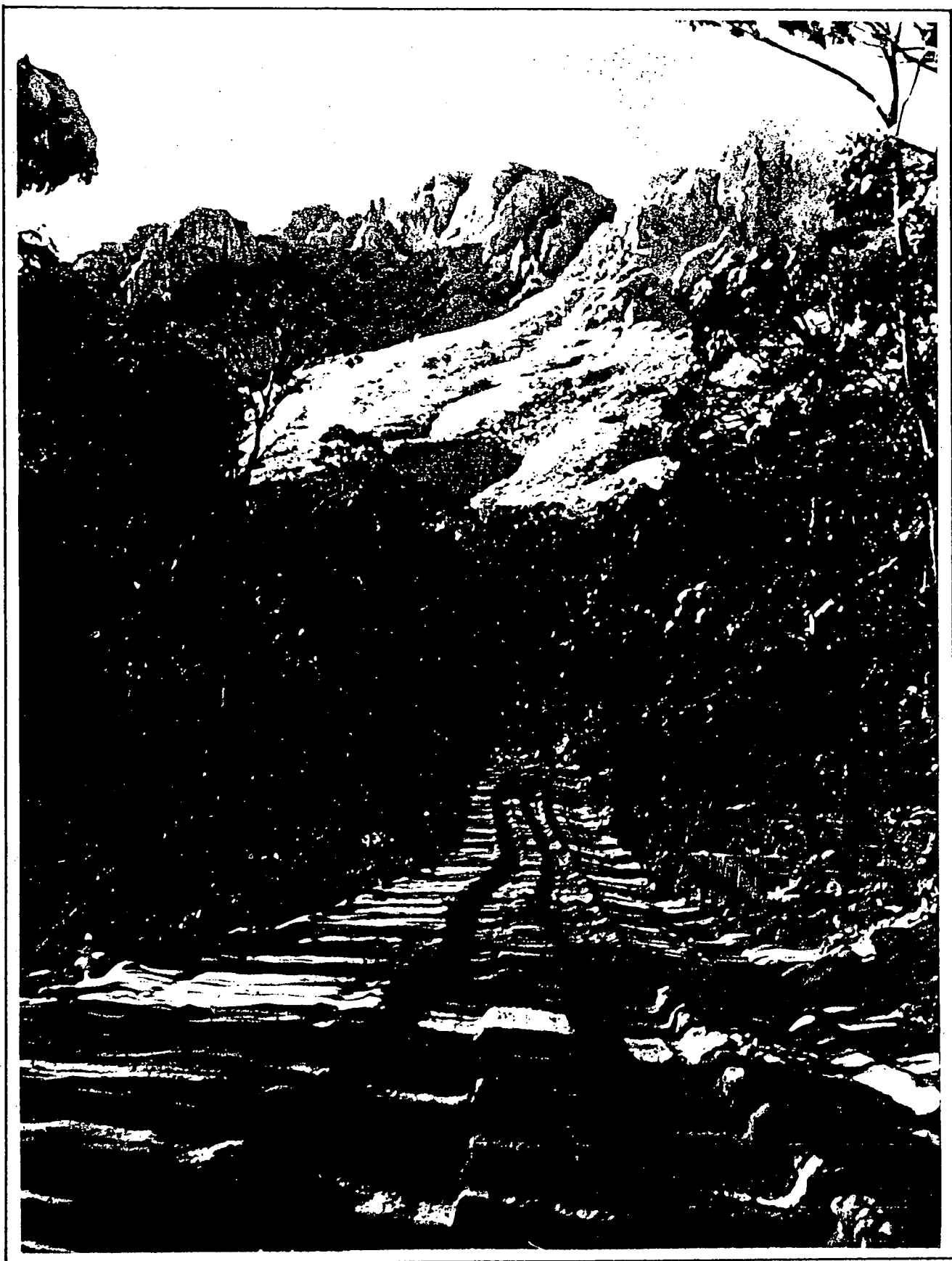
Submitted in fulfilment of the
requirements for the degree of
Master of Science

'89 graduation?

UNIVERSITY OF TASMANIA

HOBART

November, 1987



FRONTISPIECE: The northern face of Ben Lomond, 1986.

Except as stated therein, the thesis contains no material which has been accepted for the award of any other degree or diploma in any university, and that to the best of the candidates knowledge and belief, the thesis contains no copy or paraphrase of material previously published or written by another person, except when due reference is made in the text of the thesis.

A handwritten signature in black ink, appearing to be 'R. J. ...', with a long horizontal flourish extending to the right.

ACKNOWLEDGEMENTS

This study involved five years of continuous field work, mostly during the winter months when weather was bleak. A special note of thanks must go to those people on the mountain who provided me with shelter, enthusiasm and a good deal more during this time. They are Erryl Williams of Alpine Enterprises, Graham Holloway and Brian Hill of Ski Rentals.

Meteorological observations would not have been possible without the help of the National Parks and Wildlife Service rangers, John Walters, Trevor Westren and Ian Marmion. These people assisted me in every way they could. The equipment for the observations was kindly loaned by the Australian Maritime College and this debt is acknowledged.

Finally, and most importantly, I wish to thank Dr. Manuel Nunez, my project supervisor, for his expert guidance and help; my wife Beth for her constant support and professional typing and my children Andrew and Caroline, who kept the weather log in town for 5 years.

TABLE OF CONTENTS

	Page
TITLE PAGE	i
THESIS STATEMENTS	ii
ACKNOWLEDGEMENTS	iii
FRONTISPIECE: The northern face of Ben Lomond	iv
TABLE OF CONTENTS	v
LIST OF TABLES	ix
LIST OF FIGURES	x
LIST OF APPENDICES	xii
ABSTRACT	xiii
 <u>CHAPTER</u>	
1 A DESCRIPTION OF THE STUDY AND BEN LOMOND	1
1.1 INTRODUCTION	1
1.2 PHYSICAL GEOGRAPHY	5
1.2.1 Geomorphology	7
1.2.2 Biogeography	10
1.3 CLIMATE	13
1.3.1 The General Climate of Tasmania	13
1.3.2 Temperature and Frost Days	14
1.3.3 Rainfall	17
1.3.4 Snowcover	20
1.3.5 Snow and Wind	21
2 THE ENERGY BALANCE	23
2.1 THE GENERAL MODEL	23
2.2 NET RADIATION	25
2.2.1 Downward Shortwave Radiation	26
2.2.2 Reductions in Shortwave Radiation in Hilly Terrain	31

Table of Contents (Continued)

CHAPTER		Page
2.2.3	Upward Shortwave Radiation	34
2.2.4	Albedo	35
2.2.5	Solar Radiation Attenuation Within the Snowpack	36
2.2.6	Longwave Radiation	37
2.3	SENSIBLE AND LATENT HEAT	40
2.3.1	Eddy Correlation	40
2.3.2	The Bowen Ratio	41
2.3.3	The Aerodynamic Approach	42
2.4	THE GROUND FLUX	46
2.5	THE FLUX OF HEAT FROM RAIN	47
2.6	INTERNAL ENERGY	49
2.7	SNOWMELT	50
3	DATA ACQUISITION	52
3.1	CLIMATE	52
3.1.1	Temperature and Relative Humidity	52
3.1.2	Wind Direction and Speed	53
3.1.3	Precipitation	54
3.1.4	Solar Radiation	54
3.2	SNOW	55
3.2.1	Depth Measurements	55
3.2.2	Areal Measurements	57
3.2.3	Mapping and Snowcover	57
3.2.4	Snow Density	58
3.2.5	Albedo	59
3.2.6	Temperature	59
3.2.7	Free Water Content	60

Table of Contents (Continued)

CHAPTER		Page
3.3	ASSEMBLAGE OF DATA	60
3.3.1	Instrument Location and Height	60
3.3.2	Duration and Frequency of Observations	61
3.3.3	Difficulties	63
3.3.4	Processing	63
4	RESULTS	66
4.1	TEMPORAL VARIABILITY	66
4.1.1	Introduction	66
4.1.2	Calculation of the Heat Balance	66
	(a) Net radiation	67
	(b) Sensible and latent heat fluxes	67
	(c) The ground heat flux	69
	(d) The flux of heat from rain	69
	(e) Internal energy	70
4.1.3	Synoptic Weather Regimes	71
4.1.4	Time Series	76
4.2	SPATIAL VARIABILITY	86
4.2.1	Introduction	86
4.2.2	Spatial Variation in the Energy Balance for Snowmelt	87
4.2.3	Observations of Spatial Variability in Snowmelt	94
4.2.4	Environmental Factors Affecting Observed Spatial Variation in Snowmelt	102
	(a) Altitude	102
	(b) Ground cover	103
	(c) Ground water	104
	(d) Groundflux	104

Table of Contents (Continued)

CHAPTER	Page
5 SUMMARY AND CONCLUSIONS	106
5.1 SUMMARY	106
5.1.1 Temporal Variability	106
(a) Climatic factors	106
(b) The energy balance	107
(c) Snowmelt	108
5.1.2 Spatial Variability	110
(a) Climatic factors	110
(b) The energy balance	110
(c) Other factors	111
5.2 CONCLUSIONS	113
REFERENCES	115
APPENDICES	124

LIST OF TABLES

TABLE		Page
1.1	Lapse Rate	15
1.2	Climatic Statistics	15
1.3	Minimum Air Temperatures	16
1.4	Light Frost Days	16
1.5	Heavy Frost Days	16
1.6	Average Station Data	18
1.7	Snowfall Days	19
1.8	Rainfall	19
1.9	Climatic Statistics	22
3.1	Frequency of Manual Observations	61
3.2	Duration of Records	62
3.3	Temperature Profile	62
4.1	Daily Energy Flux Transfer	74
4.2	Daily Energy Flux Transfer	74
4.3	Comparative Net Radiation Data	89
4.4	Comparative Snowmelt	92
4.5	Surface Temperatures	96
4.6	Melt Calculations	96
4.7	Depth Averages	101
A1	Tow Summary	135
A2	Cloud Transmission Constants	143
A3	CR21 Input Programme Table (4)	149
A4	CR21 Output Programme Table (1)	150
A5	CR21 Output Programme Table (2)	150
A6	CR21 Output Programme Table (3)	151

LIST OF FIGURES

FIGURE		Page
1.1	Tasmania, Australia	6
1.2	The Ski Field Area in relation to the Ben Lomond Plateau	8
1.3	The Ben Lomond Ski Field Area (boundary and topography)	11
1.4	The Ben Lomond Ski Area (groundcover)	12
2.1	Zenith and azimuth used in calculating the solar zenith angle	32
3.1	Snow depth and photographic sites on the Ben Lomond Ski Field	56
4.1	Synoptic situations representative of the events described in section 4.1.3	72
4.2	Mean daily values for the three dominant components of the energy balance over snow on Ben Lomond for July, 1986	77
4.3	Mean daily values for the three dominant components of the energy balance over snow on Ben Lomond for August, 1986	78
4.4	Mean daily values for the three dominant components of the energy balance over snow on Ben Lomond for September, 1986	79
4.5	Mean daily values for the wind direction and air temperatures as well as snow melt calculated from the energy balance at the meteorological station on Ben Lomond for July, 1986	81
4.6	Mean daily values for the wind direction and air temperatures as well as snow melt calculated from the energy balance at the meteorological station on Ben Lomond for August, 1986	82
4.7	Mean daily values for the wind direction and air temperatures as well as snow melt calculated from the energy balance at the meteorological station on Ben Lomond for September, 1986	83

List of Figures (Continued)

FIGURE		Page
4.8	Spatial variability in the energy balance	91
4.9	Varying slopes on the Ben Lomond Ski Fields	93
4.10	The Ben Lomond Ski Field Area (Sep 22, 1981)	95
4.11	The Ben Lomond Ski Field Area (Sep 28, 1981)	98
4.12	The Ben Lomond Ski Field Area (Oct 6, 1981)	100
4.13	The relative aspect and snowdepth over the major rock domes in the Ski Field Area	105
5.1	A five day moving average time series of the calculated daily snowmelt for Winter, 1986 on Ben Lomond	111
5.2	A five day moving average time series of the mean daily snowmelt (including spatial variations)	112
A1	Schematic used in the calculation of shadow areas (Nunez, 1980)	140
A2	Schematic used in the calculation of sky view factors (Nunez, 1980)	142

LIST OF APPENDICES

APPENDIX		Page
1	Constants and Symbols	124
2	Descriptive Data for Ben Lomond	132
	(a) History	133
	(b) Tow Summary	135
	(c) Vegetation and Soils	136
3	Modelling Net Radiation for Mountainous Terrain	138
4	Data Acquisition	145
	(a) The Calculation of the Free Water Content of Snow	146
	(b) The Calculation of Vapour Pressure	148
	(c) CR21 Programme Tables	149

ABSTRACT

Studies were pursued in the snowfields of Ben Lomond in north-eastern Tasmania to establish the environmental factors affecting snowmelt. The approach through temporal and spatial analysis of ablation, was built upon a five year study of the climate which commenced in 1981. This was accompanied by an intensive measurement period in July to October, 1986.

Climatic results indicated that the highest and most consistent rates of snowmelt were associated with a mean rise in the daily air temperature and a reduction in snow-fall days towards the end of September. The days of strongest melt were most commonly accompanied by north-westerly winds generating regional advection. As the snowfield boundaries decreased, local advective forces enhanced heat available for melt.

The three dominant terms in the energy balance over snow were, in order of importance, net radiation, sensible and latent heat. Other terms investigated, including heat from rain, the ground and internal energy, were of minor significance in providing energy for melt. The importance of any one term was observed to depend upon the prevailing synoptic situation. The seasonal changes in the energy balance were reflected in temporal variations in snowmelt. The spatial

variability in snowmelt was not adequately described by variations in the energy balance. The differences could be explained by local characteristics in groundcover and topography.

Snow melted most slowly in grassed gullies lying under steep southward facing slopes above an altitude of 1500 metres. Within the study area, the rock domes and ridges which had the most easterly aspect and were below 1500 metres lost their snowcover first.

CHAPTER 1

A DESCRIPTION OF THE STUDY AND BEN LOMOND

INTRODUCTION 1.1

The global seasonal snowcover extends to approximately 12% of the earth's surface. All aspects of life are altered by its presence. Man has been particularly concerned with the social and economic ramifications of flood, storm, water supply and power resources from the seasonal cover. Other areas of concern involve the increasing impact of snow based recreational pursuits as well as the age old problems of travel and communication (McKay and Adams, 1981).

The 20th century has seen the emergence of research investigating specific aspects of snowmelt from the energy balance approach of Sverdrup (1936) and observational work of Seligman (1936) to recent work in the Cairngorms (Ferguson, 1985) on melt rates and modelling the bulk transfer coefficient over snow (Kondo and Yamazawa, 1986) in Japan. However, studies are hampered by an environment that is alien to both

man and instrumentation (Barry, 1981) with a resulting shortage of data.

Snow studies in ski field areas have tended towards avalanche forecasting rather than ablation (Kattelman, 1984) whilst melt rates and patterns have been specifically observed in relation to skier usage and snow making (Farwell et al, 1983). However, ski fields differ from snow fields only in their commercial development for recreational usage and research into melt factors over snow and ice in general has been well documented (Light, 1941; Gerdel et al, 1954; Kuz'min, 1961; Yosida, 1972; Fitzharris et al, 1980 and Aguado, 1985).

Consideration of environmental factors affecting snowmelt may be divided into climatic, biogeographic, geomorphic and geographic, with all these finally influencing the energy available for melt. Commonly snowmelt has been considered over a flat surface at low altitudes (U.S.A.C.E., 1956; O'Neill and Gray, 1973 and Male and Granger, 1979), whilst spatial variations due to slope and aspect typical of mountain regions have not been so well addressed (Hogg et al, 1982 and Munro and Young, 1982). The general approach is to consider a point representative of the snow field area concerned and calculate the energy budget from meteorological data available at that point. However this approach ignores the changing heat input from advective sources as reported by Treidl (1970) and Weisman (1977).

Research into melt of the seasonal snowcover in the southern hemisphere has been extremely limited (Moore, 1983) with no work published on snowmelt in Australia prior to 1986.

Investigations continue to be hampered by the paucity of meteorological data available above the seasonal snowline with no meteorological station being so situated in Tasmania prior to 1981.

The snow field on Ben Lomond in the highlands of north-east Tasmania is not only the prime winter recreational area for the State, but also part of the catchment area for two major river systems, the North Esk and South Esk. These two rivers have significant roles in supplying water for crops and stock in the surrounding rural areas as well as the City of Launceston (pop. 62,000). Serious flooding occurs in the river valleys approximately twice in every 10 years with damage sometimes estimated in millions of dollars (Examiner, 1970).

There has been a growing need for scientific research into snowmelt as costs for recreational development in the snow field escalate (Holloway, 1980). In addition, flood forecasting in Tasmania does not currently include expressions for run off from snowmelt due to lack of data, a further rationale for studies in this area.

This study describes a measurement programme to research the process of snowmelt in this maritime alpine climate. It involves the compilation of climatic data over a 5 year period as well as calculations to determine the energy balance of snowmelt. Extensions of temporal as well as spatial variations in melt and the energy balance have been attempted in addition to specifically mapping snowmelt against groundcover and terrain. However, heat from skiing, a melt factor specific to ski fields, was omitted.

The approach taken in this study commences with a description of the physical geography of Ben Lomond including details of the biogeographic and geomorphic features of the study area in the ski field. The results of the five year climatic survey are discussed and comparisons drawn with other meteorological stations in northern Tasmania as well as ski field areas in Victoria and New South Wales.

Various estimates of the energy balance calculations over snow are discussed in Chapter 2. The three dominant terms, net radiation, sensible and latent heat, are argued in some detail whilst other expressions to describe the exchange of heat from rain, the ground and internal energy are also included.

Chapter 3 describes the site of the meteorological station and data acquisition. Observations were hampered by financial constraints, poor weather, no reticulated power and difficult access. Characteristics within the snowpack were investigated in addition to the meteorological parameters essential for climatic studies and the energy balance.

The results and summary are divided into two sections, both analysed with respect to the energy balance and resultant snow-melt. In the first section dealing with temporal variability, the energy balance equation of Male and Gray (1981) was applied to construct a time series over the winter months of 1986. Further analysis was made with one week of high spring melt as well as several synoptic situations associated with high melt days, to determine the dominant energy balance terms.

The study of spatial variability commenced in 1981 when snow-melt was mapped against groundcover. Repetitions of the

patterns that emerged were noted throughout the next five years. In 1986 the energy balance was investigated for variation with space across the ski field. The model of Nunez (1980) was applied to reduce net radiation for mountain terrain and the ensuing calculated melt arising from the energy balance compared with observed data. The conclusions reached at the end of Chapter 5 draw attention to the dominant terms within the energy budget in consideration of seasonal snowmelt. The parameters arising from physical geography and synoptic events are included in the argument.

PHYSICAL GEOGRAPHY 1.2

Ben Lomond is situated in northern Tasmania and forms the southern boundary of the North Eastern Massif. This area rises immediately to the east of the Tamar Basin upon which is situated the City of Launceston. The massif is bounded to the north-west by Mt. Arthur and Mt. Victoria in the north-east (Figure 1.1).

Two major rivers rise in the massif. The North Esk skirts the northern face of Ben Lomond and descends to Launceston from the east, while the South Esk encircles the other three sides eventually approaching Launceston from the south and west. The South Esk is particularly important to the rural community and the two rivers supply the fresh water needs of over 100,000 people. The low lying areas are prone to violent flood and occasional drought. Knowledge of highland rainfall and snowcover is important in this regard.

Legges Tor in latitude $41^{\circ}32.1'S$ and longitude $147^{\circ}39.5'E$ is the second highest point in the State at 1572 metres. From this peak the northern half of the plateau maintains an

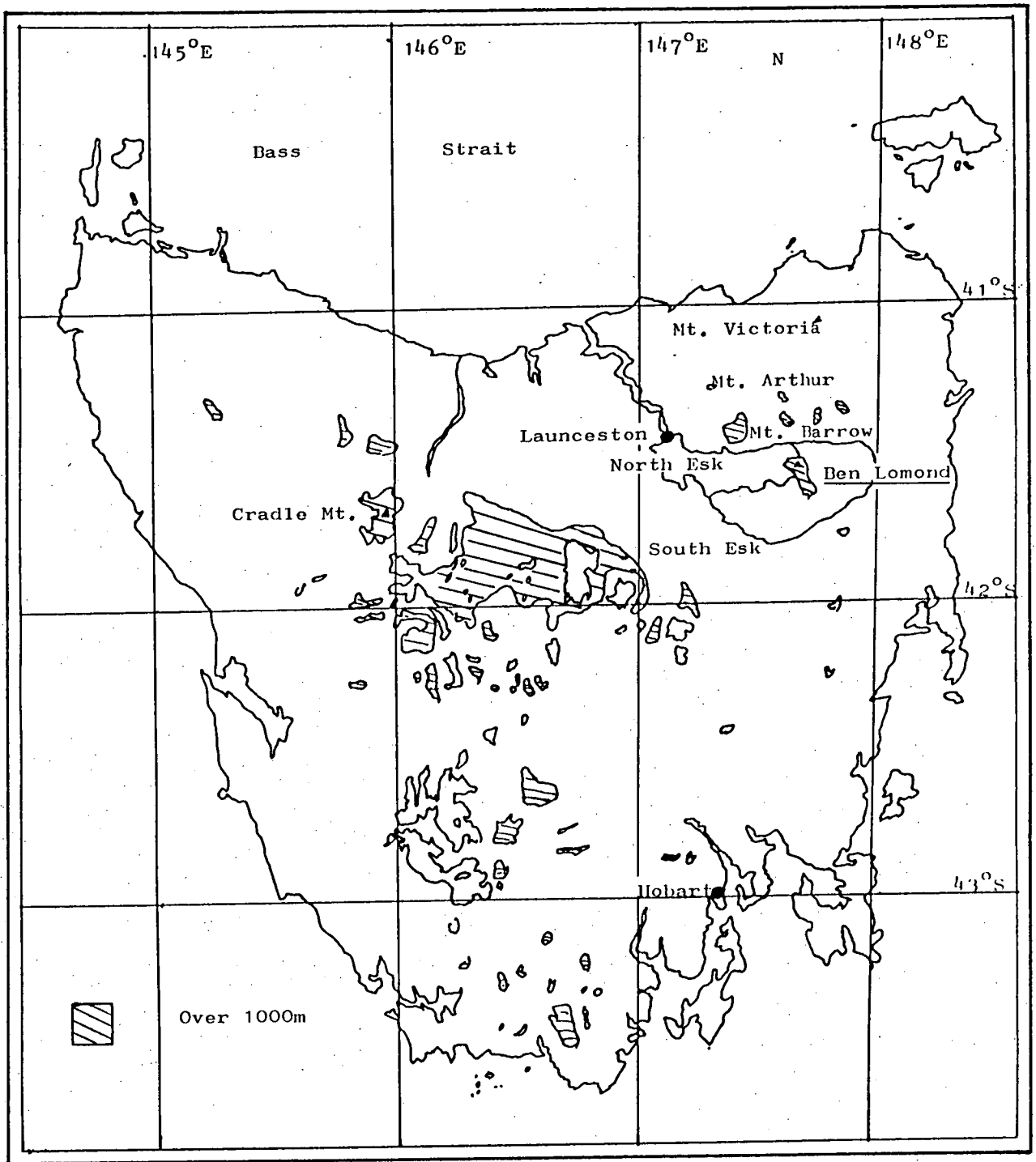


FIGURE 1.1 Tasmania, Australia

Source: The Reference Atlas for Australia and New Zealand, George Phillip and Son Limited, London, 1982.

altitude in excess of 1400 metres. The southern half is markedly lower being mostly between 1300 and 1400 metres with only Stacks Bluff rising above 1500 metres (Figure 1.2) to 1527 metres. Rodway Valley splits the plateau and descends to 1240 metres carrying the Nile River to the Speke Gorge. This is the only breach in the rim of the plateau.

Geomorphology 1.2.1

The basement rocks, peneplanation and dolerite intrusion of the Ben Lomond Plateau match the descriptions of basement rocks, peneplanation and dolerite intrusion of the Tamar Basin by Leadman and Symonds (1973). However, faulting and uplift has raised the level of the Central Plateau and Ben Lomond more than 1300 metres higher than the Tamar Basin that divides them.

The dolerite that is everywhere on the Ben Lomond Plateau is a silica and quartz poor igneous rock of medium grain (Holmes, 1964). The valleys of the uplands may have been caused by minor faulting along lines of weakness existing among the network of megajoints that cover the dolerite sheet. The rock has been further split into a series of hexagonal joints of 1.5 to 2 metres (Caine, 1968) clearly visible in the cliffs and exposed bedrock of the area today.

The features of Ben Lomond observed today are thought to have been affected by the ice cap that it held during the Pleistocene and the ensuing periglacial climate that still exists on the plateau today (Davies, 1969). However, attention must be drawn to the lack of tillite evidence of glaciation. Tillite

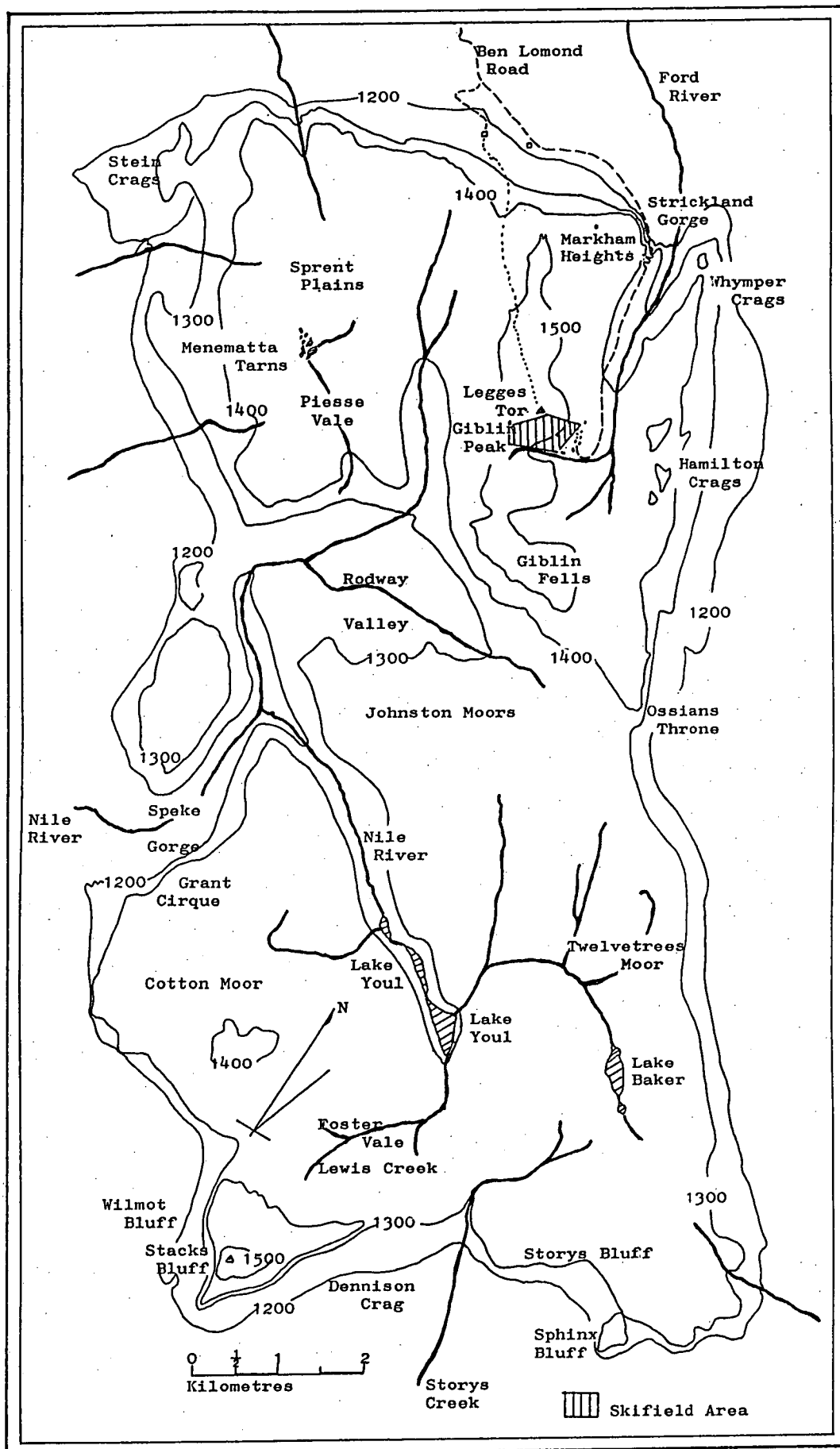


FIGURE 1.2

The Ski Field Area in relation to the Ben Lomond Plateau.

Source: Lands Department, Tasmap Series, 1:100,000, St. Pauls (1975).

is regarded by many as absolutely necessary to indicate glacial activity (Caine, 1968).

Apart from the huge domes that appear in the glaciated areas, the upland is marked by many blockfields and tors. Dolerite is subject to much chemical erosion when the right climate exists (Holmes, 1964), and it was thought by such investigators as Caine (1976B) and Davies (1969) that the tors were primarily due to such weathering, with particularly resistant plugs of dolerite standing out to heights of 10 metres from the general surface.

Frost action rapidly accelerates the breakdown of rock surfaces, talus and soils (Johns, 1977). A clear indication of the periglacial climate that exists on the Ben Lomond plateau is exhibited in the action of piprakes (Davies, 1969). These ice needles forming in the soil may be found to depths of 30 cm. They are a major factor in changing the character of the soil in this type of climate.

The frost process known as cryostatic pebble heaving has been held to account for sorted hexagonal patterns of stones found on the soils of periglacial regions. The huge domes of dolerite on the Ben Lomond plateau are also patterned with networks of hexagonals delineated by frost action (Davies, 1969).

Snow produces its own patterns of erosion and deposition. As deep patches of snow dig slightly deeper holes, more snow accumulates. This process of nivation is amply illustrated on the south eastern slopes of Legges Tor on Ben Lomond in transverse, longitudinal and circular forms, relative to the slope.

Biogeography 1.2.2

The ski field area (Figure 1.3) is typical of the plateau in terms of groundcover. Huge mammillated domes of dolerite intersperse the low alpine fellfield vegetation. This comprises shrubs, herbs, sedges and grasses (Figure 1.4).

Blockfields lie at the base of the rock walls along the upper ridge and streams follow the major gullies. Small patches of bare soil are to be found here and there.

Pinkard (1980) reported the Ben Lomond soils on dolerite as being of a strong clay loam of moderate permeability. He found a black soil with much organic material and many roots at an altitude of 1515 metres. Nichols (1958) suggested the soil is of an alpine humus type with poorly drained areas developing moor peat. The definitive work on alpine vegetation on Ben Lomond was done by Noble (1981). He found the plateau soil on dolerite to be strongly acidic and moderately to strongly leached. The sample he took near to the skifield area (and detailed in Appendix 2), supported other workers in that the soil was rich with organic material and roots, of colour dark brown grading to black. The soils in the ski-field are in general, well drained. During the summer they are quite dry even at 10 cm depth. However, throughout the winter they are wet or frozen to a depth in excess of 30 cm.

Noble (1981) identified more than 300 species of flora on Ben Lomond. Of particular significance to snowcover, are the distribution of shrublands in relation to herbs, sedges and grasslands (Figure 1.4). The most dominant of the woody shrubs are the *Richeas* and *Orites*, whilst the herb, *Gentianella diamensis* is everywhere.

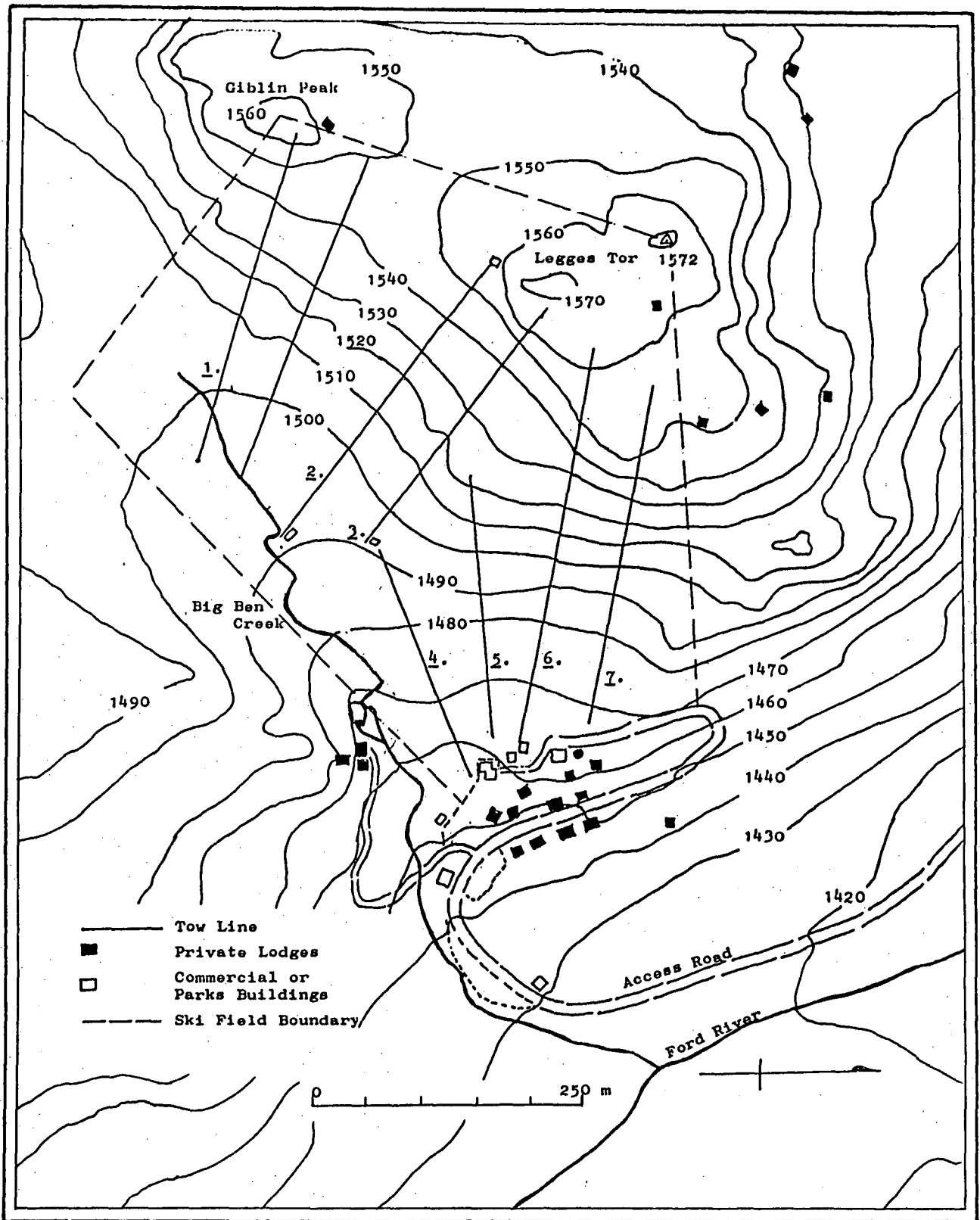


FIGURE 1.3

The Ben Lomond Ski Field Area

The Tows are numbered and named: 1. Giblin, 2. Big Ben, 3. Fannies, 4. Creek, 5. Beginners, 6. Thirty Second, 7. Summit. A new tow, Bill's, was built in 1985 between Nos. 1 and 2 tows as illustrated. The Meteorology station is denoted by (•).

Source: Lands Department, Ben Lomond National Park, 1975.

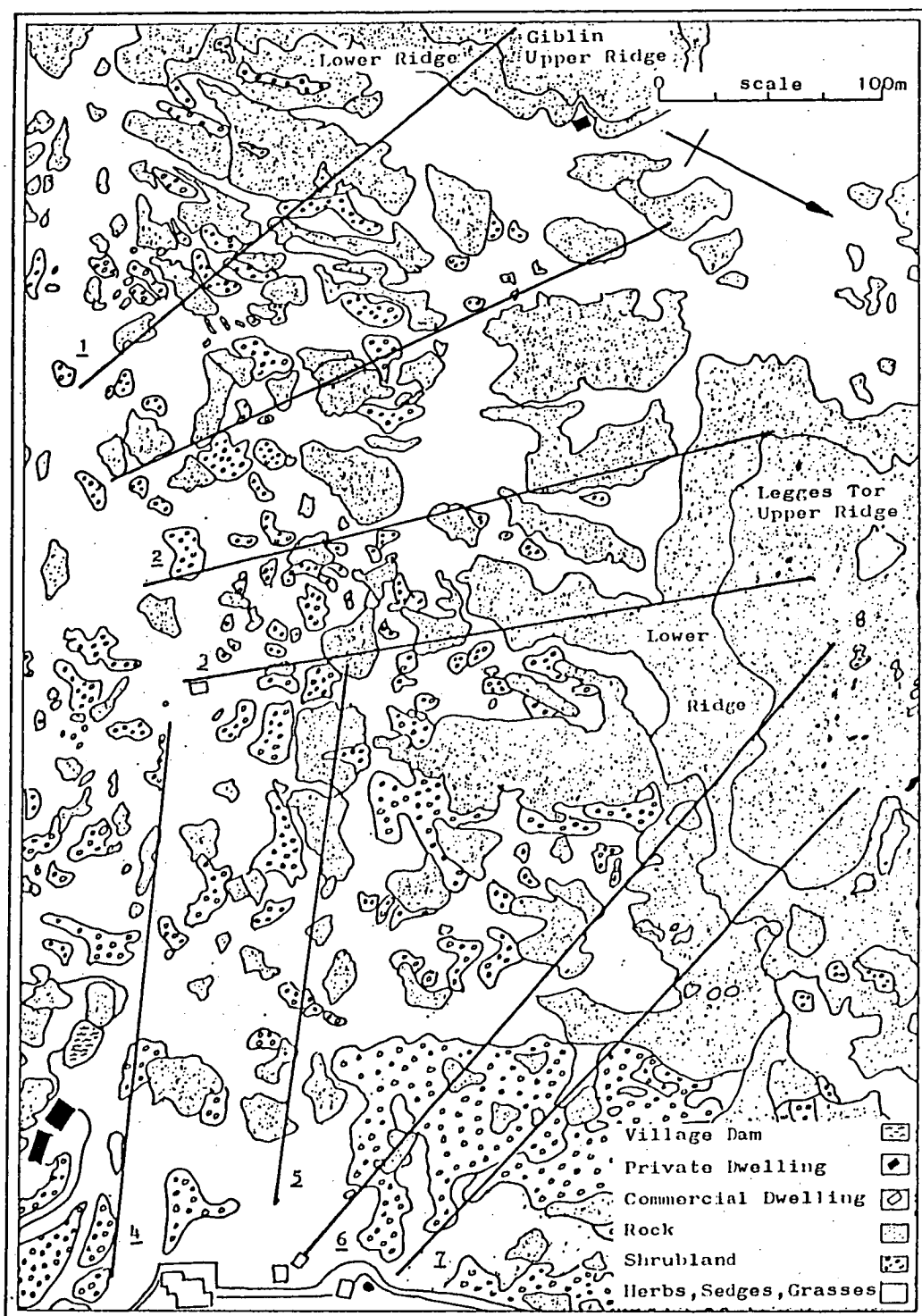


FIGURE 1.4 The Ben Lomond Ski Area

The groundcover is depicted in terms of rock, shrubland and herbs, sedges and grasses. The tows are numbered and named: 1. Giblin, 2. Big Ben, 3. Fannies, 4. Creek, 5. Beginners, 6. Thirty Second, 7. Summit. A new tow (Bill's) was built in 1985 between Nos. 1. and 2. The meteorology station is denoted by (●). Source: Lands Department aerial map of Legges Tor, 1980.

CLIMATE 1.3

The snowcover and the climate of the Ben Lomond ski area (1460 m) was investigated in terms of the statistics of temperature, precipitation and wind. Comparisons were drawn with other meteorological stations in north-eastern Tasmania as well as other ski field areas in Australia.

The study was made from June to October inclusive, these being defined as the winter months and when snowfall was most likely to occur. It commenced in 1981 and was still continuing in 1987 although this thesis concludes the five year period to 1985.

The General Climate of Tasmania 1.3.1

Tasmania has a temperate latitude, maritime climate. The prevailing weather is dominated by the mid-latitude westerly airstream (the "Roaring Forties") and the sub-tropical ridge. In the summer this belt of high pressure strengthens and is centred around 40°S, bringing mild to warm conditions especially to the north-eastern part of the State. During the winter a northward movement of the sub-tropical ridge allows a more frequent penetration of temperate depressions and polar maritime air bringing cooler and more moist conditions to the State. Rainfall is primarily frontal or orographic during the winter months with the North Eastern Massif forcing the westerly air up to over 1400 metres from the Midlands Valley and Tamar Basin.

Temperature and Frost Days 1.3.2

Temperature is perhaps the single most important indicator of snowcover (McKay and Gray, 1981). In Tasmania, the altitude above which heavy frost days occur with sufficient frequency to sustain seasonal snowcover, is referred to as the snowline, which occurs at approximately 1460 metres on Ben Lomond.

The dry adiabatic lapse rate at which the temperature reduces with altitude is $10^{\circ}\text{C km}^{-1}$. This lapse rate was altered by changing characteristics of the air mass and land mass so that the rate exhibited between Ben Lomond (1460 m) and Launceston Airport (166 m) was only $7.0^{\circ}\text{C km}^{-1}$ (Table 1.1) for the mean maximum air temperature which commonly occurred in the afternoon. This lapse rate was typical of a moist unstable air mass rising constantly. The mean minimum lapse, most often happening in the early morning, was $4.0^{\circ}\text{C km}^{-1}$ and suggested a stable air mass with inversions probably due to night time radiative cooling under clear winter skies. Noble (1981) indicated an inversion ceiling between 880 metres and 480 metres with a base from 380 metres down to sea level.

The mean minimum temperatures around which frost days are determined, did not differ markedly between Mt. Barrow (1323 m) and Ben Lomond (Table 1.3). In accordance with their lower altitudes, Cradle Valley (914 m) and Launceston Airport were respectively warmer. The lowest temperature ever recorded in Region 3 for northern Tasmania by the Bureau of Meteorology was -10.3°C at Cradle Valley. However, in July, 1981 a temperature of -11°C was recorded at the Ben Lomond meteorological station (Table 1.2). Minimum temperatures below -6°C

TABLE 1.1 LAPSE RATE

Temperature	Jun	Jul	Aug	Sep	Oct
Mean Maximum	6.7	6.7	7.0	7.9	7.0
Mean Minimum	3.6	4.4	3.8	3.9	4.3

The mean monthly lapse rates between Ben Lomond village (1460 m) and Launceston Airport (166 m), expressed in degrees centigrade per kilometre.

TABLE 1.2 CLIMATIC STATISTICS - BEN LOMOND VILLAGE

	Jun	Jul	Aug	Sep	Oct
Mean Maxima °C	2.6	2.0	1.8	3.8	7.2
Mean Minima °C	-1.6	-3.4	-1.9	-0.9	-0.0
Extreme Maxima °C	7.5	11.1	9.0	11.2	13.0
Extreme Minima °C	-5.5	-11.0	-7.4	-7.0	-6.0
Light Frost Days	26.2	30.2	30.1	29.6	27.5
Heavy Frost Days	24.5	29.4	26.3	21.7	18.5
Freeze Days	17.8	16.5	12.8	5.4	2.2

The summary of winter climatic data for Ben Lomond Village (1460 m) for the years 1981 to 1985 inclusive.

Mean maxima and minima are daily data averaged for the month and expressed in degrees centigrade.

Extreme maxima and minima represent the highest and lowest recorded temperatures during each month in the observed period expressed in degrees centigrade.

Frost and freeze days represent the mean number of days per month on which the phenomena was observed where:

Light frost days have a minimum air temperature $\leq 2^{\circ}\text{C}$.

Heavy frost days have a minimum air temperature $\leq 0^{\circ}\text{C}$.

Freeze days have a mean daily air temperature $\leq 0^{\circ}\text{C}$.

TABLE 1.3 MINIMUM AIR TEMPERATURES

	Jun	Jul	Aug	Sep	Oct
Ben Lomond	-1.6	-3.4	-1.9	-0.9	0.0
Cradle Valley	-0.2	-0.4	-0.6	0.3	1.3
Launceston Airport	3.0	2.3	3.0	4.1	5.5
Mt. Barrow	-0.9	-2.3	-2.0	-1.4	-0.0

Daily minimum air temperatures averaged per month and expressed in degrees centigrade.

TABLE 1.4 LIGHT FROST DAYS

	Jun	Jul	Aug	Sep	Oct
Ben Lomond	26.2	30.2	30.1	29.6	27.5
Cradle Valley	24.5	27.1	28.0	24.2	21.2
Launceston Airport	13.6	15.4	14.5	9.0	4.7
Mt. Barrow	26.0	29.5	30.0	29.0	22.8

Averages of the number of days per month on which light frost occurred.

TABLE 1.5 HEAVY FROST DAYS

	Jun	Jul	Aug	Sep	Oct
Ben Lomond	24.5	29.4	26.3	21.7	18.5
Cradle Valley	17.1	17.9	19.3	14.6	11.3
Launceston Airport	6.4	8.4	6.1	2.3	0.6
Mt. Barrow	-	-	-	-	-

Average of the number of days per month on which heavy frost days occurred.

were uncommon based on records over the five years from 1981 to 1985 on Ben Lomond.

The number of light frost days with minimum temperatures equal to or less than 2°C did not greatly differ between the stations above 900 metres (Table 1.4). Ben Lomond experienced more heavy frost days when the minimum temperatures were equal to or less than 0°C , when compared with Cradle Valley and Launceston Airport (Table 1.5). The coldest temperatures and the greatest number of days per month of frost coincided in July and August with the heaviest precipitation.

Rainfall 1.3.3

Precipitation decreases from west to east across the State, a leaching function of the orographic effect induced by the mountainous land mass on the prevailing westerly airstream (Lewis, 1945). Cradle Valley is situated immediately north of Cradle Mountain (Figure 1.1) which rises to 1544 m and had a higher annual rainfall at 2777 mm than mountains in the North Eastern Massif typified by Mt. Barrow which had an annual precipitation figure of 1401 mm. This latter value was considerably greater than that for Launceston Airport which received 719 mm of rain annually. Upper Blessington (420 m) is directly under the northern foothills of Ben Lomond and had the high precipitation figure of 1358 mm. All stations showed the heaviest precipitation to be in July and August (Table 1.8) with these two months supplying approximately 22% of the annual total.

The only rainfall figures for Ben Lomond stem from the work of Noble (1981) who applied regression analysis to three years

TABLE 1.6 AVERAGE STATION DATA

STATION 083081: MOUNT HOTHAM Lat. 37°00' Elevation 1750.0M							
Element	Units	Jun	Jul	Aug	Sep	Oct	Annum
Mean Daily Max. Temp.	°C	3.0	0.9	3.2	5.1	9.8	-
Mean Daily Min. Temp.	°C	-1.9	-3.7	-2.0	-1.3	1.4	-
Snow Days	Days	15	20	17	13	6	-
Frost Days	Days	20	22	21	15	11	-
STATION 071032: THREDBO (CRACKENBACK) Lat. 36°29'S Elevation 1957M							
Element	Units	Jun	Jul	Aug	Sep	Oct	Annum
Mean Daily Max. Temp.	°C	1.6	-0.1	0.3	2.7	7.1	-
Mean Daily Min. Temp.	°C	-3.7	-5.7	-5.1	-3.6	-0.5	-
Snow Days	Days	13	17	17	14	7	-
Frost Days	Days	21	21	19	21	17	-
Rainfall	mm	102.9	142.2	150.3	179.3	184.0	-
STATION 071072: PERISHER VALLEY SKI CENTRE Lat. 36°24'S Elevation 1720M							
Element	Units	Jun	Jul	Aug	Sep	Oct	Annum
Mean Daily Max. Temp.	°C	3.3	1.9	3.4	5.5	9.2	-
Mean Daily Min. Temp.	°C	-3.9	-5.8	-4.0	-2.3	0.6	-
Snow Days	Days	13	16	13	11	6	-
Frost Days	Days	19	27	25	21	18	-
Rainfall	mm	178.5	184.6	224.6	264.8	204.3	-

Data for three stations which have an altitude above the seasonal snowline in the states of Victoria and New South Wales, where skiing occurs (Bureau of Meteorology, 1975).

TABLE 1.7

SNOWFALL DAYS

	Altitude	Jun	Jul	Aug	Sep	Oct	Total
Ben Lomond	1460m	5.6	8.8	10.4	5.2	0.8	30.8
Cradle Valley	914m	5.1	7.8	9.6	6.6	5.5	34.6
Launceston Airport	166m	-	-	0.2	0.1	-	0.3
Mt. Barrow	1323m	2.6	5.9	8.1	6.3	3.7	26.6

The average number of days per month on which snowfall was recorded.

TABLE 1.8

RAINFALL

	Jun	Jul	Aug	Sep	Oct	Year
Cradle Valley	275	320	307	275	251	2777
Launceston Airport	63	84	80	65	68	719
Mt. Barrow	133	151	180	144	98	1401
Upper Blessington	114	137	127	98	95	1358

The mean monthly rainfall expressed in mm.

With the exception of Ben Lomond, the data are published with permission of the Director, Commonwealth Bureau of Meteorology, with the reservation that base data had not been quality controlled by the Bureau of Meteorology (1979) at the time.

of summer data for several stations on the north face of the mountain, arriving at 1277 mm for 1260 m altitude and a steady increase in precipitation with altitude. The ski village (1460 m) is 137 m higher than Mt. Barrow and 200 m above the north face station. It is probable then, that greater precipitation would have been experienced over the ski field area than at Mt. Barrow, following the argument of precipitation increasing with altitude (Barry, 1981).

The winter rainfall is mainly the result of cold fronts constantly sweeping across the State, generally moving at 15-25 knots. Depressions moving at lower latitudes occasionally cross the State and are sometimes "cut off" near the east coast. Such regimes produced heavy rains and snow on Ben Lomond accompanied by strong easterly winds.

Snowcover 1.3.4

All areas in Tasmania experience snowfall from time to time with more falls being recorded in the south-western region than elsewhere, a function of high precipitation in this area. Whilst snowfall is common in winter above 800 metres, only Ben Lomond of the mentioned stations had a regularly sustained seasonal snowcover. Snowfall days (Table 1.7) did not show any strong variation amongst the higher three stations, and all three had the most frequently recorded falls coinciding with frosts and precipitation in July and August.

For snowcover to be maintained, snowfall must exceed snowmelt. One outstanding factor was the higher number of heavy frost days Ben Lomond had when compared with the other stations in Tasmania. Other ski fields in Australia at Hotham, Thredbo,

and Perisher Valley had lower minimum temperatures and similar frost days to Ben Lomond (Table 1.6) but a distinctly higher frequency of snowfall days. Records showed a more sustained and deeper snowcover (Summit Sun, 1984) at these three other ski fields when compared with Ben Lomond.

Snow and Wind 1.3.5

The dominant westerlies that encompass the Southern Ocean are changed by atmospheric disturbance and landform until the winds experienced on Ben Lomond are distributed as shown in Table 1.9. The winter westerlies with their embedded cold fronts introduce air which is mainly of polar maritime origin. The resulting precipitation has been recorded falling as snow on more than one day in four during July and August on Ben Lomond (Table 1.7).

Whilst not indicated by the mean data (Table 1.9), the heaviest early season snowfalls accompanied north-easterly winds presaging the passage of a front. Snowfall was more frequent during July and August, whilst more snowfall days accompanied winds from the westerly quarter than any other quarter.

BEN LOMOND SKI VILLAGE (1460m)CLIMATIC STATISTICS

TABLE 1.9 WIND DIRECTION AND SNOW DATA

[Wind]	N	NE	E	SE	S	SW	W	NW	CALM	
Jun	1	2	0	3	2	8	3	5	6	
Jul	1	3	0	3	3	7	2	6	6	
Aug	2	5	0	2	2	6	2	8	4	
Sep	2	3	0	2	1	9	2	9	2	
Oct	3	5	0	2	2	4	1	10	3	
Tot	9	19	0	12	10	34	10	38	21	
[Snowfall]										TOTAL
Jun	0.4	0.2	0.0	0.6	0.4	1.4	0.8	1.6	0.2	5.6
Jul	0.0	1.4	0.0	0.4	0.6	3.0	0.8	2.0	0.6	8.8
Aug	0.8	1.2	0.0	0.6	0.6	2.8	1.0	2.8	0.6	10.4
Sep	0.6	0.6	0.0	0.2	0.0	1.6	0.6	1.6	0.0	5.2
Oct	0.0	0.0	0.0	0.4	0.0	0.0	0.0	0.4	0.0	0.8
Tot	1.8	3.4	0.0	2.2	1.6	8.8	3.2	8.4	1.4	30.8

Period of Records: 1st June to 31st October from 1981 to 1985 inclusive.

The upper table shows the mean number of days each month the wind was recorded from the named sectors (rounded to the nearest day).

The lower table shows the mean number of days each month on which snowfall was recorded, displayed in relation to the wind sectors (rounded to one decimal place).

Source: After Caine (1968).

CHAPTER 2

THE ENERGY BALANCE

THE GENERAL MODEL 2.1

Sverdrup was the first to apply the energy budget to the snowcover in studies on West Spitzbergen Island in 1924 (McKay and Thurtell, 1978). Since then it has gained in popularity as it allows the melting process to be studied in a systematic and objective way.

For the calculations the pack is assumed to be ripe or primed for melt. The temperature is at 0°C and each grain of snow is covered by a film of water. The water content of the pack may be 3% to 25% depending on the internal structure and grain characteristic. The application of any additional energy to the pack will result in more water being produced than the pack can hold in situ. The excess water percolates through the pack and is released as melt.

In terms of its energy balance components, the energy flux

available for melt can be written as (Male and Gray, 1981):

$$Q_M = K^* + L^* + Q_H + Q_E + Q_G + Q_P + Q_I, \quad 1$$

where

Q_M - energy flux available for melt,

K^* - net shortwave radiation flux,

L^* - net longwave radiation flux,

Q_H - convective or sensible heat flux,

Q_E - flux of the latent heat (evaporation, sublimation, condensation),

Q_G - flux of heat from the ground,

Q_P - flux of heat from rain and

Q_I - internal flux of heat from water phase changes.

Commonly the net longwave and shortwave radiation terms are reduced to a net radiation term (Q^*) so that:

$$Q_M = Q^* + Q_H + Q_E + Q_G + Q_P + Q_I \quad 2$$

The flux of heat from the ground (Q_G) is generally a small quantity and may be considered negligible over a few days (Moore and Owens, 1984). In the longer term, over weeks or months, the amount of melt generated from this source may prove significant. The diurnal melt/freeze cycle of the pack produces an internal change of energy (Q_I) often ignored in field calculations (Treidl, 1970; Aguado, 1985) where the pack is deep. The energy derived from this source is small, measurements are difficult and the process complex. As these two sources supply less than 2% of the heat budget they are often omitted, and the equation becomes:

$$Q_M = Q^* + Q_H + Q_E + Q_P. \quad 3$$

Of the four remaining terms, the energy derived from a rain on snow event (Q_p) is usually of small significance compared to the other three (Fitzharris, et al, 1980).

The equation is normally resolved for a horizontal surface. However, in mountainous terrain this is not usually the case. Net radiation is reduced to allow for slope and aspect but all other terms are treated as for the horizontal surface in the absence of alternatives (Male, 1980).

NET RADIATION 2.2

An inspection of the sum of the first two terms in Equation 1 concerning net shortwave (solar) and longwave radiation leads us to:

$$Q^* = K^* + L^* , \quad 4$$

where $K^* = K\downarrow - K\uparrow , \quad 5$

and $L^* = L\downarrow - L\uparrow , \quad 6$

for \uparrow - the upward flux and

\downarrow - the downward flux.

Problems in assessing net radiation are approached by isolating each term and investigating the impact of the atmosphere, geographic position and topography of the area under investigation upon them (Houghton, 1954; Sellers, 1965; Munro, 1970; Kondratyev, 1969; Davies et al, 1975 and Nunez, 1980).

During the resolution of the energy balance over snow it is seldom that all the terms are measured. It is common practice (Dozier, 1979; Hogg et al, 1982; and Munro and Young, 1982),

to construct a model to allow for variations occurring in mountainous regions after initial measurements have been taken over the horizontal surface.

Downward Shortwave Radiation 2.2.1

The extra terrestrial constant of the solar flux was reported as $1360 \text{ W m}^{-2} (\pm 1.5\%)$ by Barry and Chorley (1982). Solar energy is attenuated through absorption and scattering by gases and dust in the atmosphere so that only a fraction is transmitted to the Earth's surface. Garnier and Ohmura (1970) suggested a transmission coefficient of 0.75 whilst Kondratyev (1969) argued that transmission was higher in winter than summer due to the lower water vapour content of the air. Accordingly a value of $p = 0.8$ was given to the transmission of global radiation over snow in European U.S.S.R.

The question must always arise as to the minimum data necessary to ensure the proper functioning of a model. Houghton (1954) looked at transmission factors in more detail. He assumed that upon entering the atmosphere the solar beam was absorbed before scattering occurred and that half the scattered energy reached the surface of the Earth.

Schertzer (1975) applied least squares regression to Houghton's data obtaining polynomial approximations for the transmission coefficients of water vapour absorption (w_a) and scattering (w_s) and Rayleigh scattering (r_s) which are:

$$\psi_{ws} = 1.0059 - 0.0224545 (wm), \quad 7$$

$$\begin{aligned} \psi_{wa} = & 0.9972 - 0.0918415 (wm) + 0.0224301 (wm)^2 \\ & - 0.0026573 (wm)^3 + 0.0001107 (wm)^4, \quad 8 \end{aligned}$$

$$\psi_{rs} = 0.9716084 - 0.0826204 (m) + 0.0093269 (m)^2 - 0.000946 (m)^3 + 0.0000437 (m)^4, \quad 9$$

or $\psi_{ws} = 1 - 0.025 (wm), \quad (\text{McDonald, 1960}) \quad 10$

and $\psi_{wa} = 1 - 0.077 (wm)^{0.3}, \quad (\text{McDonald, 1960}) \quad 11$

where w - the precipitable water vapour and
 m - the optical air mass expressed by Kasten
 (1966) as:

$$m = [\cos Z + 0.15 (93.885 - Z)^{-1.253}]^{-1}. \quad 12$$

The length of the path of the direct solar beam through the atmosphere (the optical air mass) may be more simply stated by:

$$m = \sec Z, \quad 13$$

where z - the zenith angle of the sun.

Barry (1981) suggested this should be adjusted for altitude so that:

$$m = \sec Z (P_a/P_o), \quad 14$$

where P_a - atmospheric pressure and
 P_o - standard atmospheric pressure at mean sea level.

The precipitable water vapour may be calculated or extracted from List (1968). However, the impact upon the expression is very small and Sellers (1965) suggested a value of 18.1 mm be adequate. Davies et al (1975) suggested that the use of surface humidity data as an approximation for precipitable water be acceptable.

Houghton (1954) stated (with reservations) that absorption (da) and scattering (ds) due to dust were equal and wrote:

$$\psi_{da} = \psi_{ds} \simeq 0.975^m, \quad 15$$

so that the transmission coefficient for dust was:

$$\psi_d = \psi_{da} \psi_{ds} = (c)^m. \quad 16$$

Considerable discussion (Houghton, 1954; Davies et al, 1975; Schertzer, 1975; Nunez, 1980 and Barry, 1981) has centred around the constant (c) with values between 0.88 and 0.98 being investigated and found a good fit. An atmosphere that is heavily polluted with a high turbidity is expected to respond best to a low (0.88) value whilst a clear dust free atmosphere is best suited to a higher (0.98) constant. Nunez (1980) found 0.88 was the best fit for Tasmanian lowlands whilst Barry (1981) suggested that values in excess of 0.96 might not be uncommon for higher altitudes in clean air.

The solar radiation incident under cloudless conditions received on a horizontal surface ($K\downarrow_o$) is the sum of the direct (S_o) and diffuse (D_o) shortwave radiation components expressed by Davies et al (1975) as:

$$K\downarrow_o = I \cos Z + D_o, \quad 17$$

so that $S_o = I \cos Z, \quad 18$

and $I = I_o \psi_{wa} \psi_{da} \psi_{ws} \psi_{ds} \psi_{rs}, \quad 19$

also $D_o = S_o \psi_{wa} \psi_{da} (1 - \psi_{ws} \psi_{ds} \psi_{rs})/2, \quad 20$

where I - solar constant reduced by transmission through the atmosphere,

and I_o - solar constant.

Global radiation has so far only been considered for cloudless skies. Two approaches have generally been adopted for cloudy

conditions. The first and simplest method adopted (Paltridge and Platt, 1976; Munro and Young, 1982) was to consider the cloud cover as a single layer so that for direct radiation under cloudy skies:

$$S_c = S_o (1 - n) \quad 21$$

where n - total fractional amount of cloud.

The diffuse radiation was considered for the cloudless portion of the sky (D_1) and the multiple reflections between the clouds and the ground (D_2). The sum then became:

$$D_c = D_1 + D_2, \quad 22$$

$$\text{where } D_1 = D_o (1 - n) + n S_o (1 - a_n - \alpha_n), \quad 23$$

$$\text{and } D_2 = (S_c + D_1) n \alpha_b \alpha (1 - \alpha_b \alpha)^{-1}, \quad 24$$

for a_n - absorptivity of the cloud,

α - reflectivity of the ground (albedo),

α_b - reflectivity of the cloud base and

α_n - reflectivity of the cloud top.

Munro and Young (1982) used a modified form of Fritz' (1954) expression for the cloud base reflectivity:

$$\alpha_n = \{ \exp (-0.565 m \chi) [\chi (1 - 1.48 \alpha_n) + 3.54 m^{-1} - 2.62] - 3.54 m^{-1} - 2.62 \} \{ (\chi + 5.24) + 1 \}^{-1} \quad 25$$

where χ - cloud thickness to the mean free path of light through the cloud.

This expression accommodated the reduction in albedo (α_n) as the optical air mass (m) became small.

Suckling and Hay (1977) suggested that whilst observers tended to overestimate cloud cover, sunshine records underestimate,

and a better fit for cloud amount (n) was:

$$n = [a (1 - f_s) + b n_e] [a + b]^{-1}, \quad 26$$

where a - weight = 1 ,

f_s - fractional sunshine recorded on sun cards,

b - weight = 2 and

n_e - observer estimate of cloud amount.

Workers attempting a more detailed analysis of radiation receipt under cloudy skies have adopted a physical model rather than using the single layered empirical approach described above. Nunez et al (1971), Davies et al (1975) and Suckling and Hay (1977) used a multi layered cloud model. Considering three layers of cloud, high (h) Medium (m) and low (l), the global radiation incident on a horizontal surface for cloudy conditions was expressed (Nunez, 1980) as:

$$K\downarrow_c = K\downarrow_o \psi_{ch} \psi_{cm} \psi_{cl}, \quad 27$$

where each cloud layer (i) transmission, assuming uniform distribution was:

$$\psi_{ci} = 1 - (1 - t_i) C_i, \quad 28$$

where t_i - transmission of the cloud layer i and

C_i - the amount of cloud layer i .

Utilizing data from Haurwitz (1948):

$$t_i = K\downarrow / K\downarrow_o, \quad 29$$

$$\text{where } K\downarrow = \frac{a}{m} \exp (- b m). \quad 30$$

Values for (a) and (b) are detailed in Appendix 3.

Allowances for reflection from the lowest cloud base altered Equation 27 to:

$$K\downarrow_c = K\downarrow_o \psi_{ch} \psi_{cm} \psi_{cl} \{1 + 0.5 \alpha C_l\}, \quad 31$$

where 0.5 - mean lower cloud base albedo.

Reductions in Shortwave Radiation in Hilly Terrain 2.2.2

In mountainous country a reduction in the global radiation receipt has been found due to topographical constraints (Dozier, 1979). The angle of elevation of the horizon is commonly increased, reducing the sky view; and all slopes, particularly those pole oriented, are subject to shadowing (Seligman, 1936).

The initial problem of resolving global radiation for hilly conditions has traditionally commenced by reducing the zenith angle of the direct solar beam for slope and aspect (Figure 2.1). The three dimensional geometry applied to this problem was stated by Nunez (1980) in a similar manner to Sellers (1965) and Kondratyev (1969) so that the angle of incidence (γ) of the direct solar beam with an inclined surface became:

$$\cos \gamma = \sin Z \cos \omega \sin X \sin Y + \sin Z \sin \omega \sin X \sin Y + \cos Z \cos Y. \quad 32$$

Equation 18 describing the receipt of the direct solar beam may now be adjusted to allow for an inclined surface so that:

$$S'_o = I \cos \gamma. \quad 33$$

Hogg et al (1982) applied the model of Garnier and Ohmura (1970) to calculate the direct radiation receipt on a slope:

$$S'_o = I_o \int_{H_1}^{H_2} p^m \cos (XAS) dH \quad 34$$

The integration limits H_1 and H_2 are sunrise and sunset on the slope in question and $\cos (XAS)$ the angle of incidence of the direct solar beam upon the slope. The expression can be solved numerically by summing intervals (half-hourly or hourly) between H_1 and H_2 . Atmospheric transmissivity (p) was assumed to be 0.75 in the original study.

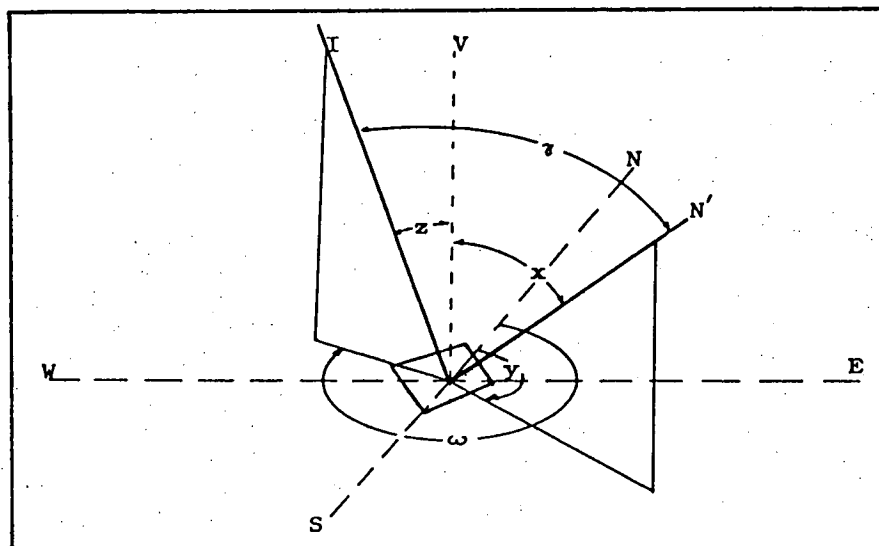


FIGURE 2.1 Zenith and azimuth used in calculating the solar incidence angle

where I - direct beam solar radiation
 N' - normal to inclined surface
 V - vertical axis
 N, S, W, E - four compass points in a horizontal plane
 z, x - zenith angles for I and N' respectively
 ω, y - azimuth angles for I and N' respectively
 γ - angle of incidence of I with the inclined surface

Calculations for the restricted access of the direct solar beam onto a slope have included modelling the topography in a suitable computer programme to allow for additional shadowing that occurs due to concavity or convexity in any slope.

A typical programme (Nunez, 1980) details the area into grids or pixels and steps towards the direct solar beam according a grid area as either in sunlight or shadow. Further details are included in Appendix 3.

In consideration of diffuse radiation an isotropic model underestimates the clear sky diffuse radiation on equator facing slopes as the incident flux is anisotropic. 75% of the diffuse radiation flux is received from the circumsolar half of the sky; that is, the half bounded by the plane normal to the solar vertical (Kondratyev and Federova, 1977). This dependence on the azimuth of the sun causes differences according to the slope azimuth.

Hay (1977) has developed a model for anisotropic diffuse radiation on slopes which yield lower systematic and random errors than either the isotropic model or one using half circumsolar and half isotropic arguments:

$$D_o' = \left[\frac{I}{I_o} \cdot \frac{\cos \gamma}{\cos Z} D_o \right] + \left[0.5 D_o (1.0 + \cos X) \left(1.0 - \frac{I}{I_o} \right) \right] \quad 35$$

and $\frac{I}{I_o} \cos \gamma$ - an 'anisotropy index' for the slope.

The first term on the right is the circumsolar component.

The last term is the isotropically distributed radiation flux.

It is difficult to calculate the component reflected from adjacent slopes. If a mean surface characteristic is assumed, Barry (1981) offers the following equation:

$$D_r = (S_o + D_o) \alpha \sin^2(X/2) \approx 0.5 (S_o + D_o) \alpha (1.0 - \cos X).$$

However, he further stated that important discrepancies arose in the term D_r from the anisotropic diffuse radiation component, especially in the presence of snowcover.

For practical reasons, isotropic models have been adopted for calculating diffuse radiation in hilly regions (Munro and Young, 1982). The equation written for diffuse radiation received on a slope allowing for a reduced sky view has been expressed (Nunez, 1980) as:

$$D'_o = D_o VF + (1 - VF) K\downarrow_o \alpha . \quad 37$$

Now, applying the zenith angle of the direct solar beam reduced for slope and aspect (Equation 33) and substituting Equation 37 in Equation 17, global radiation received on a slope under cloudless conditions is (Nunez, 1980):

$$K\downarrow'_o = I \cos \gamma + D'_o , \quad 38$$

and under cloudy skies with a reduced sky view:

$$K\downarrow'_c = I (1 - C_l)(1 - C_m)(1 - C_h) \cos \gamma + D_c VF + K\downarrow_c \alpha (1 - VF), \quad 39$$

$$\text{where } D_c = K\downarrow_c - I (1 - C_l)(1 - C_m)(1 - C_h) \cos Z. \quad 40$$

Upward Shortwave Radiation 2.2.3

An inspection of Equation 5 reveals that net solar radiation requires the upward component (reflected) to be defined as well as the downward flux. This has been traditionally expressed as a function of the reflectivity or albedo of the surface (Male, 1980):

$$K\uparrow'_c = \alpha K\downarrow'_c \quad 41$$

There arises a heavy dependence upon the value given to albedo for net radiation calculations (Schneider and Gal Chen, 1973).

Albedo 2.2.4

Langham (1981) stated that albedo was a good measure of the ability of snow to absorb radiative energy. Investigations reveal that the radiative energy absorbed by the snow is a prime melt factor. Albedo (α) may be expressed as the ratio of reflected shortwave radiation ($K\uparrow$) to the incident shortwave radiation ($K\downarrow$) (Male and Gray, 1981):

$$\alpha = K\uparrow / K\downarrow .$$

42

When snow is freshly fallen it is clean, dry and loose, with a density commonly of less than 200 kg m^{-3} . The albedo may be as high as .88, values being typically dependent on the solar zenith angle. However, as the snow ages it becomes wetter and more compact; the albedo drops to 0.55 within six days, largely due to the increase in the free water content (Diamond, 1956). Even if this old snow is frozen, the albedo does not increase. Finally, old and dirty saturated sea ice will yield albedo values of less than 0.3.

Snow cover of a shallow nature ($< 250 \text{ mm}$) has albedo values differing primarily due to ground showing through the cover. In addition, shortwave radiation has been shown to penetrate the shallow pack to be absorbed by the ground (Male and Gray, 1981).

The snowpack grain size varies with texture and density which also alter with ageing. This process known as metamorphism or firnification, affects albedo in two ways.

Initially the surface 'roughness' affects the albedo value, and the back-scattering due to subsurface grain characteristics add to the surface albedo to a varying degree. Albedo varies inversely as the square root of the grain size (Male and Gray, 1981) whilst water in the snowpack also reduces the albedo values.

Hubley (1954) found that daily albedo values over snow seldom varied by more than 30%. In mountain regions this variation may be increased in accord with the larger range of solar zenith angles due to the slope and aspect variability of mountain regions.

Solar Radiation Attenuation Within the Snowpack 2.2.5

Incoming solar radiation is absorbed to a certain extent within the snowpack. This has little effect on melt in deep snow as the energy reaching the ground is very small. However, in shallow snow (depth < 250 mm) some incoming shortwave radiation will reach the ground and be returned to the pack in the form of longwave radiation or through conduction. Thus energy is provided for melt or for thawing the soil surface to permit water percolation from the snow (Male and Gray, 1981).

If the pack is assumed homogenous, a typical state for low altitude temperate snow, then the attenuation of incoming solar radiation may be expressed by (Giddings and La Chapelle, 1961):

$$K_z = K_{\downarrow 0} \exp (- b z) \quad 43$$

where K_z - radiation intensity at any depth (z)
 b - extinction coefficient.

There is uncertainty surrounding the extinction coefficient which has been shown to be more dependent on foreign matter (dust and organic matter) within the pack than either the wetness or density of the snow (Bohren and Barkstrom, 1974).

Longwave Radiation 2.2.6

A final consideration of net radiation:

$$Q^* = K^* + L^*. \quad 44$$

After the net shortwave radiation (K^*) has been either calculated or measured, a value for net longwave radiation is required (L^*). It may be obtained as a residual from direct measurements:

$$L^* = Q^* - K^* \quad 45$$

or calculated, as shown below.

Outgoing longwave radiation may be expressed in terms of ground temperature. Paltridge (1975) found that over a day the mean surface temperature was equal to the mean air temperature, so that:

$$L\uparrow = \epsilon \sigma \theta^4 + L\downarrow (1 - \epsilon), \quad 46$$

where ϵ - surface emissivity,

σ - Stefan Boltzman constant and

θ - surface temperature.

Snow has been reported (Sellers, 1965; Munn, 1966; Anderson, 1976) as having longwave emissivities ranging between 0.97 and 1.00, whilst Moore (1983) applied a value of 0.99 to longwave calculations over snow in New Zealand.

Several expressions have been applied for ascertaining downward longwave radiation of which the most widely used, according to Male (1980), is of the form first written by Brunt (1952):

$$L\downarrow = \epsilon \sigma T_a^4 (a + b \sqrt{e_a}), \quad 47$$

where T_a - air temperature,

a and b - constants changing with time and space, and

e_a - vapour pressure.

Kuzmin (1961) offered values for (a) and (b) based on long term measurements over snow in the Russian plains and steppe regions so that:

$$L\downarrow = \epsilon \sigma T_a^4 (0.62 + 0.005 \sqrt{e_a}). \quad 48$$

However, Barry (1981) expressed reservations in applying the Brunt equation to high altitude areas due to the reduced water column in the atmosphere leading to overestimation in the model. A simple temperature and humidity profile was developed by Brutsaert (1975):

$$L\downarrow = 0.642 (e_a/T_a)^{1/7} (T_a^4), \quad 49$$

and modified by Marks (1979) for alpine use by assuming that relative humidity is constant with altitude but temperature reduces with the standard lapse rate. Prowse and Owens (1982) applied this for a net longwave radiation expression with further adjustments to allow for the reduced view factor (Lee, 1962) and cloud cover (Sellers, 1965):

$$L^* = 1.24 (e_a/T_a)^{0.16} (P_a/1013) \sigma T_a^4 (1 + \Omega n^2) \cos^2 (90 - \eta) + \epsilon \sigma \theta^4 (1 - (\cos^2 (90 - \eta))) - \epsilon \sigma \theta^4, \quad 50$$

where T_a' - air temperature adjusted to sea level,
 Ω - cloud height and temperature coefficient, and
 η - average horizon angle from the zenith.

Many calculations in mountain regions at high altitude utilise sub zero air temperatures. Satterlund (1979) as reported by Male and Gray (1981) achieved more accurate results than Marks (1979) by applying:

$$L\downarrow = (\sigma T_a'^4) 1.08 [1 - \exp(-e_a^{T_a'/2.016})] . \quad 51$$

Swinbank (1963) suggested that the dependence of the downward longwave radiation receipt on water vapour present in the atmosphere was not warranted and a better fit relating the receipt to air temperature was more accurately expressed as:

$$L\downarrow = 5.31 \times 10^{-14} T_a'^6 . \quad 52$$

Nunez (1980) applied the Swinbank equation with allowances for hilly terrain, whilst following Paltridge's (1975) practise of assuming isotropism for incoming longwave radiation and allowing an increase of $6 \text{ J m}^{-2} \text{ s}^{-1}$ per one tenth cloud cover, to write:

$$L\downarrow_c = (5.31 \times 10^{-13} T_a'^6 + 6.0n)VF + \epsilon\sigma\theta^4(1 - VF) . \quad 53$$

Finally, net longwave radiation is simply the difference arising between the incoming and outgoing components:

$$L^* = L\downarrow - L\uparrow , \quad 54$$

which over snow normally assumes a negative value through nocturnal cooling of the pack. Idso and Jackson (1969) expressed this as:

$$L^* = \sigma T_a'^4 \{ -c \exp[-d(273 - T_a')^2] \} , \quad 55$$

where the constants (c) and (d) were given the values 0.261 and 7.77×10^{-4} respectively, whilst the air temperature was in degrees Kelvin.

SENSIBLE AND LATENT HEAT 2.3

An inspection of Equation 3 reveals that two of the three most important sources of energy for melt are sensible and latent heat. The mathematics of heat transfer involved in these two terms are dependent upon turbulent theory. Three approaches to the resolution of the problems will now be discussed.

Eddy Correlation 2.3.1

Measurements of temperature and vapour pressure gradients within the millimetric boundary layers above the snow surface are exceedingly difficult, whilst Male and Gray (1981) suggest that sensible and latent heat fluxes are governed by complex turbulent exchange processes. Ignoring advection and assuming constant fluxes with height, the vertical transport of sensible and latent heat can be written (Munn, 1966):

$$Q_H = C_p \overline{\rho_a u'_N T'}, \quad 56$$

and
$$Q_E = L_v \overline{\rho_a u'_N q'}, \quad 57$$

where C_p - specific heat of air at constant pressure,
 ρ_a - density of air,
 u'_N - the fluctuating component of wind normal to the earth's surface,
 T' - the fluctuating component of temperature, T ,
 defined by the relationship, $T' = T - \bar{T}$.

L_v - latent heat of vaporization/sublimation, and
 q' - the fluctuating component of specific humidity,
 q , defined by the relationship, $q' = q - \bar{q}$.

The instruments required in eddy correlation techniques are expensive and consideration of the data thought too difficult for general application to snow hydrology. However, Hicks and Martin (1972) and McKay and Thurtell (1978) both used this approach in an endeavour to ascertain more accurate values for the turbulent exchange fluxes. Such accuracy was thought desirable before various models of the energy balance over snow (O'Neill, 1972; Outcalt et al, 1975; Anderson, 1968, 1976) could be properly tested.

The Bowen Ratio 2.3.2

The Bowen ratio approach in resolving the turbulent terms Q_H and Q_E has been previously applied in micro-meteorology because of the simplicity of the instruments required and the theory. If other terms in the energy balance, net radiation and energy available for melt are known, the residual dominant terms may be represented as (Sellers, 1965):

$$Q_H = Q_M - Q^* - Q_E, \quad 58$$

$$Q_E = Q_M - Q^* - Q_H. \quad 59$$

Assuming no advection, constancy of turbulent fluxes, and that eddy diffusivities of sensible heat (A_H) and latent heat (A_E) are equal:

$$A_H = A_E, \quad 60$$

Q_H and Q_E may now be expressed against each other in a manner known as the Bowen ratio:

$$B_r = Q_H / Q_E. \quad 61$$

This method was used by McKay and Thurtell (1978) to compare results for Q_H and Q_E arising from eddy correlation practises with those achieved through applying gradient data for temperature and vapour pressure. Under normal circumstances over snow, the melt term Q_M is difficult to measure and is therefore determined as a residual of the remaining terms (Equations 58 and 59). Because of this the Bowen ratio is not commonly used in calculating turbulent fluxes over snowmelt.

Aerodynamic Approach 2.3.3

Alternate approaches centre around the constraints of instrumentation. To overcome the problems encountered in eddy correlation techniques without resorting to the Bowen ratio, an aerodynamic approach has been applied. This assumes that the fluxes are proportional to the vertical gradients of temperature and water vapour. The relationships describing the turbulent fluxes for sensible and latent heat using this method have been expressed as (Owens, Marcus and Moore, 1984; Prowse and Owens, 1982; and Male and Granger, 1979):

$$Q_H = \rho_a C_p D_H (T_a - T_s), \quad 62$$

$$Q_E = \rho_a L_v D_E (0.622 P_a)(e_a - e_s), \quad 63$$

where D_H - bulk exchange coefficient for sensible heat,

T_a - air temperature,

T_s - snow surface temperature,

D_E - bulk exchange coefficient for latent heat,

P_a - air pressure,

e_a - vapour pressure in air, and

e_s - vapour pressure over ice.

There is general agreement (Sellers, 1965 and Anderson, 1976) that under near neutral conditions when the change of temperature with height approaches the adiabatic lapse rate:

$$D_H \approx D_E \approx D_M, \quad 64$$

where D_M , the bulk exchange coefficient for momentum can be described by:

$$D_M = (k^2 u) / [\ln(z/z_o)]^2 \quad 65$$

and k - Von Karman's constant,

u - wind speed,

z - height,

also z_o - roughness coefficient.

Under normal melt conditions either neutral or stable conditions exist where the air temperature equals or exceeds the snow surface temperature. An expression applied to describe the dampening effect of stable conditions upon turbulent exchange pursuing the work of Price (1977) as reported by Moore (1983) is:

$$D_s = D_M / (1 + a R_i). \quad 66$$

The constant (a) was given a value of approximately 10 and the Richardson number (R_i) may be approximated by (Price, 1977):

$$R_i = [g/T_a][T_a z/u^2] \quad 67$$

where g - gravitational acceleration.

This represents a mechanical energy rate for turbulent motion expressed as a ratio of free or naturally corrected buoyancy forces to forced or inertial forces. Neutral conditions are represented when $|R_i| < 0.012$ so that:

$$D_s = D_M \quad 68$$

and stable conditions when the Richardson number is positive (Rosenberg, 1974).

Central to all approaches in the estimation of turbulent exchanges is the wind profile term. For any height, the wind speed can be written in terms of the logarithm of the height and a constant (f) (Sellers, 1965; Holmgren, 1971):

$$u = f \ln (z/z_0). \quad 69$$

This relation assumes that the wind speed approaches zero at some non zero height (z_0). The constant (f) is a function of the rate of lateral momentum and the density of air so that,

$$f = (1/k) (\mathcal{T}/\rho_a)^{0.5}, \quad 70$$

where \mathcal{T} - vertical momentum;

$$\text{alternately } f = u^*/k, \quad 71$$

and u^* - friction velocity;

$$\text{finally } u = (u^*/k) \ln (z/z_0). \quad 72$$

The roughness length (z_0) may be calculated from:

$$z_0 = \exp [(u^* \ln z)/k] . \quad 73$$

For practical snow hydrology, vertical momentum (\mathcal{T}) has been considered constant with wind speed (u) at any height (z).

Expressing the bulk exchange coefficient in terms of vertical momentum:

$$D_M = (\mathcal{T}/\rho_a)(1/u), \quad 74$$

$$\text{where } \mathcal{T}/\rho_a = u^{*2} . \quad 75$$

Rearranging Equation 71 in terms of the square of the friction velocity:

$$u^{*2} = (k^2 u^2) / [\ln (z/z_0)]^2. \quad 76$$

Substituting Equation 75 into Equation 73 the bulk exchange coefficient for momentum in neutral conditions is described by (Equation 65):

$$D_M = (k^2 u) / [\ln (z/z_o)]^2 .$$

The bulk transfer coefficients have been given many values by different investigators ranging from $1.06 \times 10^{-3} \text{ kJ m}^{-3} \text{ }^\circ\text{C}^{-1}$ for D_H (Hicks and Martin, 1972) and $2.17 \times 10^{-1} \text{ kJ m}^{-3} \text{ Pa}^{-1}$ for D_E (Granger, 1977) to $15 \times 10^{-3} \text{ kJ m}^{-3} \text{ }^\circ\text{C}^{-1}$ (D_H) and $25 \times 10^{-1} \text{ kJ m}^{-3} \text{ Pa}^{-1}$ (D_E) (Gold and Williams, 1961), as reported by Male and Gray (1981).

Recently, Kondo and Yamazawa (1986) investigating the bulk transfer coefficients for drag and sensible heat over snow found only a small dependence on the friction velocity (u^*) and geometric roughness of the surface (z_o). They suggested that for all practical purposes a constant value could be assumed for the coefficients so that at a reference height of 1 metre, $D_H = 2.0 \times 10^{-3} \text{ kJ m}^{-3} \text{ }^\circ\text{C}^{-1}$ and $D_E = 2.1 \times 10^{-1} \text{ kJ m}^{-3} \text{ Pa}^{-1}$. A study of the various investigations suggests that each value remains unique to the conditions prevailing at the time, and consequently the bulk transfer coefficients should be calculated afresh for each new meteorological situation. This would involve applying Equations 65, 66 and 67 to calculate D_H and D_E using u , z and u^* .

The bulk aerodynamic models (Equations 62 and 63) discussed to date are one dimensional and do not consider the conditions when moist warm air is advected over a snow field. Advection may be said to be significant when isotherms and surface wind streamlines intersect. Treidl (1970) studied the advection of warm

air over a snow surface during a nine hour passage. He noted that the heat of air advected into the area was reduced until the temperature of the air reached 0°C . The resultant loss in the snowpack implied that the heat advected into the area was used largely for melt.

Weisman (1977) addressed this problem by creating a two dimensional model. A steady turbulent flow of moist warm air was assumed passing over flat bare homogenous ground to a flat homogenous snow surface. Net radiation was taken as constant over the snow field and minor terms in the energy balance ignored, so that only sensible and latent heat were examined for changes in space. The melt at the leading edge of the snow field was seen to decrease by one third in the first fifteen to twenty-five metres and thereafter according to the power law. However, air temperature was observed as only changing gradually and Weisman suggested that in the light of this, one dimensional measurements in the centre of a snow patch would suffice for the turbulent exchanges.

Observations in mountain areas do not usually find steady turbulent flows, flat homogenous terrain or even a fetch (200 m) adequate for measurements at a height of two metres (Sellers, 1965). Reservations should be exercised in viewing the results of the turbulent exchanges in all the models discussed under such conditions (Prowse and Owens, 1982).

Consideration of the latent heat flux should include the two possible exchanges which may occur. These are sublimation or evaporation and condensation. The former will lead to heat loss from the pack, whilst the latter needs to be considered for two

cases. Weisman's (1977) study considering warm moist air illustrated heat gained by the snow through condensation. However when condensation occurs at sub zero temperatures, a frequent event in temperate latitude snowfields, the resulting hoar frost contributes to the snowcover.

THE GROUND FLUX 2.4

The problem of accurately measuring heat flux from the ground under varying snow conditions has yet to be solved (U.S.A.C.E. 1956). For short periods of time, less than a week, the literature suggests that energy received by the snowpack from this source is insignificant (Male, 1980). This may not be so if the snowcover is shallow enough (<250 mm) to allow incoming shortwave radiation to penetrate through the snowpack to the ground. Over a season the ground flux is likely to offer a small but significant heat flux to the snowpack to assist in melt. This heat conduction is given by Male and Gray (1981) as:

$$Q_g = -h \partial T_g / \partial z , \quad 77$$

where T_g - ground temperature, and

h - thermal conductivity of soil.

Thermal conductivity values range from 0.4 to 2.1 W m⁻¹ °C⁻¹ for silt and clay soils to sand at 0.25 to 3.0 W m⁻¹ °C⁻¹ depending on density and moisture. Values of Q_g available for snowmelt over a 24 hour period have been noted as 270 kJ m⁻² d⁻¹ (U.S.A.C.E., 1956) with values as high as 860 kJ m⁻² d⁻¹ by Gold (1957) at Ottawa.

The difficulties of ascertaining heat flux and water movement under snow covered ground lie in the changing phase of the

ice/water content of the soil. Whilst under a deep snowpack conditions might be stable, under a shallow snowpack freeze/thaw conditions may exist on a daily basis (Barry, 1981).

THE FLUX OF HEAT FROM RAIN 2.5

The energy received by a snowpack from a rain on snow event can be considered for two cases:

- (i) Rainfall on a melting pack where the rain does not freeze.
- (ii) Rainfall on a pack with a temperature below 0°C where the water freezes and releases its latent heat of fusion.

The temperature for falling rain is usually taken as the wet bulb temperature and the equation offered by Male and Gray (1981) for the heat flux is:

$$Q_p = \rho_w C_{pw} (T_r - T_s) P_r / 1000, \quad 78$$

in which ρ_w - density of water,

C_{pw} - specific heat of water,

T_r - temperature of rain, and

P_r - depth of rain.

Taking the density of water as 1000 kg m^{-3} and the specific heat of water as $4.2 \text{ kJ kg}^{-1} ^{\circ}\text{C}^{-1}$, the equation reduces to:

$$Q_p = 4.2 T_r P_r . \quad 79$$

The second case is more complicated as rain falling on a freezing pack will release energy on freezing at the rate of 333.5 kJ kg^{-1} (latent heat of fusion). The temperature of the snow will rise according to the specific heat of snow, $\approx 2.1 \text{ kJ kg}^{-1}$ until melt is reached at 0°C when water will penetrate the pack.

Rain on snow events are common in mountainous areas but McKay and Thurtell (1978) did not find this term dominant. In New Zealand (and Tasmania) under warm, moist north westerly conditions Fitzharris et al (1980) suggested that under exceptional conditions, the temperature and extent of the rainfall could offer sufficient heat to dominate the energy balance for snowmelt.

INTERNAL ENERGY 2.6

When considering the energy balance over deep snowpacks, the magnitude of the internal change has been found small enough to be ignored (Treidl, 1970).

The shallow snowpack (250 mm depth) experiences diurnal cycles of melt and freeze throughout the pack. In deep snow, this only occurs in the upper layers. Each change from freeze to thaw to freeze implies a change in internal energy as phase changes occur in the water cycle. During daytime melt there is an excess of energy in the energy balance which must be lost before freezing can occur. The pack cools primarily due to longwave radiation emission at night. Again, before melt can proceed, the energy balance must indicate the excess of energy necessary for water to move freely through the pack after it has been primed for melt.

The phase changes of water through solid, liquid and vapour generate the internal energy of the pack. Male and Gray (1981) suggest:

$$Q_I = d (\rho_i C_{pi} + \rho_l C_{pl} + \rho_v C_{pv}) \cdot T_m \quad 80$$

where d - depth of snow,

ρ - density of snow,

C_p - specific heat.

T_m - mean snow temperature, and

i, l and v refer to - ice, liquid and vapour.

In the equation, if the air in the snowpack is assumed to have 100% humidity, the term for the vapour phase becomes small enough to be disregarded. In addition, during freeze cycles the liquid term goes toward zero so that the equation reduces to:

$$Q_r = d (\rho_i C_{pi}) T_m \quad 81$$

This simple expression is not easy to apply in the field. Only microwave methods in remote sensing technology are available to measure ice and free water content (Goodison et al, 1981). For more detailed work calorimetry has to be pursued which is cumbersome and slow.

Male and Granger (1979) indicate that discrepancies between observed and calculated melt in shallow packs where the energy balance is used, may be attributable to errors arising from the internal energy term.

SNOWMELT 2.7

When the energy available for snowmelt, represented by the term (Q_m) has been determined, the ensuing snowmelt may be calculated using the following expression from Male and Gray (1981):

$$M = Q_m / (\rho_i L_f B), \quad 82$$

where M - snowmelt water equivalent,

L_f - latent heat of fusion,

ρ_w - density of water, and

B - thermal quality of the fraction of ice in
a unit mass of wet snow.

The latent heat of fusion is 333.5 kJ kg^{-1} and for normal conditions the density of water is 1000 kg m^{-3} . The equation may now be reduced to:

$$M = Q_M / (3335 B). \quad 83$$

The thermal quality may be determined from:

$$B = 1 - W_f, \quad 84$$

in which W_f - free water content of a unit mass of wet snow
(expressed as a decimal).

The free water content may be between .03 and .14 although values at the lower end, .03 to .05, are more common as representative of water held by the pack against water in free drainage through the pack.

CHAPTER 3

DATA ACQUISITION

CLIMATE 3.1

Temperature and Relative Humidity 3.1.1

Wet and dry bulb thermometers manufactured by Dobbie with ranges of -30 to 50°C were used in a Stevenson screen to measure air temperatures. Dobbie maximum and minimum thermometers, model numbers 4425 and 4430 respectively, were also used. The maximum thermometer had a range between -30 and 55°C whilst the minimum thermometer was -45 to 50°C . The stated accuracy for all the thermometers by Dobbie was $\pm 0.2^{\circ}\text{C}$ and their graduations were to 0.5°C . A Dobbie HI-Q seven day thermograph was also installed in the Stevenson screen. The range of the instrument was 60°C with an accuracy of $\pm 1\%$.

The relative humidity was calculated using the dry bulb in conjunction with the wet bulb depression and standard meteorology tables (List, 1968). Temperature and relative

humidity were also measured with a Phys-Chemical model 201 sensor which gave 2 millivolt signals and was interfaced to a Campbell Scientific CR21 Micrologger. The printed board contained a PCRC-11 RH sensor which had a $\pm 1\%$ deviation error, a range of 10% to 97% and a Fenwal UUT-51J1 thermistor for temperature with a calibrated error within $\pm 0.1^\circ\text{C}$ between -35°C and 48°C .

Wind Direction and Speed 3.1.2

Wind velocities were measured using hand held instruments as well as a sensor attached to the micrologger. The hand held instrument was a Davis 'Wind Wizard' anemometer. The graduations were to 0.5 m s^{-1} with an accuracy of 0.4 m s^{-1} . The instrument was magnetically dampened and had an oscillating paddle settled on sapphire bearings with a gold plate spring balance. It was light and compact measuring only $60 \times 60 \times 20\text{ mm}$. Wind speed was also monitored using a Met One, three cup anemometer. As the cups turned, a magnet-reed switch initiated a series of pulses through the contact closure at each revolution, which was proportional to the wind speed. The range of operation was 0.5 to 60 m s^{-1} with the lower threshold at 0.5 m s^{-1} and an accuracy of $\pm 1.5\%$.

Manual estimates of wind direction were made from an intimate knowledge of local mapping and topography. Occasionally a Silva pocket compass with graduations of 10° was used to verify the direction. Data was only required to 45° (i.e. S, SW, W, etc.) of azimuth. A Met-One wind vane was used for wind direction. The vane drove a potentiometer which produced an output varying

according to the direction of the vane. It had an 0.44 m s^{-1} lower threshold with an accuracy of $\pm 5^\circ$.

Precipitation 3.1.3

Precipitation was measured using a 25 mm standard raingauge bucket for manual observations. In addition a tipping rain-gauge bucket accurate to $\pm 0.5 \text{ mm}$ was attached to the micro-logger. For each tip of the bucket, 1 mm of water was measured and a pulse initiated to the micrologger. Four snowstakes recorded snowfall in the vicinity of the Stevenson screen. They were graduated in 5 cm divisions and a vernier was used to interpolate to 1 cm.

Solar Radiation 3.1.4

Incoming solar radiation was observed with a Li-Cor 200S pyranometer which is essentially a silicon photodiode. A second similar pyranometer was installed downward facing to gain the net shortwave figure. These pyranometers were calibrated to deliver 6.55 and 6.61 $\text{mV.kW}^{-1}\text{m}^{-2}$ respectively. The net longwave radiation was also available by comparing the net shortwave result with the net allwave radiation which was measured as well. The 200S pyranometer offered a signal normally between 6 and 9 millivolts for each kilowatt per square metre of shortwave radiation energy received. Calibration was against an Eppley PSP Pyranometer with an accuracy $\pm 6\%$. The relative spectral response was in the range of 0.4 to 1.2 microns peaking at 0.95 microns and reducing to zero at either end of the range. Great care was taken to ensure that the radiation sensors in particular were level.

A Fritschen type net radiometer (Model 3030) was used for allwave net radiation, with a calibration of $5.30 \text{ mV.kW}^{-1} \text{ m}^{-2}$. The spectral response ranged between 0.3 and 60 microns with a $\pm 2\%$ accuracy against a factory standard. The emittance of a millivolt signal was in response to the temperature differences of two blackened plates with one facing up and the other down. The thermal contact between the plates was made by alternate junctions of a manganin-constantan thermopile. A protective dome of polyethylene covered each plate.

SNOW 3.2

Depth Measurements 3.2.1

Methods of ascertaining snowcover characteristics vary from remote sensing to field stakes. Remote sensing was initially considered but rejected as not suitable for the purpose. The skifield area is only 13 hectares and the combination of specific dates and necessary resolution was not available in 1981. Depth stakes are commonly used (Goodison et al, 1981) and 43 sites were chosen in the skifield area as detailed in Figure 3.1. The probe positions were fixed by attempting to encompass all types of ground including bushes, grasses, rock domes and gullies found along each ski tow. It was not possible to erect permanent stakes because of their danger to skiers. A portable depth probe was made of an old ski stock, graduated in 1 cm divisions. A 10 metre electrical conduit tube was used to sound the deepest drifts.

Positions for the depths were taken by cross bearing and transit from the ski tows. Where the surface of the snow

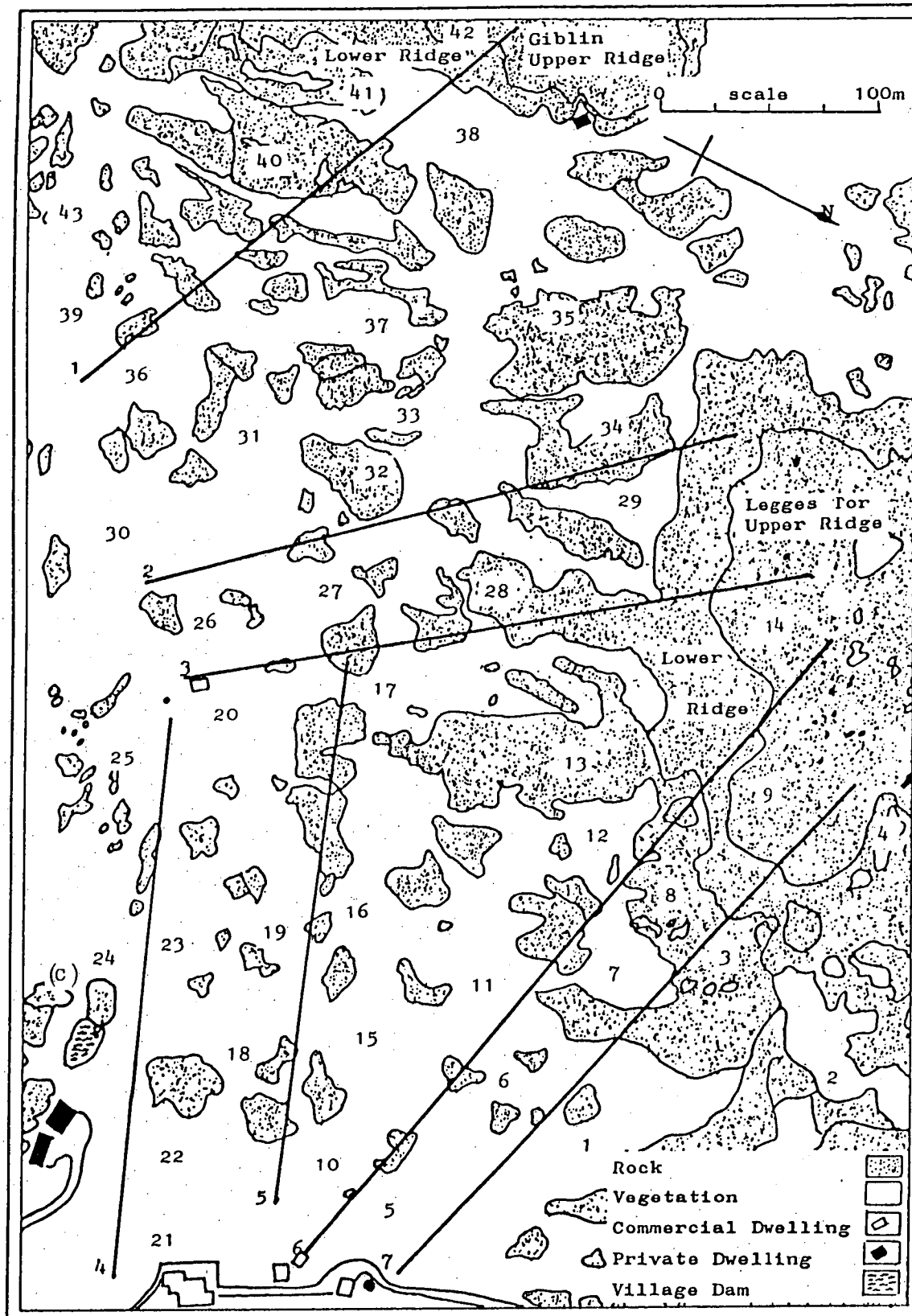


FIGURE 3.1 Snow depth and photographic sites on the Ben Lomond Ski Field.

Tows are numbered at their bases (1 - 7) whilst the photographic site is marked (C).

The snow depth sites are numbered 1 to 43 and • represents the meteorological station.

Source: Lands Department aerial map of Legges Tor, 1980.

was smooth, every attempt was made to read depths to the nearest centimetre. However, if the surface was rutted (through skiing) the depths were averaged to the nearest 5 cm for some practical solution. Various workers including Taylor (1953) and Bilello (1966) did not offer any guidelines in this area.

Areal Measurements 3.2.2

Aerial photography was initially considered for the purpose of recording the areal snowcover (Sporns, 1976) but rejected on financial and operational grounds. Instead a series of photographs was taken on the 22nd and 28th September, and 6th of October. The photographs overlapped and the site from which they were taken (Figure 3.1) encompassed a view of the entire skifield from an outcrop of rock facing the skifield slopes. Strip pictures of the total skifield were composed by putting the photographs together. Data from the photographs were supported by fieldwork observations and measurements.

Mapping and Snowcover 3.2.3

The first maps for this study were constructed on the base of the excellent aerial survey by the Department of Lands on 12th of April, 1980. The primary details required were the tow positions and ground cover, in particular dolerite domes. Legges Tor was used as a survey point.

The aerial photograph was enlarged using a photocopier until a scale of 1:1500 was achieved. The copy was used as a base to draw the maps of the skifield area in terms of

groundcover. Details of flora were omitted from the maps showing snowmelt patterns for the sake of clarity.

Data from areal and depth studies of the snowcover for each of the three days in 1981 mentioned earlier in this chapter, were mapped on perspex overlay sheets superimposed on the 1:1500 maps. These were then reduced to a format suitable for A4 presentation.

The tow built in 1985 (Bill's) was not included in the aerial photograph or the mapping of the snowcover. However, it was marked on the descriptive maps of the area (Figures 1.3 and 1.4).

Snow Density 3.2.4

Apparatus for measuring the density of snow was made according to ideas from Seligman (1936), the U.S. Army Corps of Engineers (1956) and Kojima (1966). Two portable scales were used depending on the distance involved in field work. A Salter 200 gm spring scale with 2 g graduations was portable and accurate (± 2 g) when checked in the laboratory. A small Ohaus electronic balance (C200) was also used with a readout to 0.1 g and a range of 254 g. Laboratory checks indicated a field accuracy of ± 0.1 g.

Two 100 cm³ tubes were used to collect snow samples for weighing. The first, an aluminium tube of bore 25 mm and wall 1 mm, cut very well through denser snow but did not perform well with new snow. Under these circumstances a density tube was cut from a section of plastic plumbing pipe of bore 35 mm and wall 3 mm. Each tube had one end serrated

for better penetration of the snowpack. Special cradles were made to allow easy handling of the tubes when weighing in slippery alpine conditions.

The appropriate tube was screwed into the snow, the ends guillotined off and the contents weighed. A direct measurement of the density of the snow was possible with an accuracy of $\pm 20 \text{ kg m}^{-3}$.

The inside of the tubes was sprayed with a hydrophobic agent and polished to assist in a clean sample of snow being taken, in particular in new, damp snow which has a putty-like character and is made sticky by the crystal shape.

Albedo 3.2.5

The albedo of snow was calculated using the formula from chapter 2: $\alpha = K\uparrow/K\downarrow$ (42.). The values were obtained from two Li-Cor 200S pyranometers described in the solar radiation section of 3.1, one of which was mounted facing upward for the incoming shortwave radiation and one facing down for the reflected component.

Temperature 3.2.6

Snow as well as soil and groundcover temperatures were taken with a Kane-May model 3002 thermocouple probe which had a range from -50°C to 200°C . The accuracy of the instrument was stated as $\pm 0.02^{\circ}\text{C}$ and a digital reading was possible to 0.1°C . The probe length was 30 cm and the instrument was battery powered. The instrument was checked at 0°C each week in an ice bath in the Australian Maritime College laboratory.

Free Water Content 3.2.7

Kojima (1966) indicated that using calorimetry to determine free water content was the most accurate method. It is limited in application to large areas but thought suitable for this small study. Ordinary thermos calorimetry was used and details are shown in Appendix 4. The instruments for calorimetry included the density tube, thermocouple and electronic scale described previously in this chapter. The calorimeter was a wide necked 750 ml thermos flask and a portable 'Gaz' stove heated the water.

ASSEMBLAGE OF DATA 3.3

Instrument Location and Height 3.3.1

A meteorological station comprising the Stevenson screen contents and raingauge had been established by National Parks and Wildlife personnel prior to 1981. It was north of the Day hut and east of the foot of tow number 7, at an altitude of 1460 metres. The automatic weather station, which comprised a Campbell Scientific CR21 micrologger and several meteorological sensors mounted on a galvanized iron mast, was sited within five metres of the meteorological station. Their combined position is marked on Figure 3.1. All air temperatures were taken at a height above the ground of 1.2 metres. The wind vane and anemometers on the micrologger were at a height of 3 metres as were the sensors for solar radiation.

Duration and Frequency of Observations 3.3.2

Records have been kept constantly during the winter months on Ben Lomond from the 1st of June to the 30th of October each year during the period 1981 to 1986 inclusive. The frequency of observations taken manually, which were in accordance with the Bureau of Meteorology (1984) guidelines, are recorded in table 3.1. Data recorded automatically were logged every ten seconds.

Table 3.1 FREQUENCY OF MANUAL OBSERVATIONS

Observation	Frequency
Wet bulb temperature	9 a.m. 3 p.m.
Dry bulb temperature	9 a.m. 3 p.m.
Relative humidity	9 a.m. 3 p.m.
Wind direction	9 a.m. 3 p.m.
Wind speed	9 a.m. 3 p.m.
Precipitation	9 a.m. 3 p.m.
Cloud	9 a.m. 3 p.m.
Maximum daily temperature	3 p.m.
Minimum daily temperature	3 p.m.
Rainfall	3 p.m.
Snowfall	3 p.m.
Thermograph air temperatures	Every 7 days

The records of all manual observations persisted throughout the six year period from 1981 to 1986. However, the duration of records for solar and allwave radiation was only possible after the micrologger system was installed in 1983, summarized in Table 3.2.

On days selected for energy balance modelling, a temperature profile of a vertical column extending from 30 cm below ground level to 1 metre above the snow surface (Table 3.3) was taken every 3 hours. In addition at least two sets of measurements of snow albedo, density and free water content were made near the meteorological station.

Table 3.2 DURATION OF RECORDS

	1981	1982	1983	1984	1985	1986
Manual records						
Automatic records						
Global radiation						
Net shortwave radiation						
Net allwave radiation						

A summary of the duration of records of meteorological data.

Table 3.3 TEMPERATURE PROFILE

Medium	Depth/Height	
Air	1 metre	above the snow surface
Air	1 cm	above the snow surface
Snow	1 cm	below the snow surface
Snow	1 cm	above the ground
Ground	1 cm	below the ground
Ground	30 cm	below the ground

A description of the relative heights and depths of the temperature observations in a column of air, snow and soil, after Sellers (1965).

Difficulties 3.3.3

The problems experienced with the riming of instruments have been reported since last century (Buchan, 1890) by observers in alpine meteorology. Snowfall and heavy frosts on Ben Lomond have caused the Stevenson screen and automatic weather station to become covered in ice many centimetres thick. Rainfall monitoring was so badly affected by icing that no reliable records are available for the period 1981 to 1986. Poor data arising from other instruments icing up was not included in the climate summary given in Chapter One.

A further problem with the net radiometer was internal condensation. This was reduced to some extent by silica gel on the intake tube. Blown air or a heating ring could not be used due to lack of power and restricted access prevented the use of compressed air bottles.

The automatic weather station was completely out of action for two days in 1985 due to vandalization; however, records were retrieved intact for the preceeding period. During severe spells of cold weather, the cassette tape used for permanent record storage with the CR21 micrologger became a poor receptor and data retrieval was a delicate matter. It was suggested by technicians at the Australian Maritime College that this was possibly due to a change in tape stretch.

Processing 3.3.4

Vapour pressure was not measured directly but calculated from air temperature and relative humidity using the formulae

detailed in Appendix 4 . Atmospheric pressure was extrapolated from readings taken at the Australian Maritime College meteorological station (altitude 40 m). A rate of reduction in pressure due to altitude was realized after 50 trials yielded a mean of $1140 \text{ Pa } 100 \text{ m}^{-1}$ with a standard deviation of $\pm 30 \text{ Pa}$.

No compaction rate was allowed for in the spring snow depth measurements. Commonly fresh snow has a density less than 200 kg m^{-3} . As the snow ages and metamorphosis occurs, the pack compacts and density can increase over several days to around 400 kg m^{-3} (Bilello, 1966). Spring snowfall on Ben Lomond is uncommonly wet and dense with readings within 24 hours of snowfall varying between 380 and 440 kg m^{-3} . Measurements of snow density in 1981 did not show any more densification during the three weeks of snow melt observed and therefore no compaction of the snowpack.

The CR21 micrologger in the automatic weather station scanned the sensors every 10 seconds, logging the data and eventually processing it in a variety of programmes detailed in Appendix 4 . A suite of input programmes converted the signals received from the sensors to engineering units, e.g. mV to W m^{-2} . The readout was to the fourth decimal place, often implying a greater accuracy than the sensors could deliver.

Output programmes were written for hourly, six hourly and daily analysis. Data processed for the hourly input was intended for use in the energy balance equation for snowmelt whilst the six hourly programme was written primarily for the purposes of snowmaking so that factors of temperature,

relative humidity and wind were of importance. The daily analysis for meteorological records included maximum and minimum air temperatures in addition to total precipitation and other averages described in the programme outline in Appendix 4.

The study of the climate of Ben Lomond incorporated both manual and automatic records for temperature, wind, precipitation and fallen snow data between 1981 and 1985.

Temporal and spatial investigations applying the energy balance to snowmelt were pursued in 1985 and 1986 following the installation of a net allwave radiation sensor linked to the micrologger. Automatic records were the primary data source whilst manual records were searched for data pertaining to cloud, precipitation, fallen snow and thermal soil regimes. Net radiation data was applied directly to temporal analysis whereas spatial variations required both upward and downward shortwave radiation data as well.

Initial observations in spatial variability in snowmelt commenced in 1981 and concluded in 1986, although the main study was in 1981. These observations were confined to fallen snow and called on manual records for data in areal and depth analysis as well as free water content, density and crystal characteristics.

CHAPTER 4

RESULTS

TEMPORAL VARIABILITY 4.1

Introduction 4.1.1

The energy available for snowmelt was calculated using the energy balance approach which required meteorological data. The model used for calculation is detailed, followed by the application to four common synoptic regimes. Finally a time series was constructed so that an investigation of the daily values for the dominant components of the energy budget for the winter months could be made. In addition, the calculated daily melt was set against selected weather parameters for analysis.

Calculation of the Heat Balance 4.1.2

As detailed in Equation 2, the energy budget for the melting snow can be described as

$$Q_M = Q^* + Q_H + Q_E + Q_G + Q_P + Q_r$$

Daily values for each of the above terms were either

measured or calculated from daily meteorological data.

Q_p , Q_a and Q_r are shown to contribute less than 6% of Q_m in the heat balance of the four common synoptic regimes (section 4.1.3). Therefore, they were not included in the estimation of the energy balance time series.

(a) Net radiation: This was measured directly using the Fritschen type net radiometer which was described in Chapter 3. Hourly averages from the Campbell system CR21 micrologger were summed to yield a 24 hour daily value.

(b) Sensible and latent heat fluxes: Bulk aerodynamic formulae were used for both sensible and latent heat fluxes. Applying Equation 62, calculations for the former were expressed as

$$Q_H = \rho_a C_p D_H (T_a - T_s).$$

Values for the density of air (ρ_a) were taken from standard meteorological tables (List, 1968) whilst the specific heat of air at constant pressure (C_p) was given a value of $1 \text{ kJ kg}^{-1} \text{ K}^{-1}$. A mean air temperature (T_a) was obtained as the average of a 24 hour value from the thermistor linked to the micrologger. The snow surface temperature (T_s) was taken as 0°C under melt conditions (U.S.A.C.E., 1956). However, under freeze day conditions (see Chapter 1) the mean daily snow surface temperatures were measured and applied in the above relationships.

The latent heat flux was described using Equation 63 where

$$Q_E = \rho_a L_v D_E (0.622 P_a)(e_a - e_s).$$

The latent heat of vaporization of water (L_v) was taken as 2500 kJ kg^{-1} for melt conditions while the vapour pressure

at the snow air interface (e_s) was established by assuming that the air in contact with the snow was saturated. The standard meteorological tables for saturated vapour pressure over ice (List, 1968) were then consulted to obtain a value of 6.1 hPa when the temperature at the interface was zero. The vapour pressure of air (e_a) was computed from the hourly average air temperature and relative humidity and summed for the day as described in Chapter 3. The air pressure (P_a) was a 24 hour mean figure extrapolated from readings at the Australian Maritime College (Chapter 3).

The exchange coefficient varied according to atmospheric stability so that applying Equations 64 and 65 under neutral conditions (Prowse and Owens, 1982; Sellers, 1965):

$$D_H \approx D_E \approx D_M$$

$$\text{and } D_M = (k^2 u) / [\ln (z/z_0)]^2.$$

Von Karman's constant (k) was taken as 0.4 (Businger, 1973) and the height (z) at which the wind speed was read was 1.2 m. The roughness parameter (z_0) accepted was 2.5×10^{-3} m (Sverdrup, 1936) whilst the wind speed (u) was calculated as a 24 hour average from Li-Cor cup anemometer measurements (Chapter 3).

When a normal melt situation prevails, the air temperature exceeds the snow temperature and stable conditions exist (Barry, 1981). The stability adjustment to the exchange coefficient was given as a function of the Richardson number described by Moore (1983) and Price (1977) in Equation 66 as

$$D_s = D_M / (1 + aR_i)$$

Under unstable conditions the transfer coefficients were calculated from

$$D_v = D_m / (1 - aR_i) \quad 85$$

where the constant (a) was given a value of 10 (Price and Dunne, 1976) and the Richardson number (R_i) was described (Equation 67) by

$$R_i = [g/T_a(^{\circ}\text{K})] \cdot [T_a(^{\circ}\text{C}) z/u^2].$$

(c) The ground heat flux: Calculations for heat conduction from the ground used the expression from (Equation 77):

$$Q_g = -h \Delta T_g / \Delta z$$

where the thermal conductivity of the soil (h) was taken as $1.2 \text{ W m}^{-1} \text{ }^{\circ}\text{C}^{-1}$ (U.S.A.C.E., 1956). Temperatures were measured at the meteorological station at depths that were 1 cm and 30 cm below the ground surface. Measurements were averaged every other day during July, August and September between 1983 and 1985 with observations taken every 4 hours.

Observations showed that the ground was frozen under snow at night during the study period. It was not possible to insert the probe under such conditions and therefore it was assumed that the heat flux to the snow was negligible. Similar results were assumed when the pack was below zero since the ground was nearly always frozen under such circumstances. Neglecting this term under these conditions was felt justified since it has been shown (Table 4.2) that even under strong melt conditions the soil heat flux did not exceed 1% of the total melt energy.

(d) The flux of heat from rain: The energy received by a

snowpack from a rain on snow event was only considered for the situation when rain was falling on a melting pack and freezing did not occur. Equation 78 describing the heat flux is:

$$Q_p = \rho_l C_{pl} (T_r - T_s) P_r / 1000.$$

The density of water (ρ_l) was taken as 1000 kg m^{-3} and the heat capacity (C_{pl}) to be $4.2 \text{ kJ kg}^{-1} \text{ }^\circ\text{C}^{-1}$. Now taking the temperature of rain as the wet bulb temperature (T_r) (Fitzharris et al, 1980) and expressing it in $^\circ\text{C}$, whilst keeping the snow surface temperature (T_s) at 0°C and expressing the daily aggregate rainfall in mm, Equation 79 is:

$$Q_p = 4.2 T_r P_r.$$

(e) Internal energy: Under non freezing conditions the exchange of energy due to water phase changes within the pack (Equation 80) is:

$$Q_i = d (\rho_i C_{pi} + \rho_l C_{pl} + \rho_v C_{pv}) T_m.$$

This investigation considered the melting snowpack when the mean internal temperature (T_m) was taken as near zero (Male and Gray, 1981) and the pack primed for melt. Under these circumstances, if the air in the snowpack was assumed to have 100% humidity, the vapour phase ($\rho_v C_{pv}$) became small enough to disregard. With the liquid term ($\rho_l C_{pl}$) at zero, the expression reduced to only consider snow depth melt loss (d) in metres, against the temperature and ice term ($\rho_i C_{pi}$) so that (Equation 81) became:

$$Q = d (\rho_i C_{pi}) T_m,$$

where the specific heat of ice (C_{pi}) was taken as

$2.115 + 0.00779T$ kJ kg⁻¹ and snow density (ρ_s) measured with the snow density tube described in Chapter 3 had a mean value of 380 kg m⁻³.

Synoptic Weather Regimes 4.1.3

Light (1941) addressed the problem of predicting high melt rates in snow from specific meteorological events. Factors of high air temperature, humidity and wind velocity were all deemed important, and the situation when warm moist air was advected over the snowfield investigated. Triedl (1970) and Weisman (1977) looked at similar synoptic events whilst McKay and Thurtell (1978) compared advection of warm dry air with a stable air mass for snowmelt terms that dominated the energy balance.

Prowse and Owens (1982) and Moore and Owens (1983) were involved with smaller snow fields in New Zealand and noted the effects of regional advection when winds exceeded 5 m s⁻¹ against advection induced by heating of local valleys when winds were less than 5 m s⁻¹.

High snowmelt had been observed on Ben Lomond, when north west winds advected warm air into the region under both cloudy and clear conditions (Figures 4.1a and 4.1b).

Excessive snowmelt had also been found when a warm airmass with a small pressure gradient prevailed, particularly when accompanied by local advective conditions (Figures 4.1c and 4.1d).

From the above discussion it was decided to partition the synoptic events into four dominant types as they would affect

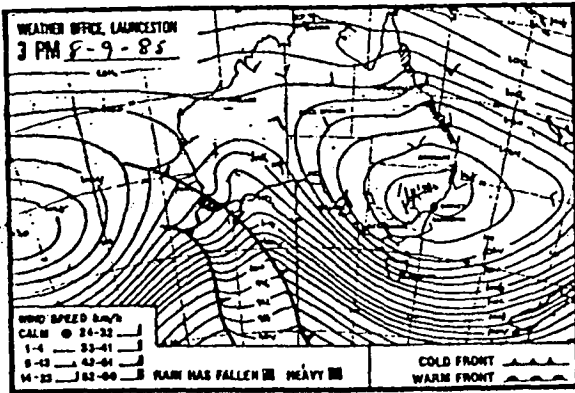


FIGURE 4.1a

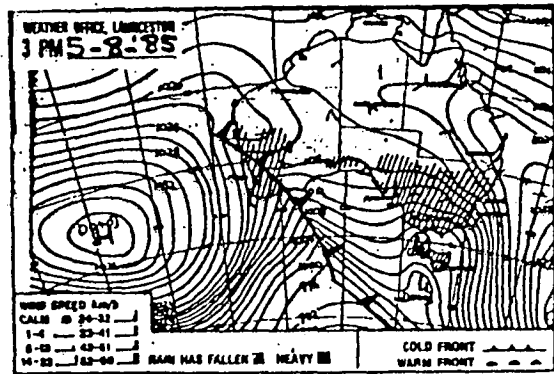


FIGURE 4.1b

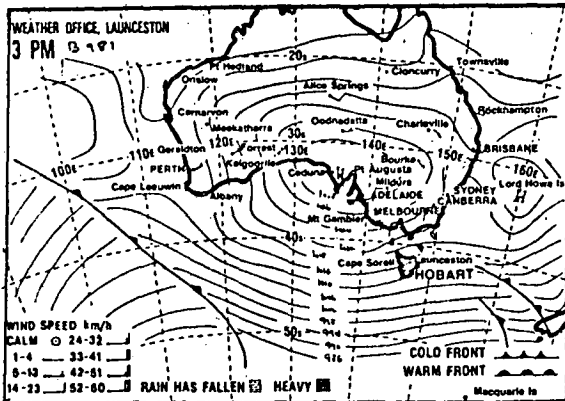


FIGURE 4.1c

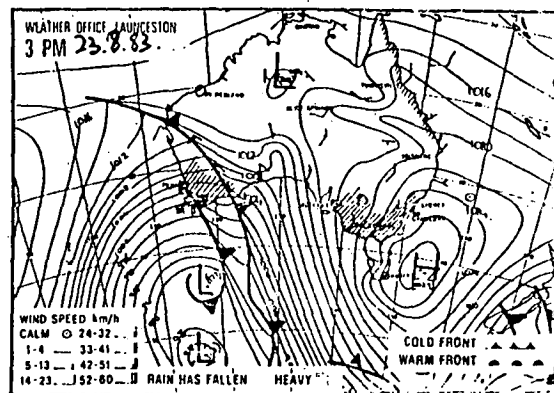


FIGURE 4.1d

FIGURE 4.1 Synoptic situations representative of the events described in section 4.1.3.

The synoptic charts are published with the kind permission of the Examiner, Launceston.

melt. Furthermore it was assumed that a particular weather type would persist for the entire day. Table 4.1 lists the four categories considered. All have been denoted as 'warm', that is with a mean air temperature greater than the monthly mean. 9am and 3pm cloud observations were used to define the days as cloudy or clear. In actual fact, in this mountain environment, days denoted as cloudy were nearly always overcast, with mountain cloud or uphill fog dominating. Clear days were typically less than one tenth cloud cover. A threshold mean daily wind speed of 5 m s^{-1} was used to separate regional from local advection.

The daily energy balance (Equation 2) was resolved for the horizontal snow surface at the meteorological station and the results of 5 days of selected observations averaged for the mean day for each selected meteorological situation. Event 1 was typical of light wind conditions dominated by a high pressure region over the north east of the state (Figure 4.1c). Under such conditions, net radiation was by far the dominating melting agent, followed by sensible heat and with a very small component from latent heat (Table 4.1).

It may be observed that net radiation for events 1 and 2 differ by approximately 10%. Inspection of incoming global radiation for these same days revealed a difference of 90% ($4.2 \text{ MJ m}^{-2} \text{ d}^{-1}$ to $0.4 \text{ MJ m}^{-2} \text{ d}^{-1}$). The variability in these differences may be partially attributed to an increase in longwave radiation which according to Paltridge (1975) is $6 \text{ J m}^{-2} \text{ s}^{-1}$ per tenth cloud cover.

Similar meteorological conditions existed for event 2. However, whereas clear skies prevailed for the former,

TABLE 4.1

DAILY ENERGY FLUX TRANSFER

Event	Q^*	Q_H	Q_E	Q_P	Q_G	Q_z	Q_n
1	4.2194	1.2107	0.0520	—	0.0180	0.072	5.5931
2	3.7979	1.5224	-0.1935	0.134	0.0660	—	5.3268
3	4.7118	5.8342	-1.1843	—	0.0370	0.114	9.5127
4	3.1969	3.9533	1.1914	0.194	0.0770	—	8.5356

Mean daily values ($\text{MJ m}^{-2} \text{d}^{-1}$) of energy flux transfers for selected synoptic events during snowmelt on Ben Lomond where the events were:

1. Warm and sunny with local advection and winds $< 5 \text{ m s}^{-1}$.
2. Warm and cloudy with local advection and winds $< 5 \text{ m s}^{-1}$.
3. Warm and sunny with regional advective conditions and winds $> 5 \text{ m s}^{-1}$.
4. Warm and cloudy with regional advective conditions and winds $> 5 \text{ m s}^{-1}$.

TABLE 4.2

DAILY ENERGY FLUX TRANSFER

Event	Q^*	Q_H	Q_E	Q_P	Q_G	Q_z
1	75	22	1	0	1	1
2	71	28	-4	3	1	/
3	50	61	-12	/	0	1
4	37	46	14	2	1	/

Mean daily values of energy flux transfers expressed in percentage, where each term was rounded to the nearest percent.

cloudy skies marked the latter event (Figure 4.1d). Although there was a decrease in heat supplied by net radiation for snowmelt, the term still dominated over sensible heat which was found again to supply a significant amount of energy (Table 4.2). Whilst some rainfall was experienced, the heat supply was less than latent or sensible heat with heat from the ground providing only 1% towards melt. The internal energy which was a very small component in event 1, was not measured. The majority of events 1 and 2 occurred in September when local advection due to the decreased boundaries of the snow field and increased heat budget in the surrounding countryside assumed mounting importance.

Event 3 was marked by warm dry north westerly winds brought down from the continent marking the trailing edge of a high pressure region (Figure 4.1a). Under clear skies, this was one of two situations where sensible heat was found to exceed net radiation, whilst latent heat indicated a significant cooling of the pack through evaporation (Table 4.1).

The warm and cloudy conditions associated with moist north westerly air being advected into the region as a front passed through was again marked by sensible heat being more important than net radiation for snowmelt in event 4. The heat received by the pack through condensation in the latent heat term exceeded the other 3 events investigated (Figure 4.1b) whilst the flux of heat from rain was again of minor importance.

Net radiation provided most energy for melt under warm local conditions, whilst sensible heat dominated when

regional advection was associated with warm north westerly air. Latent heat was seen to play a small but significant role in the energy budget whilst the remaining terms representing heat from the ground, rainfall or internal energy were regarded as of only minor importance. Days when the highest melt rates were observed occurred under regional advective conditions when net radiation and sensible heat provided between 80% and 90% of the total energy available for melt.

Time Series 4.1.4

The three most important sources of heat for snowmelt have been reported as net radiation, sensible and latent heat (Male, 1980; Owens, Marcus and Moore, 1984; and Aguado, 1985). Similar results have been found in this study, with heat from the remaining terms (the ground, rain and internal energy) providing less than 6% of the total flux on average. The energy balance was reduced to three terms so that

$$Q_M = Q^* + Q_H + Q_E \quad . \quad 86$$

The daily totals were investigated for July, August and September 1986, these being the months when sustained snowcover was most likely found on Ben Lomond. Only intermittent snowcover was recorded during June and October. The results were then plotted for each month (Figures 4.2, 4.3 and 4.4).

Snowmelt was calculated from the total energy flux using (Equations 82 and 83):

$$M = Q_M / 3335B,$$

where $B = 1 - W_f$.

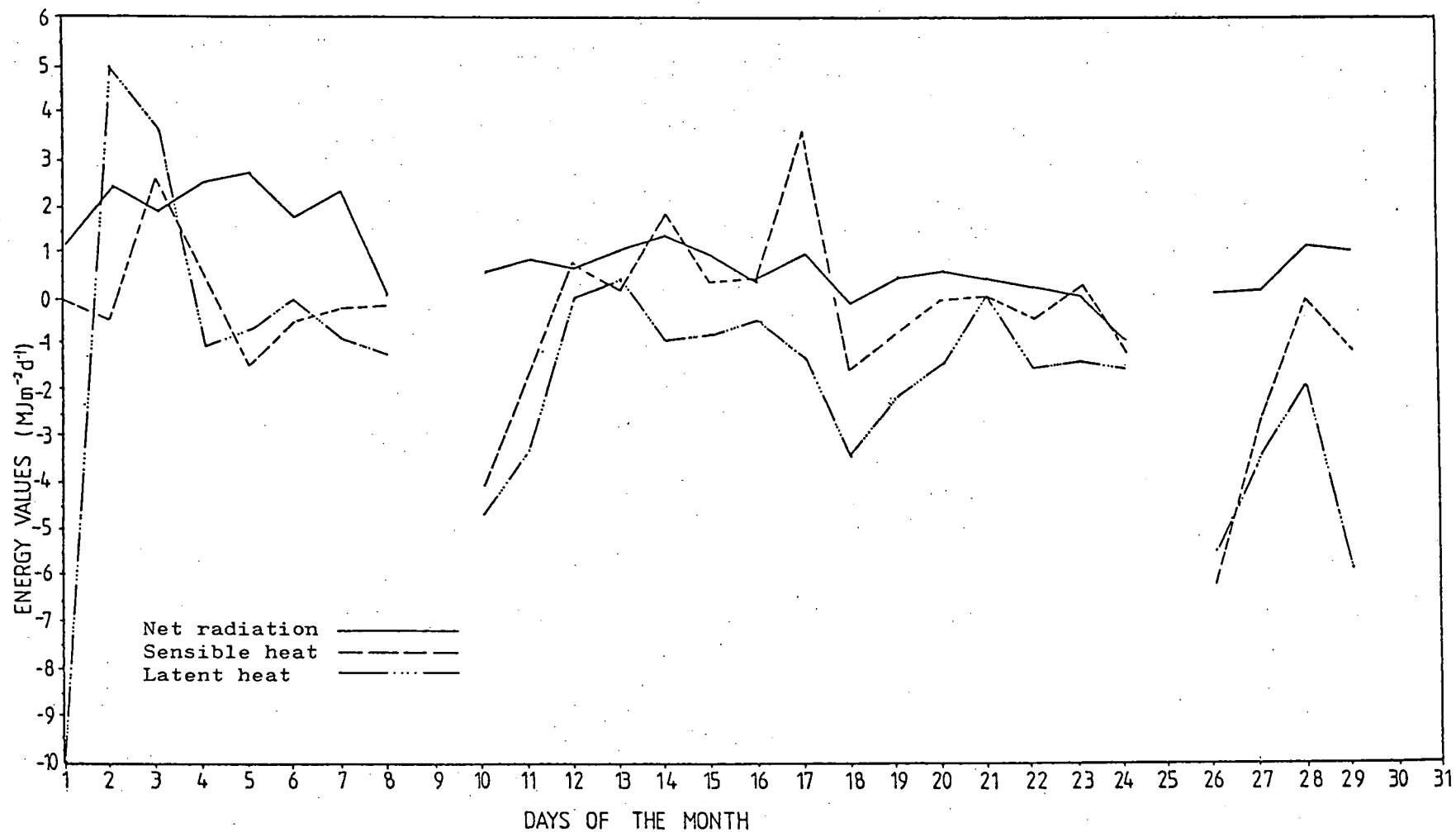


FIGURE 4.2 Mean daily values for the three dominant components of the energy balance over snow on Ben Lomond for July, 1986. Some data were omitted due to instrument malfunction.

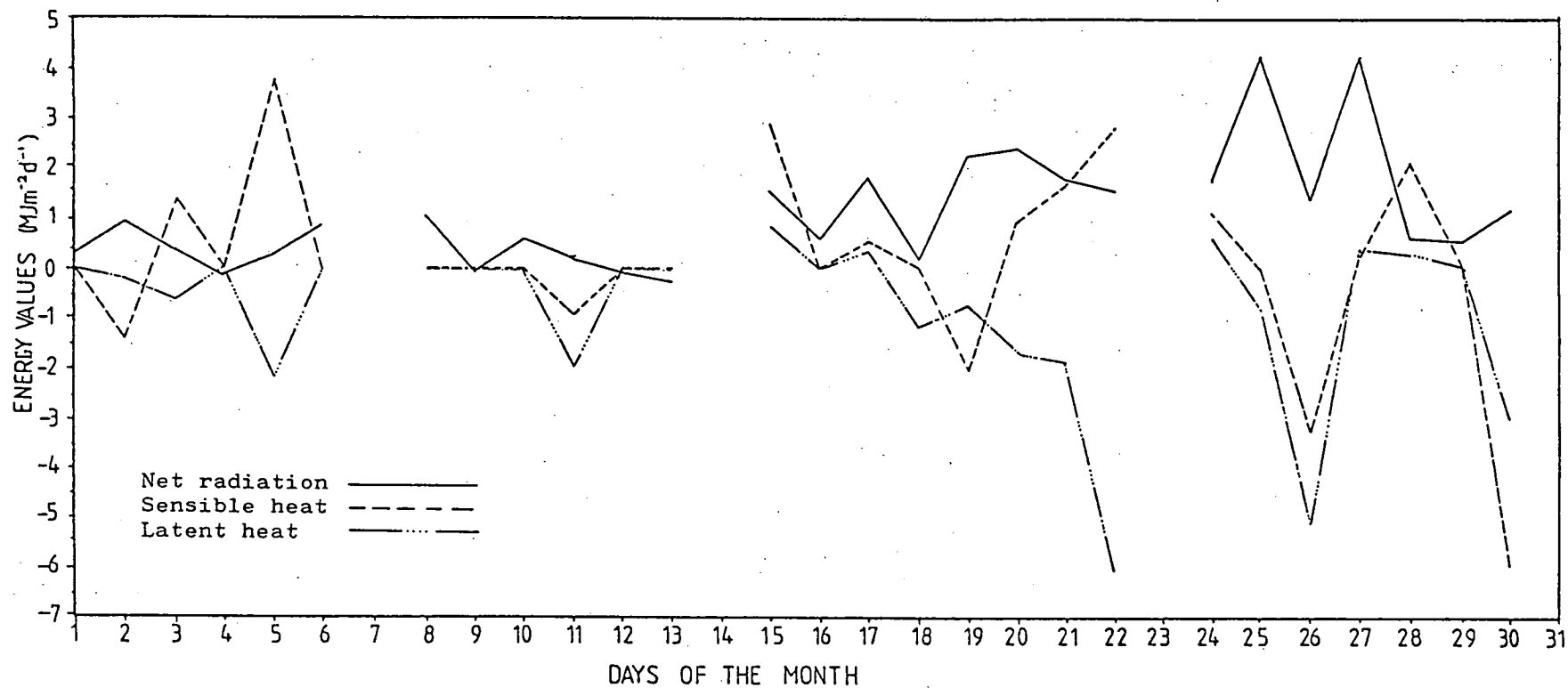


FIGURE 4.3 Mean daily values for the three dominant components of the energy balance over snow on Ben Lomond for August, 1986. Some data were omitted due to instrument malfunction.

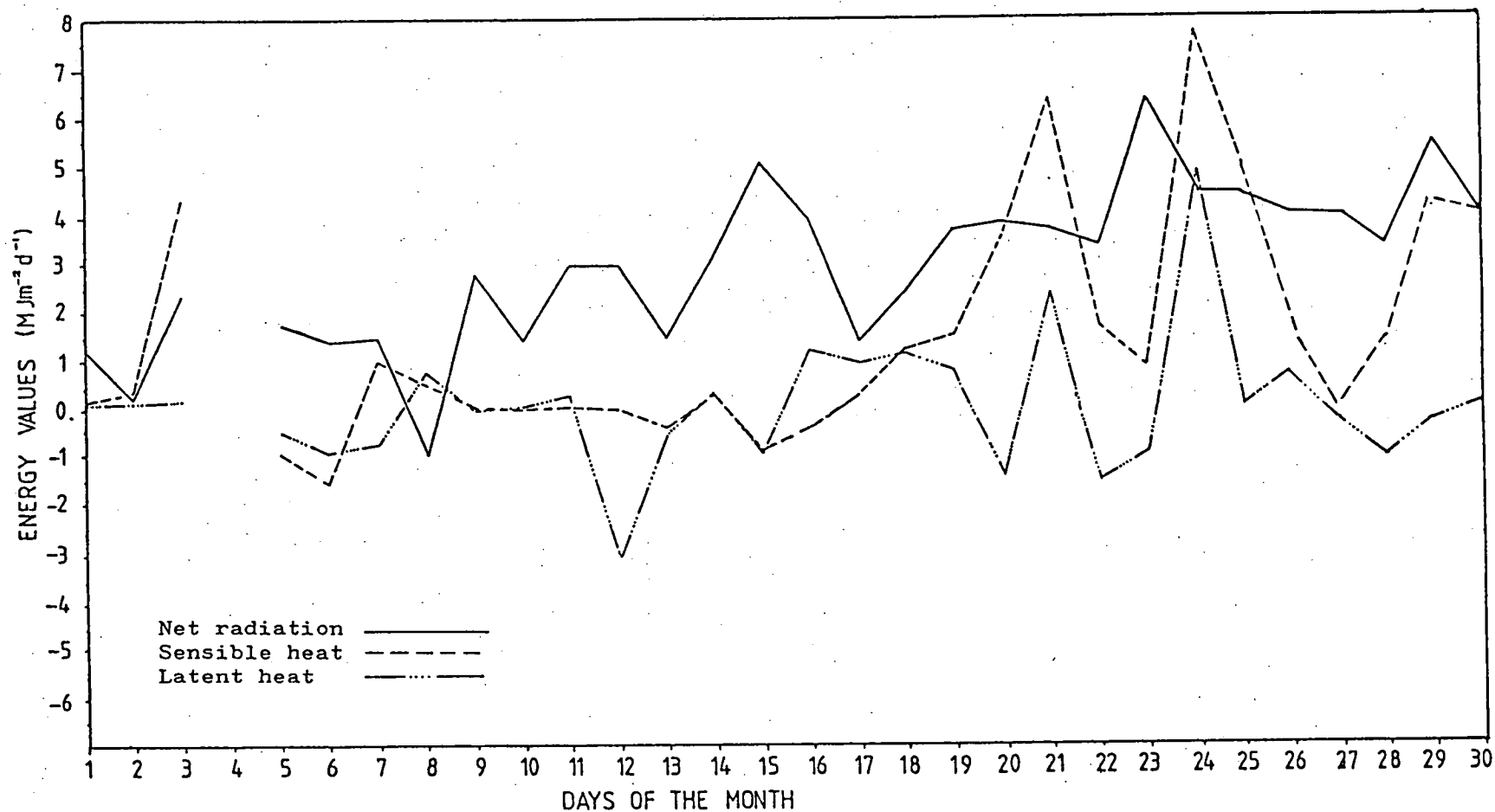


FIGURE 4.4 Mean daily values for the three dominant components of the energy balance over snow on Ben Lomond for the month of September, 1986. Some data were omitted due to instrument malfunction.

The snow on Ben Lomond was typically dense and wet with values for the free water content being between 0.04 and 0.14. The two meteorological parameters which were selected for analysis with snowmelt were the mean daily temperature and wind direction. Seligman (1936), U.S.A.C.E. (1956), Male and Gray (1981) and many other workers in the field have indicated the importance of air temperature to snowmelt whilst discussions in the previous section have highlighted the part that wind direction had to play in estimating snowmelt. Daily mean values were graphed and displayed over a monthly time scale (Figures 4.5, 4.6 and 4.7).

High melt days were chosen as those exceeding 15 mm d^{-1} arising from the sum of the seasonal daily mean of 104 mm d^{-1} and the half standard deviation. It was these days that were of particular interest although all days for which data were available were plotted including those upon which no melt occurred.

Missing data in Figures 4.2, 4.3 and 4.4 represent a malfunction of the micrologger. Zero ablation in Figures 4.5, 4.6 and 4.7 is related to conditions where the energy available for melt (Equation 86) indicated a heat loss by the snowpack. Stars represent days when energy values were missing.

A barely discernible pattern was found apparent for all terms with values decreasing towards zero from the first week in July and then unsteadily increasing from the last week in August. Net radiation continued to decrease throughout July despite the fact that the shortest solar radiation was the

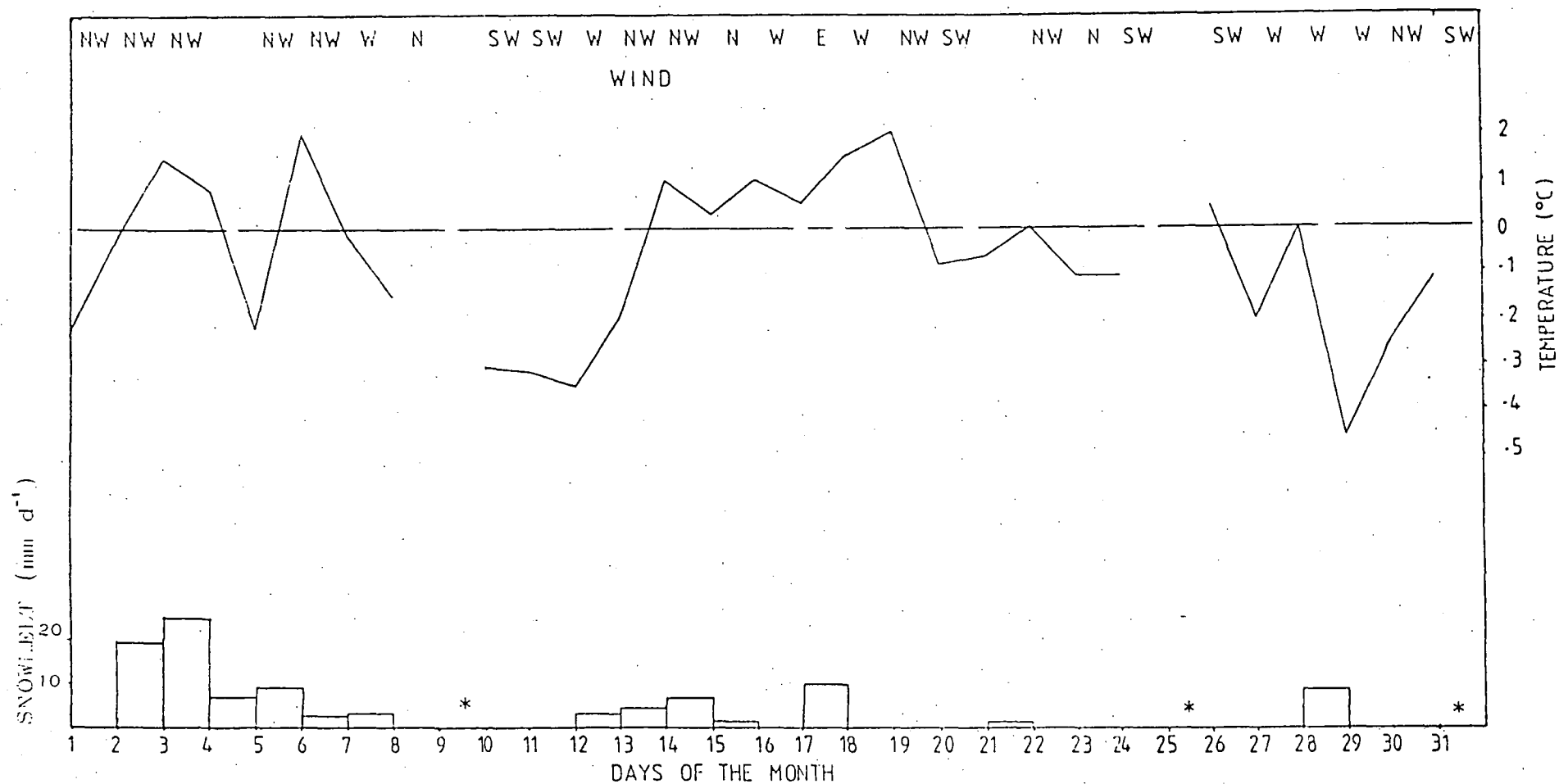


FIGURE 4.5 Mean daily values for the wind direction and air temperatures as well as snowmelt calculated from the energy balance at the meteorological station on Ben Lomond for July, 1986. Stars represent days for which micrologger data were missing.

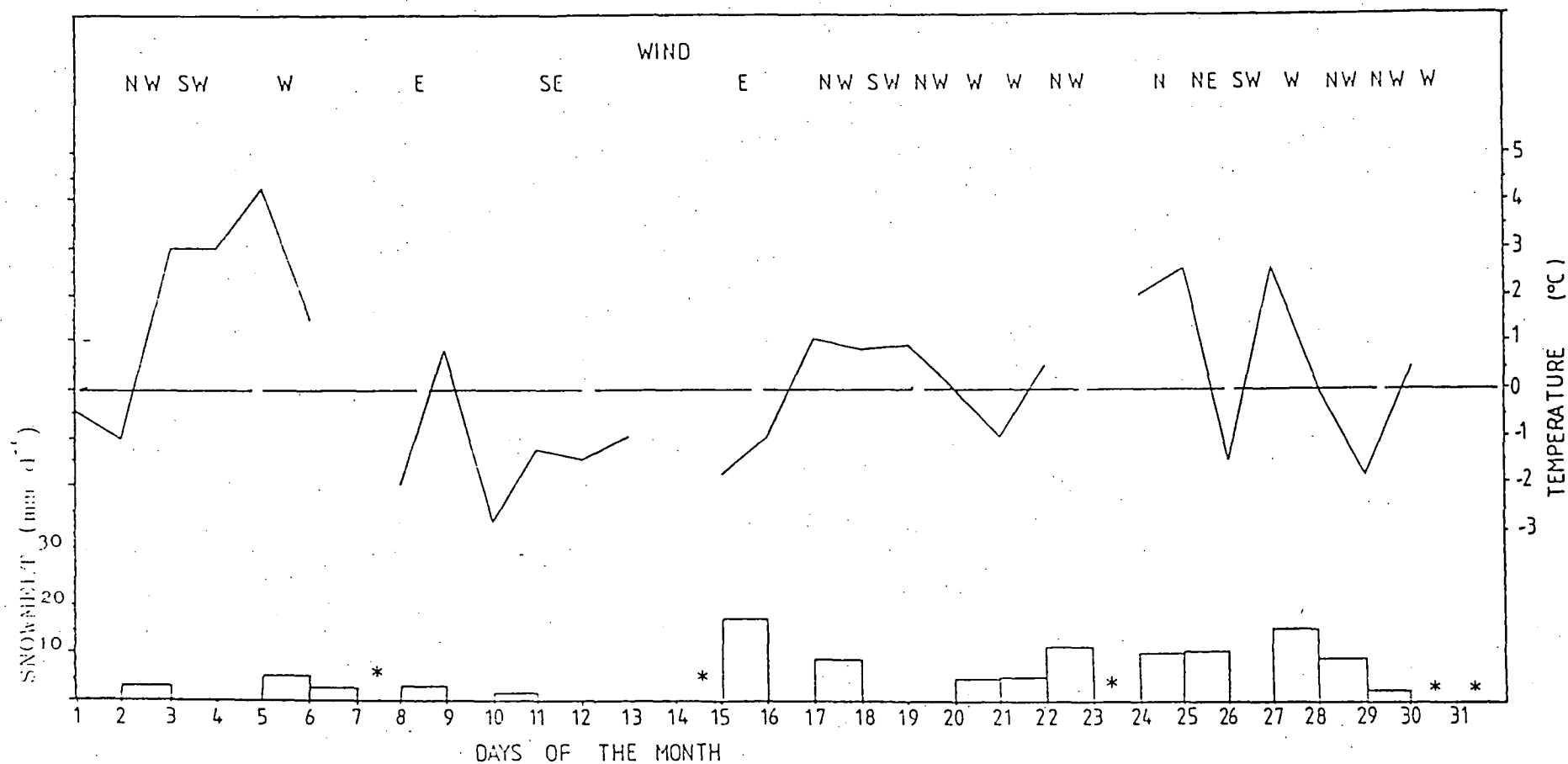


FIGURE 4.6 Mean daily values for the wind direction and air temperatures as well as snowmelt calculated from the energy balance at the meteorological station on Ben Lomond for August, 1986. Stars represent days for which micrologger data were missing.

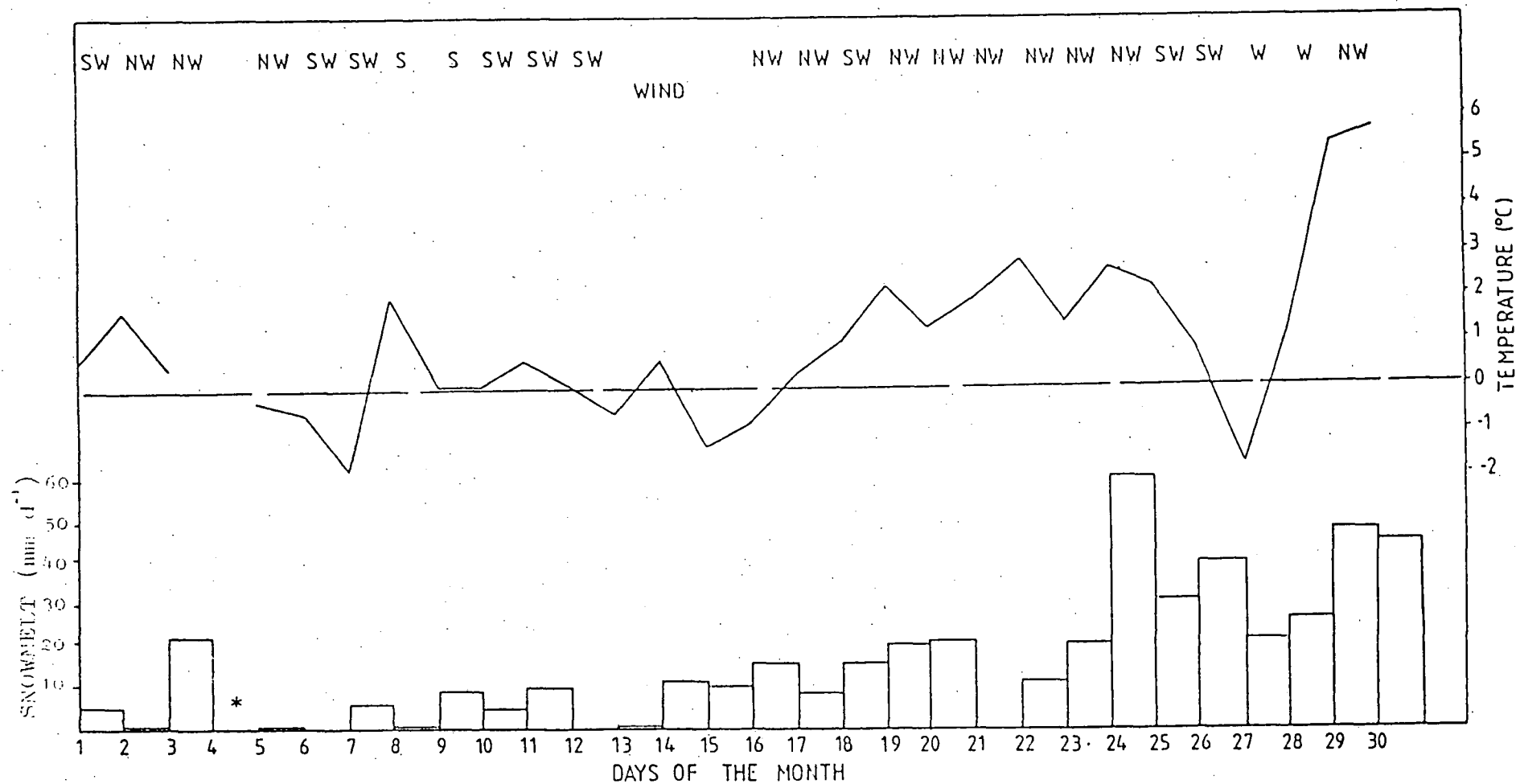


FIGURE 4.7 Mean daily values for the wind direction and air temperatures as well as snowmelt calculated from the energy balance at the meteorological station on Ben Lomond for September, 1986. Stars represent days for which micrologger data were missing.

21st of June. This decrease is undoubtedly due to increased cloud cover which arises as a function of the weakening and northward movement of the sub-tropical high pressure ridge, centred in summer around 40° south. This change is accompanied in winter by increasing intrusion of frontal systems over Tasmania. Lowest values are measured in late July or early August when snow bearing clouds are most frequent. This period also encompasses the most frequent snowfall recorded for the year.

The month of August saw no discernible change in net radiation since the pattern was highly variable. With the onset of spring the combination of climatological factors and astro-nomic arguments marked a definite increase with time. The study had shown September, when spring occurs, to be characterized by a decrease in cloudiness and precipitation.

Sensible heat gained by the pack occurred on only ten days in July as opposed to August, when this number of days was seen to increase to seventeen. It was only in mid-September that Q_w consistently applied heat to the snowpack. This arose from warming regional and local advective conditions and a steady rise in air temperature.

The contribution of energy for melt from latent heat during July and August was insignificant. These calculations must be treated with caution as temperatures often dropped below zero and heavy riming occurred on the sensor housing.

Barton (1984) had noted the hazards of operating automatic weather stations permanently exposed to heavy riming conditions. It was only in the second half of September

that the latent heat term became an important component. During this period of early spring, heavy riming on the sensor housing became less frequent and a greater accuracy of data was assumed.

During the early part of July, the ski field boundaries were relatively small and it was possible to see some local effect to the advective component in snow melt. Examples of this may be seen during high melt days accompanied by north-westerly winds on the 2nd and 3rd of July. These days were typically associated with a small ski field area when local advection as evidenced by a high Q_a value may be acting. As the season progressed the ski field area increased in size and localized advection was minimised.

As winter gave way to spring, increasingly warm air was brought in through regional advection. In addition the ski field boundaries were steadily reducing so that local advection could once more play a part in snowmelt. The importance of these mechanisms was highlighted on the 25th of September when both sensible and latent heat exceeded net radiation in providing energy for snowmelt.

There were 54 melt days recorded during the three months with 17 of these designated as high melt days. These days occurred with increasing frequency as September progressed until the snowcover was no longer sustained. This pattern was reflected in the larger values recorded for net radiation and sensible heat (Figures 4.4 and 4.7). North westerly winds were found associated with 9 of the 17 high melt days, with 6 of these 9 having winds exceeding 5 m s^{-1} ,

whilst no particular relationship appeared to link high melt days with high air temperatures.

SPATIAL VARIABILITY 4.2

Introduction 4.2.1

As part of the study of snowmelt patterns, the energy balance was investigated for variations in space. There are two aspects to be considered. Firstly, the changes that occur in the energy available for melt with topographical variations within the ski field; secondly, the changing pattern of snowmelt reflecting the results of the energy balance and other factors. These processes could include variations in the microclimate, altitude and groundcover. No specific attempt was made to relate the effects of skiing on snowmelt.

Due to constraints in time, it was decided to observe the energy balance for one week only of the spring snowmelt in late September. The period chosen (25/9/86 - 2/10/86) included the reduction of the snowcover below 100%, so that some areas were clear of snow by the end of the week. If only one day had been observed, this reduction in snowcover might not have been representative of that single day.

In the estimation of the energy balance, a point calculation of Q_m was made at the meteorological station. All terms with the exception of Q^* were applied across the skifield (Weisman, 1977; Male, 1980). Net radiation, however, was resolved to allow for the variation in receipt due to the topography of the ski field.

A survey was made in the early spring of 1981 in the ski field area, to determine snowmelt patterns by measuring the areal and depth aspects of snowcover. Observations were made on the 22nd and 28th of September as well as the 6th of October, as this period included the reduction of the snowcover from 100% to 53%.

Field work pursued information regarding surface as well as snow temperatures. The free water content and density of the snowpack was measured although no specific attempt was made to measure compaction rates (Taylor, 1953).

Spatial Variation in the Energy Balance for Snowmelt 4.2.2

Net radiation was adjusted for slope and aspect through application of the model of Nunez (1980). The solar radiation incident on a surface of arbitrary slope and aspect can be given as (Equation 39) (see Appendix 3):

$$K'_{\downarrow c} = I(1 - C_l)(1 - C_m)(1 - C_h)\cos\gamma + D_c VF + K'_{\downarrow c} \alpha(1 - VF)$$

The reflected shortwave solar radiation component is a function of albedo and expressed as (Equation 41):

$$K'_{\uparrow c} = \alpha K'_{\downarrow c},$$

so that net shortwave radiation may be described as the difference between Equations 39 and 41. Similarly net longwave radiation is the difference between the upward and downward components and pursuing the practice of Nunez (1980) is (Equations 53 and 46):

$$L^* = [(5.31 \times 10^{-13} T_a^6 + 6.0n) VF + \epsilon\sigma\theta^4(1 - VF)] - [\epsilon\sigma\theta^4 + L'_c(1 - \epsilon)]. \quad 87$$

In equation 39, the first term on the right denotes the receipt of direct solar radiation by the surface which presents an angle of incidence (γ) to the direct beam radiation. The second term is the contribution from sky radiation and term three the contribution from surface reflection.

Equation 39 was calculated on an hourly basis to arrive at a daily total figure for each day of the study period (25/9/86 - 2/10/86). Values for the extra terrestrial radiation were taken for the 30th of September and assumed constant for the week in question.

Hourly cloud data between 9 a.m. and 3 p.m. were obtained by interpolating the 9 a.m. and 3 p.m. cloud records from the National Parks and Wildlife Service. Sunrise to 9 a.m. and 3 p.m. to sunset required extrapolation from the same records.

Albedo figures used in the estimation of reflected solar radiation (Equation 41) were adjusted each hour according to the mean zenith angle (γ) and snow conditions arising from observed September data from 1983 to 1986 inclusive.

Hourly air temperatures were applied to Equations 53 and 46 and a surface temperature of 0°C was assumed. Hourly estimates of sensible and latent heat, as well as the flux of heat from rain were applied as described in the previous section (Equations 62, 63 and 78).

The observed and modelled daily data were finally averaged for the week to produce a mean day in which the observed

net radiation exceeded that which was modelled by $1.2 \text{ MJ m}^{-2}\text{d}^{-1}$ (Table 4.3). The majority of this margin may be seen reflected in the net longwave flux. It was thought that the observed net radiation had been affected by condensation in the instrument, particularly in the lower bowl, reducing the reflected shortwave flux as well as the outgoing longwave component. Incoming global solar radiation values were within 9% with the model under-predicting. The mapping of the region is on a small scale and possibly the view factor and shading errors were slightly overestimated. Nunez (1983) found solar radiation within 10% with calculated values exceeding observed values.

TABLE 4.3 COMPARATIVE NET RADIATION DATA

	$K\downarrow$	K^*	L^*	Q^*
Modelled	9.7473	5.9459	3.1513-	2.7946
Observed	10.6333	6.2737	2.2772-	3.9965
Differences	0.8860	0.3278	0.8741	1.2019

Data ($\text{MJ m}^{-2}\text{d}^{-1}$) is designated positive where the net receipts for shortwave radiation (K^*), longwave radiation (L^*) and allwave radiation (Q^*) are downward. Downward solar radiation ($K\downarrow$) is also positive.

To calculate spatial variation in Q^* , a grid was superimposed over the ski field area, each square being 50 m x 50 m. Altitude, slope and aspect were loaded into each square along with a view factor and shading error (see Appendix 3). Finally, isolines were drawn defining $1 \text{ MJ m}^{-2}\text{d}^{-1}$ differences in the energy available for melt calculated for each square (Figure 4.8). This interval was

chosen as a result of differences between measured and computed values for Q^* (Table 4.3). Other terms in Equation 2; Q_M , Q_E , Q_G , Q_P and Q_R , were assumed constant throughout the study area.

Immediately adjacent to Legges Tor and crossing the head of towlines 2, 3 and 6, the ground topography changes quickly over a little distance. The isoline representing $5.0 \text{ MJ m}^{-2} \text{ d}^{-1}$ was interpolated between calculated data for 4.0 and $6.0 \text{ MJ m}^{-2} \text{ d}^{-1}$.

Overall the ski field enjoys an easterly aspect with slopes of less than 13° . This is reflected in the small variation in the energy balance across the ski field. The small variability does not totally reflect the variation in observed snow loss (see next section). The snow cover was not deep (30 cm) at this time and local differences in surface properties and elevation resulted in a greater variation in snow loss than is implied in the energy balance results.

The weekly mean that is represented by the energy balance comprises both clear and cloudy days. If the week had been clear, greater spatial variation might have been expected. Inversely, cloudy conditions throughout the week would have further reduced variability.

The differences arising between observed and calculated snowloss in 1986 could be split into two groups; areas that were clear of snow by the end of the week and areas still maintaining a good snow cover. The control area (●) at the meteorological station was clear of snow by the 30th of September and the calculated loss agreed within 10% to the

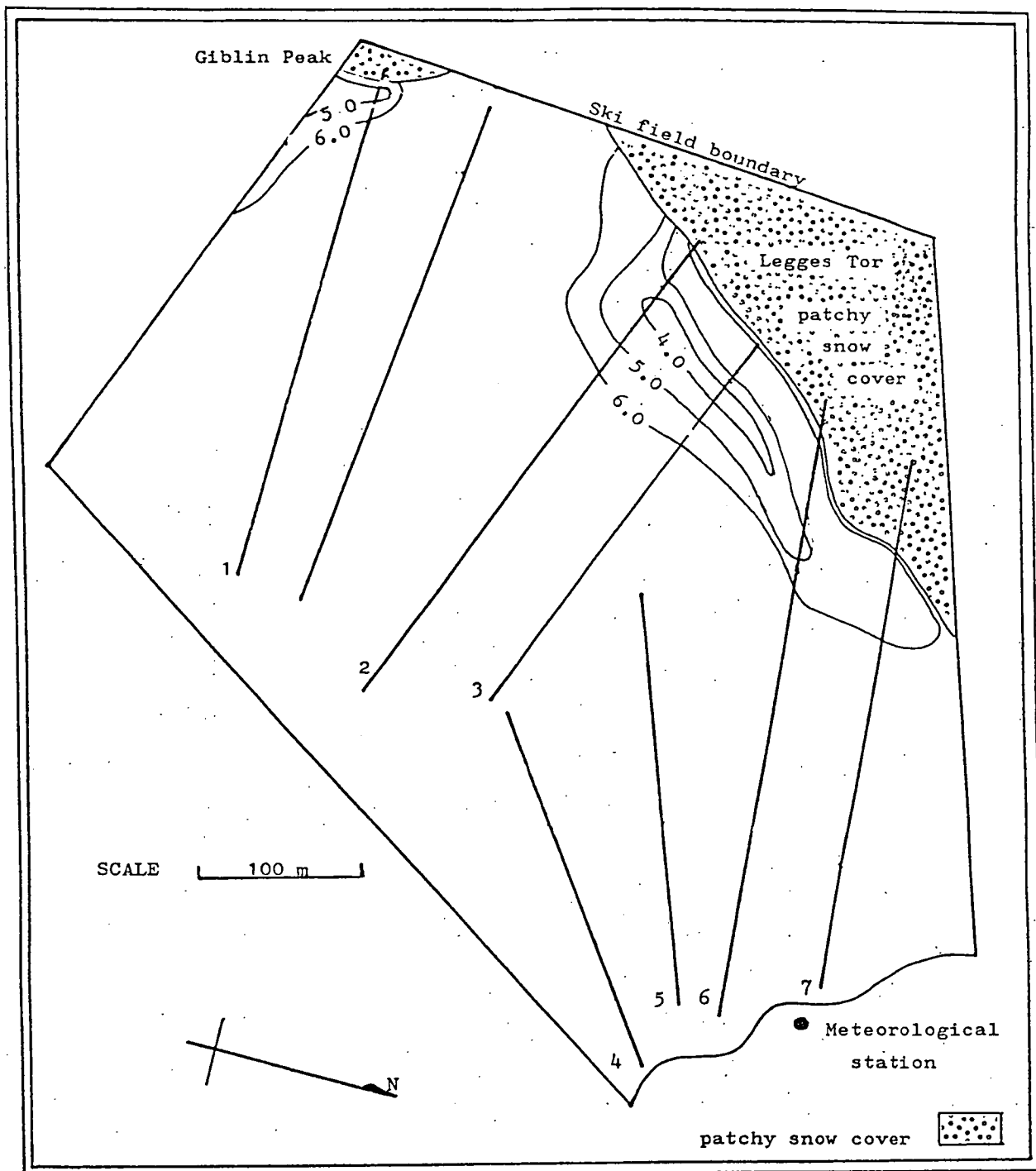


FIGURE 4.8 Spatial variability in the energy balance

The mean daily energy balance available for melt on a unit surface ($\text{MJ m}^{-2} \text{d}^{-1}$) for the week from the 26th of September to the 2nd of October, 1986 for the Ben Lomond ski field area. Variability varies with net radiation since Q_H , Q_E , Q_G , Q_F , and Q_r are assumed constant and equal with the values at the station.

observed loss of snow (Table 4.4).

It was not certain when the lower slopes (Figure 4.9) became clear of snow and therefore a direct comparison of snowmelt rates could not be specifically stated. However, if it is assumed that these areas were finally clear some time between the fifth and sixth day of the week, the calculated rates agree within 10% to the observed rates.

The middle and upper slopes showed some differences between calculated and observed values whilst mainly reflecting the energy available for melt when reduced for slope and aspect (Figure 4.8). The lower melt rates that were observed in these areas could be explained by local climatic differences that may be expected in any mountain region according to Seligman (1936) and Barry (1981). It was not possible to obtain a climate profile for each area and therefore fully state how the differences in snowloss arose.

TABLE 4.4 COMPARATIVE SNOWMELT

	Melt rates		
	Upper slopes (lowest)	Lower slopes (highest)	Meteorological station
Daily rate of energy receipt Q_m ($\text{MJ m}^{-2}\text{d}^{-1}$)	4.4	6.9	6.5
Calculated melt rate (cm d^{-1})	2.3	3.5	3.3
Observed melt rate (cm d^{-1})	2.1	3.3	3.0

Melt rates were calculated for the period 26/9/86 to 2/10/86 by applying Equation 2 to each 50 m x 50 m square and these averaged for the upper and lower slopes (Figure 4.9). The observed data were averaged from snow stake depths described in Chapter 3.

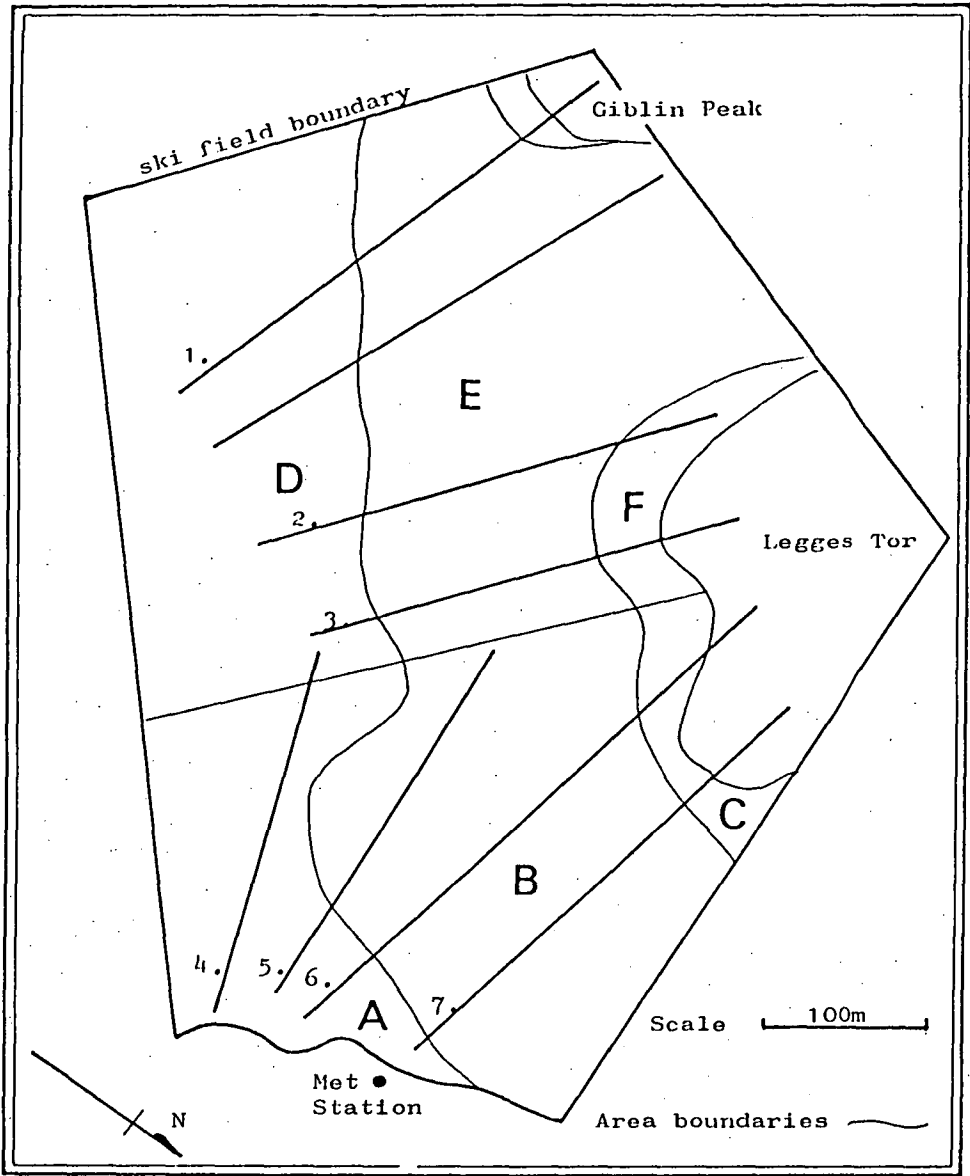


FIGURE 4.9 Varying slopes on the Ben Lomond
Ski Field

Letters A and D refer to the lower slopes
whilst C and F are the upper slopes. The middle
slopes are denoted by the letters E and B.

Observations of Spatial Variability in Snowmelt 4.2.3

In the winter of 1981 the last heavy snowfall was recorded on the 16th and 17th of August and on the 14th September there was still a 100% snowcover in the skifield area. The north-west side of the ridge from Giblin to Legges Tor had only a sparse cover. The first survey day (22/9/81) indicated rock denuded of snow along the upper ridges and some rock domes (Figure 4.10). Field work showed that melt commenced on the upper section of the domes where they dipped towards vegetation, presenting a north-westerly aspect in contrast to the general south-easterly aspect of the area.

Thermocouple temperature measurements taken of snow free surfaces (Table 4.5) did not indicate any strong difference between rock and vegetated cover. Water that flowed over the rock beneath the snowcover maintained a temperature of 3°C. The base of the snowcover over running water was 0.5°C. Rock under snow tended to be generally wet with running water whilst vegetated areas were merely damp, with running water confined to specific water courses.

The lower section of each tow has a lesser slope (6°) than the centre or upper sections. These lower sections all had depths of less than 25 cm. The areas that had been most heavily skied in the lower sections of the ski field, across tows 5 and 6, had no snowcover at all. This is not a rock area but has a more easterly and northerly aspect than the lower areas of tows 1, 2 and 3, as well as being 30 metres lower in altitude. The upper rock ridge is a generally

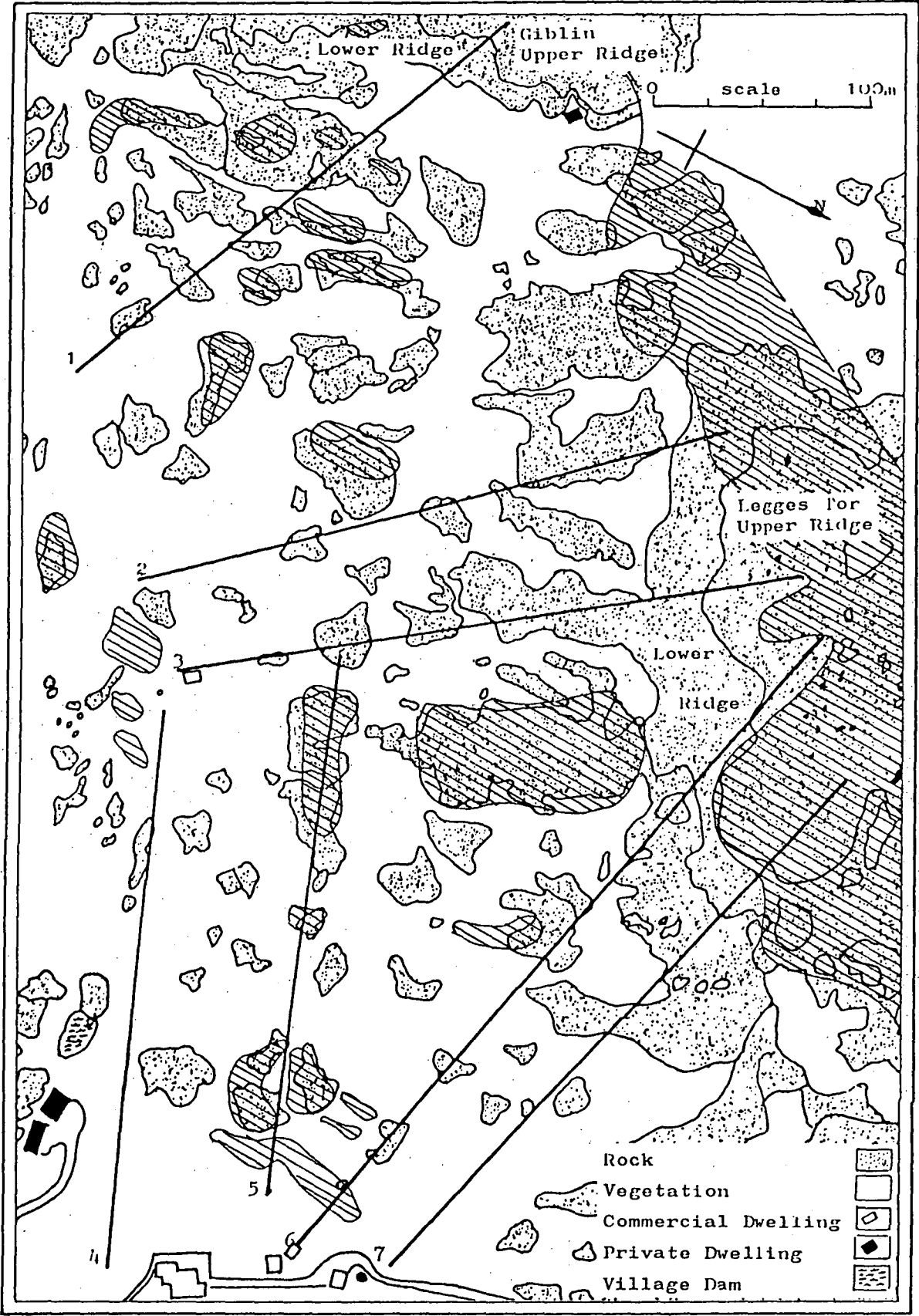


FIGURE 4.10 The Ben Lomond Ski Field Area


The areal snowcover and melt patterns on September 22, 1981, where ground clear of snow is denoted by: 

TABLE 4.5 SURFACE TEMPERATURES

Rock	11.5
Grasses	11.0
Water	3.0
Richeas	11.0
Air	10.0
Snow	0.5

Comparative surface temperatures of ground cover expressed degrees centigrade. The measurements were taken at the foot of tow No. 3 at an altitude of 1490 metres. Readings were averaged over a 4 hourly period from 10 am. to 2 pm. on October 4, 1981.

TABLE 4.6 MELT CALCULATIONS

Date	1981	Area Covered	Reduction
14th	September	100.0%	-
22nd	September	80.3%	19.7%
28th	September	78.8%	1.5%
6th	October	53.0%	25.8%

Areal snowcover reduction expressed as a percentage.

flat area with no particular slope. This is the second highest point in the State. It has no reduction in its sky view thereby accepting the maximum possible direct sunshine between sunrise and sunset, which for the 22nd of September was 13 hours.

Between the 14th and 22nd of September, the areal snowcover had been reduced to 80.3% (Table 4.6), with a mean depth of 46.8 cm and a standard deviation of 9.7 cm. The depths varied between vegetated areas and the rock domes so that, in general, the domes had only one third the depth of cover of the adjacent gullies and bowls that were vegetated. The free water content of the snow varied considerably in the pack as did density, the mean figures being 14.6% and 443 kg m^{-3} respectively. The mean figures did not vary particularly throughout the period and agree with data presented by Kojima (1966).

A further reduction of 1.5% in the areal snowcover was noted on the 28th of September with an accompanying mean depth of 383 mm. The upper ski field remained in nearly the same state whilst the lower tows, 4, 5, 6 and 7, all showed a marked increase in snow free zones (Figure 4.11) at their lower levels. There had been several light snowfalls during the week with no apparent increase in depth. It is possible that the falls were too light to be measured. Using a manual snow probe, snowfalls of less than 5 cm are difficult to measure due to irregularities in the snow surface and the underlying ground.

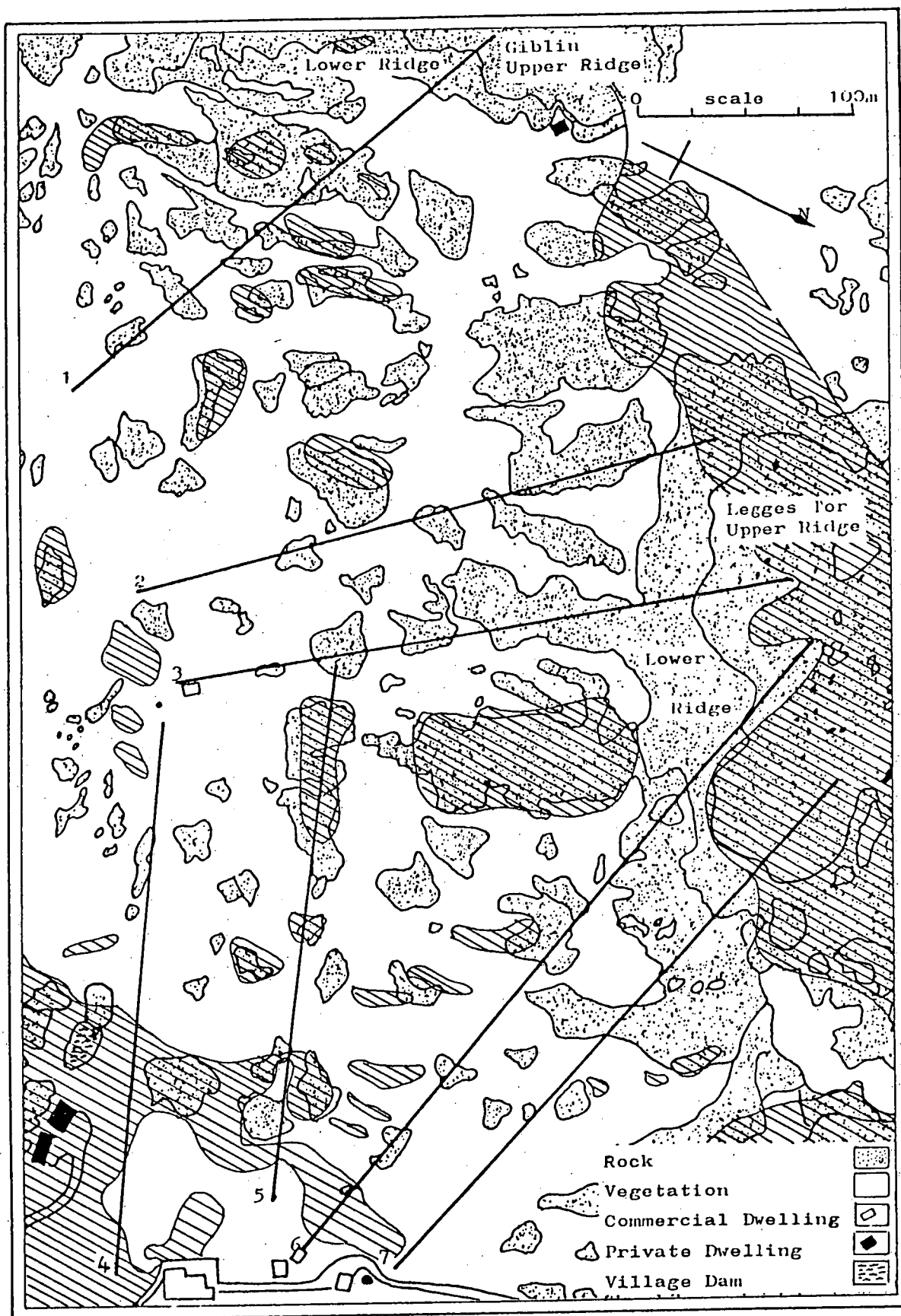



FIGURE 4. 11 The Ben Lomond Ski Field Area

The areal snowcover and melt patterns on September 28, 1981, where ground clear of snow is denoted by: 

Snow depths and areal measurements made on the 6th of October indicated a week of strong melt. Areal reduction was 25.8% since the 28th of September, with depths averaging 225 mm., a decrease of 41.3%. Nearly all rock areas were denuded of snow as were all the lower parts of the ski field below 1470 metres (Figure 4.12). Of particular interest were the mean depths calculated for the skiable snowcover (Table 4.7). The vegetated gullies and bowls that still held snow represented more than half the ski field area with depths averaging 350 mm

The lower ridge areas at the head of tows 3 and 6 have slopes in excess of 50° . The reduced sky view means a loss of direct solar radiation by 1500 L.N.T. at this time of year. There are no opposing slopes at a sufficient angle to offer any reflected solar radiation to this area and drifts here were measured to depths of 8 metres. Snow was still evident on the 25th of November. Immediately to the north of tow 3 on the rock wall, an ice fall is formed as winter progresses each year. In 1981 this ice wall still held its integrity on the 13th of October and could be climbed using crampons and ice axes. This condition is clearly indicative of mean daily subzero temperatures prevailing in this area during spring.

At a lower altitude, deep drifts were also found exceeding 4 metres under the south-east face of "Normans Folly", the large rock dome half way up tow 2 on the southern side. However, this snow had all disappeared by the 3rd of November. Pits excavated in these regions did not disclose any undue departure from snowpack temperatures of $\pm 0.5^{\circ}\text{C}$ and densities

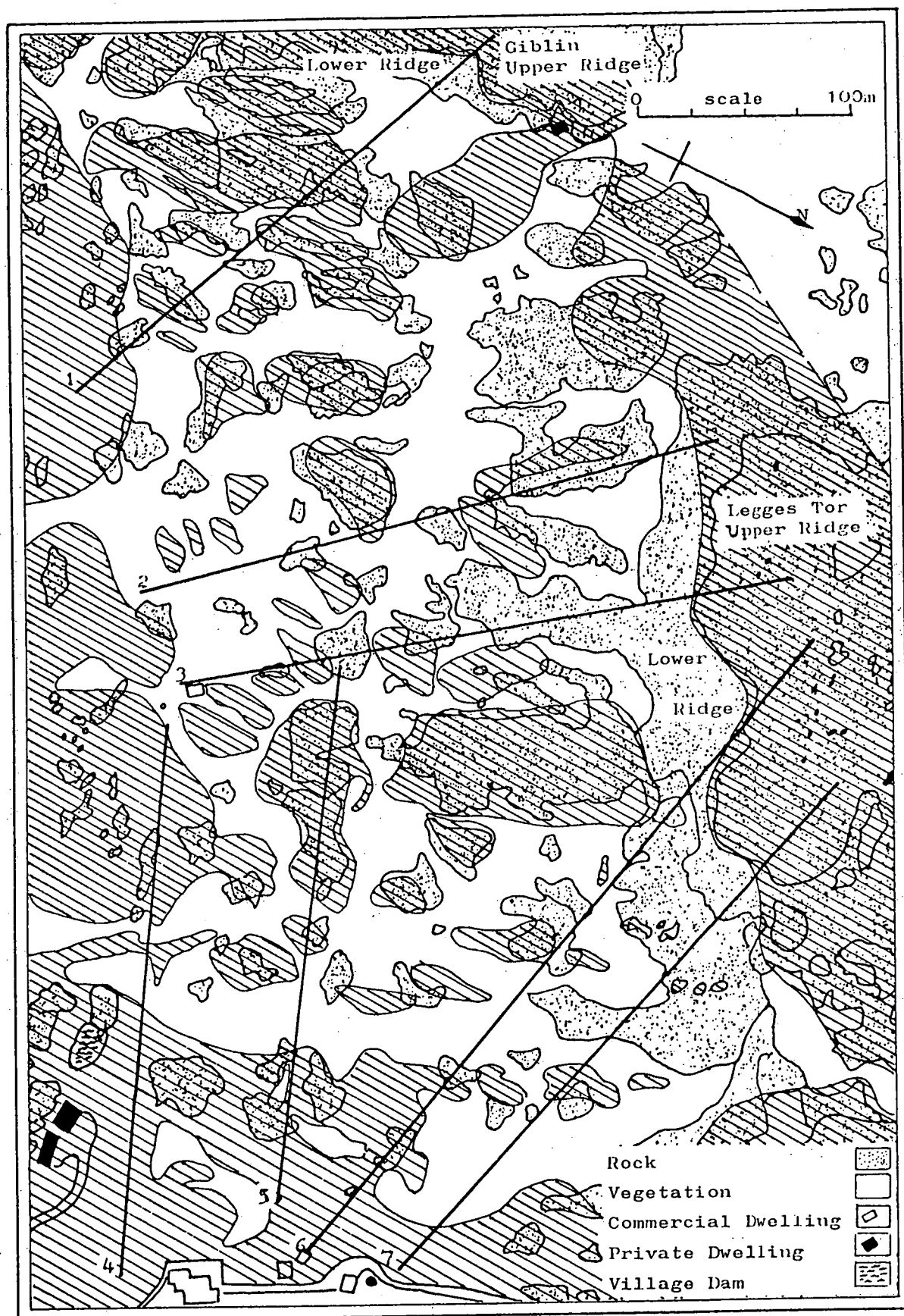


FIGURE 4.12

The Ben Lomond Ski Field Area


The areal snowcover and melt patterns on October 6, 1981, where ground clear of snow is denoted by: 

TABLE 4.7

DEPTH AVERAGES

DEPTH AVERAGES (mm) 1981								
Towlines								
Code	1	2	3	4	5	6	7	Total Date
1	488	308	463	540	533	310	411	468)
2	557	463	463	540	533	517	528	568) 22/9/81
3	483	463	463	425	533	517	386	525)
1	306	300	426	490	425	270	333	383)
2	350	450	425	490	425	450	500	478) 28/9/81
3	350	450	425	363	425	450	400	443)
1	88	225	263	340	175	180	250	225)
2	350	338	350	567	263	450	563	409) 6/10/81
3	350	338	350	350	263	450	417	350)
DEPTH LOSSES (%) 1981								
1	37.3	2.6	8.2	9.3	20.3	12.9	18.8	18.1) 22/9/81
2	37.1	2.8	8.2	9.3	10.3	13.0	5.3	15.8) 28/9/81
3	27.5	2.8	8.2	14.6	20.3	13.0	+3.6	15.6)
1	71.2	25.0	38.1	30.6	58.8	33.0	24.9	41.3) 28/9/81
2	0	24.9	16.5	+15.7	38.1	0	+12.6	14.4) 6/10/81
3	0	24.9	16.5	3.5	38.1	0	+4.3	21.0)
1	82.0	26.9	43.2	37.0	67.2	41.0	39.1	51.9) 22/9/81
2	37.2	27.0	24.4	+5.0	31.9	13.0	+6.6	28.0) 6/10/81
3	37.2	27.0	24.4	17.7	31.9	13.0	+8.0	33.0)

Code

- 1 Mean depths including all measurements for each tow and the ski field area.
- 2 Mean depths excluding bare ground (zero depths).
- 3 Mean depths excluding bare ground and drifts with depths exceeding 1 m.

Code 2 was calculated to allow a more accurate volumetric analysis of snow.

Code 3 was calculated to present data pertinent to skiable snow-cover with regard to depth.

Data expressing snowcover in terms of depth (mm) and loss of snow expressed as a percentage of depth.

approximating 433 kg m^{-3} . No particular layering was observed and the pack appeared to have similar characteristics throughout with crystals typical of three months old firnified snow (la Chapelle, 1969).

Environmental Factors Affecting Observed Spatial Variation in Snowmelt 4.2.4

Factors of ablation arising from the results generally accord with Moore (1983). The single area of contention surrounds the role of groundwater and snowmelt at the base of the pack. The flux of heat from the ground to the pack has been generally considered too difficult to evaluate (Male and Gray, 1981) and not of short term significance. Each factor will now be discussed individually.

(a) Altitude: The rate of snowmelt was seen generally to vary as a function of altitude. The majority of the areal snow cover reduction (78.8 to 53%, Table 4.6) which occurred between the 28th of September and the 6th of October was found below an altitude of 1490 m in the ski field area. It was difficult to accurately assess the change in climatological characteristics between the crest of the ridge (Legges Tor to Giblin) and the ski village. The rise is only 100 metres and local anomalies in air mass characteristics typical of mountain weather (Barry, 1981) have been observed.

Tows 6 and 7 commence at 1460 metres, rising to approximately 1550 metres and have the greatest change in altitude. Depth measurements taken on the 6th of October showed more than 50 cm of snow lying in areas above 1490 metres whilst most

of the ground below this level was clear of snow. Tow 4, which is contained completely in the lower zone of the ski field, had only a few small patches of snow left by the 6th of October (Figure 4.12). Tows 1, 2 and 3 are entirely above 1490 metres and continuous snowcover could be found along the lengths of the tows with depths ranging from 100 mm at the bottom to over 500 mm at the top.

(b) Ground cover: The northern half of the Ben Lomond plateau may be described in terms of ground that is covered by shrubs, herbs, sedges and grasses or rock. The skifield area is no exception. The non-vegetated areas identified as dolerite (rock) domes and illustrated in Figure 1.4 have been noted to lose snowcover before any other ground except the upper ridge, which is also rock. Areas that are grassed, particularly the gullies and bowls, were observed to hold snow even when the pack was shallow, for longer periods than adjacent areas covered in bush. This was highlighted in field work on the upper areas between tows 1 and 2. There are two grassed bowls, each 40 m x 20 m, surrounded by rock here. In 1981 and again in 1986, there was still snow in the bowls in excess of 150 mm in depth in mid-October when all the surrounding rock was quite clear of snow. It did not appear to matter what type of grasses and shrubs were compared, the essential boundary was between the two types of vegetation.

The lower areas of tows 3, 5 and 7 have had the bushes cut down to the base exposing soil and bare stems above the ground. The Richeas in particular leave a mass of ground wood when this is done. The snow in these areas was found to have melted as

fast as over the shrubs that had been left and more quickly than adjacent grassed areas, such as found fifty metres up tow 5.

(c) Ground water: The energy from water on the ground as a melt factor against the base of the snow pack has not been established in this study. The area containing the larger water courses and pools, especially in the south-eastern region of the ski field adjacent to tow 4, was noted in particular to lose snowcover early in spring. The area between the lower levels of tows 5 and 6 which holds much ground water, also loses snow more readily than the adjacent areas.

Studies comparing grassed areas and adjacent rock domes for ground water found the rock wet with a film of water coursing over the dome under the snowcover, whilst the grasses appeared dry enough to leave no moisture on the hand, after the snow had been excavated.

(d) Groundflux: In this study it was thought that the meltwater observed over the rock domes might play a significant part in a higher melt rate of snow. Snowdepth over the domes was generally less than in the surrounding gullies so that an even melt rate would expose the domes first, despite other factors. Conclusions are complicated by the change in energy flux as the pack reduces in depth to below 250 mm (O'Neill and Gray, 1973). The pack was observed to reduce below this depth over the domes first (Figure 4.13) and melt observed to be highest where the aspect of the domes was north-west.

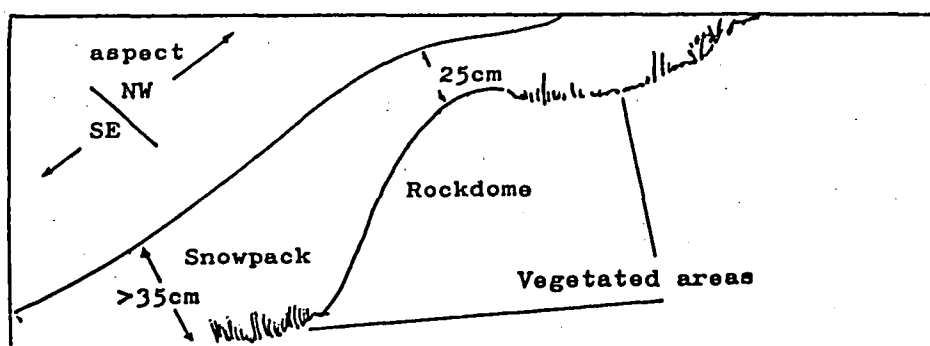


FIGURE 4.13

The relative aspect and snowdepth over the major rock-domes in the Ski Field.

Solar shortwave radiation penetrates the shallow pack (less than 250 mm) and is absorbed by the ground, some of which is returned to the pack as longwave radiation. In this instance the increased energy flux to the pack, a function of shallow snow, low rock albedo (0.17) and meltwater over the rock, could describe the mechanism that accelerates the melt in an already shallow area of the snowpack. As the rock domes become exposed to solar radiation, heat is conducted from the warmed surfaces to those immediately below the pack generating melt. In addition sensible heat from air warmed locally by the rock being advected over the snow again increases melt.

In contrast, the vegetated gullies were observed to maintain a snowdepth of 35 cm even on the 6th of October when most of the domes were uncovered. If the rock and vegetated areas were to be covered at an even depth, the higher albedo of the vegetation (0.22) and the lack of meltwater would infer a smaller return of longwave energy to the pack in comparison with adjacent rock areas (Monteith, 1959).

CHAPTER 5

SUMMARY AND CONCLUSION

SUMMARY 5.1

Temporal Variability 5.1.1

(a) Climatic factors: Snow may be expected to fall and stay on the ground for periods in excess of 7 days during any of the winter months between June and October inclusively above 1400 m on Ben Lomond. This period is most commonly reduced to July, August and September with only unusually long winters providing seasonal snowcover extending into June and October (1981, 1986).

The seasonal snowcover is a function of geographic factors and the climatic parameters of air temperature and precipitation. Highland stations in north-eastern Tasmania (Table 1.3) all show a reduction in the mean monthly minimum temperature with an accompanying increase in snowfall days (Table 1.7) from June to August.

The change in climate as winter gave way to spring was marked on Ben Lomond by a rise in the mean maximum air temperature from 1.8°C in August to 7.2°C in October (Table 1.2). This warming was further evidenced by a reduction in freezing days from 12.8 to 2.2 per month, and a decrease in snowfall days from 10.4 to 0.8 per month (Table 1.7).

Most snowfall days were accompanied by south-westerly winds which also dominated the months of June and July. More winds were recorded from the north-west than elsewhere during August, September and October (Table 1.9). These winds were also associated with the majority of days when (high) snowmelt exceeded 15 mm per day (Figures 4.5, 4.6 and 4.7).

Advective forces play an increasingly important role in snowmelt as snowcover diminishes and the edge of the snow-pack is approached (Weisman, 1977; Treidl, 1970). In addition to warm air being brought in through regional advection, local winds moved air, warmed in the surrounding valleys, over the mountainside during the latter half of winter as the mountain snowcover reduced. Most likely in July and early August, the snowcover on the plateau was generally too extensive to allow local advective warming to reach the skifield area.

(b) The energy balance: The energy balance was applied to four specific synoptic events (Figure 4.1) to determine the functions of various terms for snowmelt in each situation.

When warm conditions were associated with local advection, net radiation provided most energy for melt. Sensible heat dominated under regional advection accompanied by warm north-westerly winds (Tables 4.1 and 4.2). Of the remaining terms, latent heat contributed a small but significant component to the energy balance, whilst heat from rain, the ground and internal energy were only of minor importance.

The three dominant terms (net radiation, sensible and latent heat) were applied to a 1986 time series incorporating the months of most common snowfall, these being July, August and September. During July and August a weak trend was observed as the three terms converged toward zero. However, from the last week in August and throughout September there was a steady increase in net radiation and sensible heat (Figures 4.2, 4.3 and 4.4).

The increase in net radiation was in conjunction with astronomic arguments and more favourable climatic conditions. Sensible heat dominated on 3 days when suitable regional advective conditions prevailed. In general, latent heat played a secondary role in the energy balance, but as warm and moist advective conditions increased, accompanying the reducing ski field boundaries in late September, more heat became available from this source. Overall, net radiation followed by sensible heat emerged as providing the most energy for snowmelt throughout the winter.

(c) Snowmelt: Temporal variability in snowmelt pursued the pattern outlined by energy balance results and climatic studies (Figure 5.1). There were only 4 high melt days

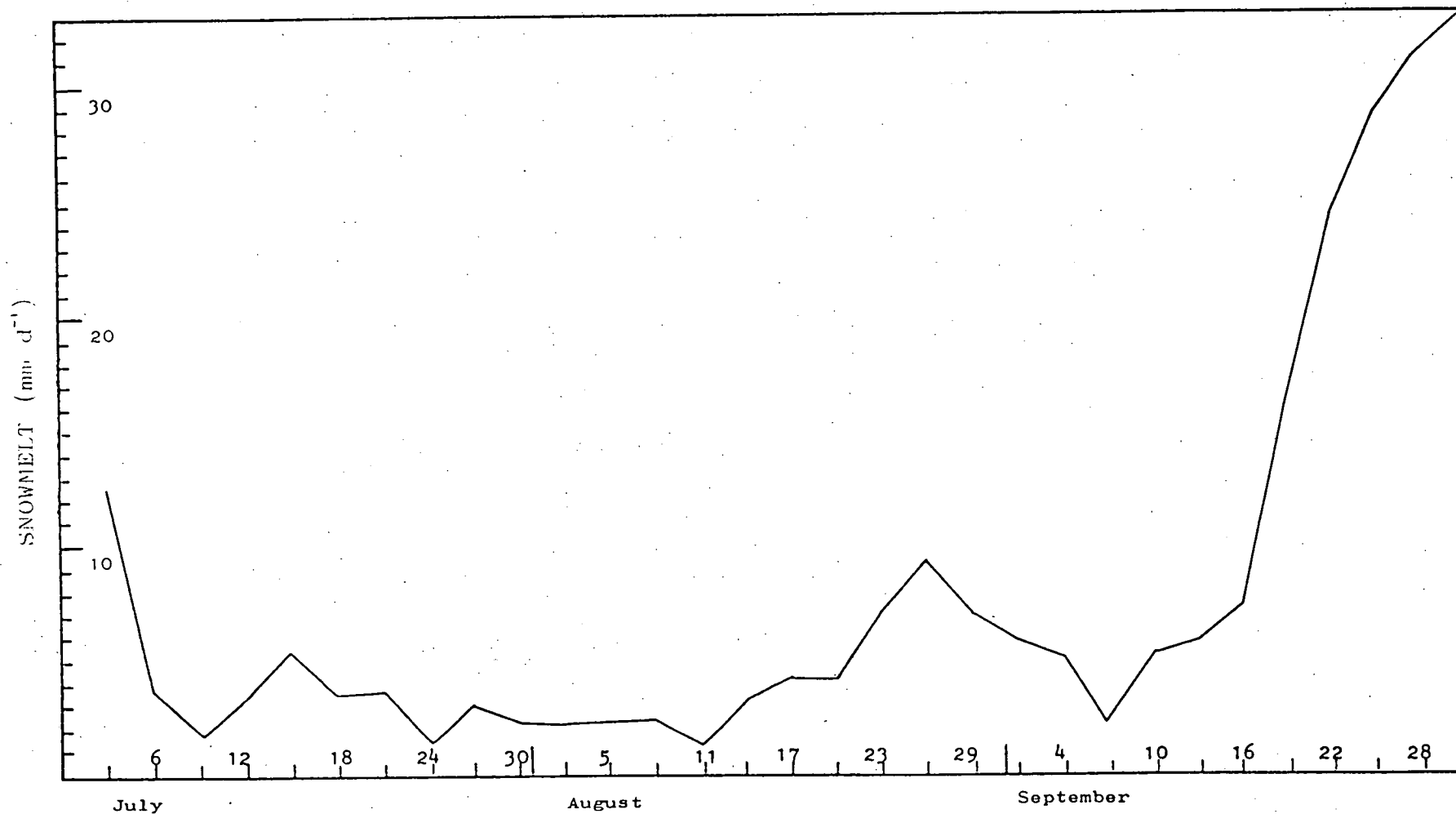


FIGURE 5.1. A 5 day moving average time series of the calculated daily snowmelt expressed in centimetres for Winter 1986 on Ben Lomond. Days with no melt were taken as zero and used in the running mean. Where data for certain days were missing, the series were averaged over the remaining days.

($M > 15 \text{ mm d}^{-1}$) in July and August as opposed to 13 days in September (Figures 4.5, 4.6 and 4.7). An investigation of the total number of days when melt was recorded reveals a similar pattern with 13 occurring in July, 15 in August and the balance of 26 days out of a season total of 54 days being in the month of September.

In 1986 there was a sustained snowcover commencing at least 7 days prior to the beginning of July which lasted until the end of September, with a mean depth of 350 mm being recorded on the 25th of September. The period of higher sustained melt, 163 mm in 5 days, during the final week in September, coincided with the end of the 100% snowcover for the winter in the ski field area.

Spatial Variability 5.1.2

(a) Climatic factors: Barry (1981) indicated that each small valley or ridge in a mountainous area might be expected to have its own climatic characteristics. It was not possible to monitor climatic parameters across the ski field area and the point measurement at the ski field meteorological station had to be applied throughout. However, profiles of temperature change with altitude between the meteorological station (1460 metres) and Legges Tor (1573 metres) were taken on many occasions during the period 1981 to 1986 during the winter months, revealing a mean lapse rate of $6^{\circ}\text{C km}^{-1}$.

(b) The energy balance: The energy balance (Equation 2) was investigated for correlation with the differing melt rates that had been observed in various parts of the ski

field. The net radiation term was reduced for slope and aspect with allowances made for a reduced sky view and shadowing by applying the model of Nunez (1980). The remaining sources of energy were applied across the ski field from point measurement at the meteorological station.

The model underestimated net radiation by $1.2 \text{ MJ m}^{-2} \text{ d}^{-1}$ (Table 4.3) when compared with observed values, whilst differences arising from changes in slope and aspect were primarily within $1 \text{ MJ m}^{-2} \text{ d}^{-1}$. There were only two areas where the variation in calculated rates exceeded the underestimated error. Directly under Legges Tor and Giblin Peak, calculations for daily melt were 4 and $5 \text{ MJ m}^{-2} \text{ d}^{-1}$ respectively as against $6 \text{ MJ m}^{-2} \text{ d}^{-1}$ for the majority of the ski field (Figure 4.8). Spatial variations in daily melt arising from the energy balance are indicative of differences of up to 1 cm per day in melt rates (Figure 5.2). This is a significant margin over a week when seen against a mean ski field depth of 350 mm and a daily rate of 33 mm.

These data suggest that whilst the energy balance and net radiation in particular may be seen to act as an agent in reduced snow melt rates for the steeper south-easterly slopes where strong afternoon shadowing occurs, some other factors must be held to account for the local variations in melt with space in other parts of the ski field.

(c) Other factors: In Figure 5.2, the effect of slope and aspect on the melting process can be seen. However, mechanisms other than slope and aspect are important factors in reducing snowcover. Observations of spatial variations in

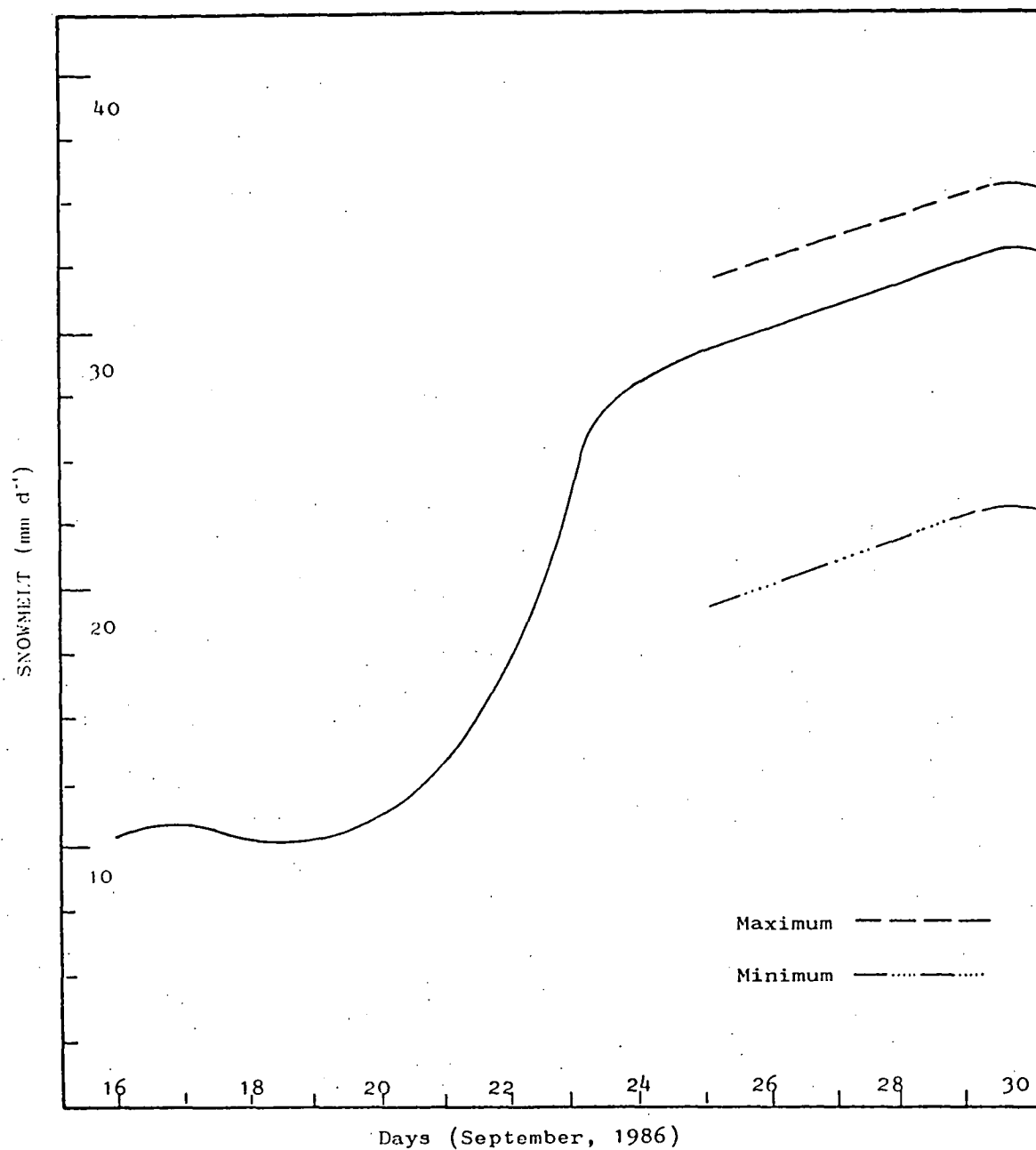


FIGURE 5.2 A five day moving average time series of the mean daily snowmelt calculated from the energy balance established at the meteorological station. Maximum and minimum rates of melt arising from spatial variations in the energy balance are also shown.

snowmelt (1981) have revealed a reduction in melt with increasing altitude (Figures 4.10, 4.11 and 4.12). Snow-cover reduced by approximately 26% during the week following the 28th of September and the majority of this reduction may be seen contained below an altitude of 1490 metres (Figures 4.11 and 4.12).

Variations were observed in snowmelt within the confines of the maximum and minimum rates calculated in 1986 (Figure 5.2) which reflect local topographic changes and the differing nature of the groundcover. The entire ski field is comprised of small shallow gullies and ridges interspersed with rocky outcrops. Drifting processes ensured that snowfall accumulated in the gullies, over the ridges and under the rocky outcrops until a fairly even surface was established. Melt quickly cleared the shallow snowcover on the ridges (Figure 4.10) whilst some of the gullies still held snow two weeks later (Figure 4.12). This pattern was repeated each year of the study period (1981-1986) as the final snowmelt for the season progressed. The gullies that held the snow longest were not water courses and had a grass or herb groundcover in preference to rock or scrub.

CONCLUSIONS 5.2

The effect of geographic position and climate have been observed and comparisons made with other meteorological stations above the seasonal snowline in Australia. Data suggested that the two most reliable indicators of seasonal snowcover were the number of heavy frost days and the number of snowfall days between the 1st of June and the 30th of October.

The strongest and most consistent snowmelt occurred in September and was associated with a mean rise in the daily air temperature accompanied by a reduction in snowfall days. The winds most commonly associated with high melt days were from the north-west. During spring this warm air, brought in through regional advection, was occasionally enhanced through local advection also bringing warm air from the north to the ski field area.

In order of importance, energy available for melt was determined to come primarily from net radiation, sensible and latent heat sources. Other terms in the energy balance were of minor significance. The dominance of any one term as a heat source was dependent upon the existing synoptic situation and the proximity of the snow field boundaries. Temporal variations in snowmelt reflected the seasonal changes in the energy balance whilst spatial variations indicated the superimposition of local differences in groundcover and terrain upon energy available for melt.

The geomorphic and biogeographic parameters on Ben Lomond indicated that snow stayed on the ground longest, and accumulated to the greatest depths in grassed gullies lying under poleward and eastern facing steep walls above 1500 metres. Within any small part of the ski field the rock covered ridges lost their snowcover first.

Arguments concerning snow loss and thermodynamic changes within the pack due to skier traffic, whilst considered outside the scope of this thesis, are duly noted.

REFERENCES

REFERENCES

- AGUADO, E., 1985; Snowmelt, energy budgets in southern and east central Wisconsin; Ann. Assoc. Amer. Geog. Vol. 75, No. 2, 203-211.
- ANDERSON, E.A., 1968; Development and testing of snowpack energy balance equations; Water Resour. Res. Vol. 4, 10-27
- ANDERSON, E.A., 1976; A point energy and mass balance model of a snowcover; NOAA Tech. Rep. NWS - 19, U.S. Dept. Commer., Washington, D.C.
- ATMOSPHERIC ENVIRONMENT SERVICE, 1973b; Snow Surveying, 2nd Ed. Environ. Can., Downsview, Ont.
- BARRY, R.G., 1981; Mountain Weather and Climate, 66-73; Methuen, London.
- BARRY, R.G. and CHORLEY, R.J., 1982; Atmosphere Weather and Climate; Methuen & Co. Ltd., New York.
- BARTON, J.S., 1984; Observing mountain weather using an automatic weather station; Weather, Vol. 38, 298-303.
- BILELLO, M.A., 1966; Relationship between climate and regional variation in snow cover density in North America; Physics of Snow and Ice, Vol. 1, Part 2, Sapparo Conference.
- BEN LOMOND SKI ASSOCIATION, 1981; Annual Report, Launceston.
- BOHRENS, C.F. and BARKSTROM, B.R., 1974; Theory of the optical properties of snow; J. Geophys. Res., Vol. 79, 4527-35.
- BRUNT, D., 1952; Physical and Dynamical Meteorology,; Cambridge Univ. Press, Cambridge, Mass.
- BRUTSAERT, W., 1975; On a derivable formula for longwave radiation from clear skies; Water Resour. Res., Vol. 11, 742-744.
- BUCHAN, A., 1890; The Meteorology of Ben Nevis; Trans. R. Soc. Edinb., 34.
- BUREAU OF METEOROLOGY, 1975; Climatic Averages, Victoria; Canberra.
- BUREAU OF METEOROLOGY, 1975; Climatic Averages, New South Wales; Canberra.
- BUREAU OF METEOROLOGY, 1979; Climatic Survey, Tasmania, Region 3, Northern; Australian Government Publishing Service, Canberra.

- BUREAU OF METEOROLOGY, 1984; Observing the Weather;
Australian Government Publishing Service, Canberra.
- BUSINGER, J.A., 1973; Turbulent transfer in the atmospheric
boundary layer; In Workshop on Micrometeorology, Boston,
1972, 67-100.
- CAINE, N., 1967b; The texture of talus in Tasmania; J.
Sedim. Petrol., Vol. 37, 796-803.
- CAINE, N., 1968; The Blockfields of North Eastern Tasmania;
A.N.U., Canberra.
- CAMPBELL SCIENTIFIC, 1980; CR21 Micrologger User's Manual;
Logan.
- DAVIES, J.L., 1969; Landforms of Cold Climates; A.N.U. Press,
Canberra.
- DAVIES, J.A., SCHERTZER, W. and NUNEZ, M., 1975; Estimating
global solar radiation; Boundary Layer Meteorol. Vol. 9,
33-52.
- DAVIES, J.A., ROBINSON, P.J. and NUNEZ, M., 1970; Radiation
measurements over Lake Ontario and the determination of
emissivity; McMaster University Report No. HO 81276.
- DIAMOND, M., 1956; Evaporation or melt of a snowcover; Snow
Ice and Permafrost Res. Est. U.S.A.C.E., Illinois.
- DOZIER, J., 1979; A solar radiation model for a snow surface
in mountainous terrain; Proc. Modelling Snow Cover Run-
off (S.C. Colbeck and M. Ray, eds.), U.S. Army Cold Reg.
Eng. Lab., Hanover, 144-153.
- EXAMINER, 1979; North-west flood damage (17 Aug.); The
Examiner Press, Launceston, Tas.
- FARWELL, T. and ASSOCIATES, 1983; The economic feasibility
of proposed snowmaking for the Panorama Ski Hill Company
Ltd., Group Delta, Boulder.
- FAULKNER, P.S., 1984; Report for National Parks and Wildlife
Service of Tasmania, Hobart.
- FERGUSON, R.I., 1985; Melt rates of snow in the Cairngorms;
Weather, Vol. 40, 272-276.
- FITZHARRIS, B.B., STEWART, D. and HARRISON, W., 1980;
Contributions of snowmelt to the 1978 flood of the
Pomoka and Fraser Rivers, Otago; J. of Hydrol. (N.Z.),
Vol. 19, No. 2, 84-93.
- FRITZ, S., 1954; Scattering of solar energy by clouds of large
water drops; J. Meteorol.,

- GARNIER, B.J. and OHMURA, A., 1968; A method of calculating the direct shortwave radiation income of slopes; J. Appl. Meteorol. Vol. 7, 796-800.
- GARNIER, B.J. and OHMURA, A., 1970; The evaluation of surface variations in the solar radiation income; Solar Energy, Vol. 13, 21-34.
- GERDEL, R.W., DIAMOND, M. and WALSH, J.K., 1954; Nomographs for computation of radiation heat supply; Snow Ice and Permafrost Research Establishment, Corps of Engineers, U.S. Army, Illinois.
- GIDDINGS, J.C. and LA CHAPELLE, E., 1961; Diffusion theory applied to radiant energy distribution and albedo of snow; J. Geophys. Res., Vol. 66, 181-189.
- GOLD, L.W., 1957; Proc. Int. Geod. Geophys. Gen. Assembly, Toronto, Vol. 4, 13-21.
- GOLD, L.W. and WILLIAMS, G.P., 1961; Energy balance during snowmelt period at an Ottawa site; Int. Union Geod. Geophys. Gen. Assem., Helsinki, Snow and Ice, Int. Assoc. Sci. Hydrol. Publ. No. 54, 288-294.
- GOODISON, B.E., FERGUSON, H.L. and McKAY, G.A., 1981; Measurement and Data Analysis; Handbook of Snow, 191-274, Pergamon, Toronto.
- GRANGER, R.J., 1977; Energy exchange during melt of a prairie snowcover; M.Sc. Thesis, Dept. Mech. Eng. Univ. Sask., Saskatoon.
- GRANGER, R.J. and MALE, D.H., 1978; Melting of a prairie snowpack; J. Appl. Meteorol. Vol. 17, No. 12, 1833-1842.
- HAURWITZ, B., 1948; Insolation in relation to cloud type; J. Meteorol. Vol. 5, 110-113.
- HAY, J.E., 1977; An analysis of solar radiation data for selected locations in Canada; Climat. Studies, 32.
- HICKS, B.B. and MARTIN, H.C., 1972; Atmospheric turbulent fluxes over snow; Boundary Layer Meteorol. Vol. 2, 496-502.
- HOGG, I.G.G., PAREN, J.G. and TIMMIS, R.J., 1982; Summer heat and ice balances on Hodges Glacier, South Georgia, Falkland Islands Dependencies; J. Glaciol., Vol. 28, No. 99, 221-238.
- HOLLOWAY, G., 1980; Annual General Report, Ben Lomond Ski Association, Launceston.
- HOLMES, A.H., 1964; Principles of Physical Geology; Nelson, London.

- HOLMGREN, B., 1971; Climate and energy exchange on a sub polar ice cap in summer; Arctic Institute of North America Devon Island Expedition, 1961-63, Pt. D; On the vertical turbulent fluxes of water vapour at ice cap station Meddelanden från Uppsala Universitets Meteorologiska Institution, Nr. 110.
- HOUGHTON, H.G., 1954; On the annual heat balance of the northern hemisphere; J. Meteorol. Vol. 11, 1-9.
- HUBLEY, R.C., 1954; Measurement of diurnal variations in snow albedo on Lemon Creek Glacier, Alaska; J. Glaciol.
- IDSÖ, S.B. and JACKSON, R.D., 1969; Thermal radiation from the atmosphere; J. Geophys. Res., Vol. 74, 5397-403.
- JOHNS, B.S., 1977; The Ice Age, Past and Present; Collins, London.
- KASTEN, F., 1966; A new table and approximation formula for the relative optical air mass; Arch. Meteorol. Geophys. Bioklimatol. Vol. 14, 206-223.
- KATTELMAN, R., 1984; Wet slab instability; Proc. Int. Snow Science Workshop, Aspen.
- KOJIMA, K., 1966; Densification of snow cover; Physics of Snow and Ice, Vol. 1, Part 2, Sapporo Conference.
- KONDO, J. and YAMAZAWA, H., 1986; Bulk transfer coefficient over snow; Boundary Layer Meteorol. Vol. 34, No. 1-2.
- KONDRATYEV, K.Y., 1969; Radiation in the Atmosphere, 441-449; Academic Press, New York.
- KONDRATYEV, K.Y., 1970; Solar radiation and solar activity; Quart. J. Roy. Meteorol. Soc. Vol. 96, 509-522.
- KONDRATYEV, K.Y. and FEDOROVA, M.P., 1977; Radiation regime of inclined slopes; W.M.O. Tech. Note. No. 152, Geneva, W.M.O.
- KUZ'MIN, P.P., 1961; Melting of Snow Cover; Gidrometeorol. Izd. Leningrad (Eng. transl. TT71-50095, Israel Program Sci. Transl. Jerusalem, 1972).
- LA CHAPELLE, E.R., 1969; A Field Guide to Snow Crystals; University of Washington Press, Washington.
- LANGHAM, E.J., 1981; Physics and properties of snowcover; Handbook of Snow, 275-337, Pergamon, Toronto.
- LEADMAN, D.E. and SYMONDS, P.A., 1973; Gravity Survey of the Tamar Region, Northern Tasmania; The Dept. of Mines, Tasmania.
- LEE, R., 1962; Theory of the "Equivalent Slope"; Mon. Weather Rev., Vol. 90, 165-166.

- LEGGE, W.V., 1907; An investigation into the Physiography of the Ben Lomond Plateau, Tasmania; Report of the eleventh meeting of the Australian Association for the Advancement of Science, Adelaide.
- LEWIS, A.N., 1945; Pleistocene Glaciation in Tasmania; Royal Society of Tasmania (December).
- LIGHT, P., 1941; Analysis of high rates of snow-melting; Snow Survey Conference, Sacramento.
- LIST, R.J. (ed.), 1968; Smithsonian Meteorological Tables; Smithsonian Institute, Washington.
- LOWE, P.R., 1976; An approximation polynomial for the computation of saturation vapour pressure; J. Appl. Meteorol. Vol. 16, 100-103.
- MALE, D.H., 1980; The seasonal snow cover; Dynamics of Snow and Ice Masses, 305-395; Academic, Toronto.
- MALE, D.H. and GRANGER, R.J., 1979; Energy mass fluxes at the snow surface in a prairie environment; Proc. Modelling Snow Cover Runoff (Colbeck, S.C. and Ray, M. eds.) U.S. Army Cold Reg. Res. Eng. Lab. Hanover, N.H., 101-124.
- MALE, D.H. and GRAY, D.M., 1981; Snowcover ablation and runoff; Handbook of Snow, 365-436; Pergamon, Toronto.
- MARKS, D., 1979; An atmospheric radiation model for general alpine application; Proc. Modelling Snow Cover Runoff (Colbeck, S.C. and Ray, M. eds.) U.S. Army Cold Reg. Res. Eng. Lab. Hanover, N.H., 167-178.
- MCDONALD, J.E., 1960; Direct absorption of solar radiation by atmospheric water vapour; J. Meteorol., Vol. 17, 319-328.
- McKAY, G.A. and ADAMS, W.P., 1981; Snow and the environment; Handbook of Snow, 1-32; Pergamon, Toronto.
- McKAY, G.A. and GRAY, D.M., 1981; The distribution of snow-cover; Handbook of Snow, 153-191; Pergamon, Toronto.
- McKAY, D.C. and THURTELL, G.W., 1978; Measurements of the energy fluxes involved in the energy budget of a snow cover; J. Appl. Meteorol., Amer. Meteorol. Soc. Vol. 17, 339-349.
- MONTEITH, J.L., 1959; Reflection of short-wave radiation by vegetation; Quart. J. Roy. Meteorol. Soc. Vol. 83, 386-390.
- MONTEITH, J.L., 1962; Attenuation of solar radiation: a climatological study; Quart. J. Roy. Meteorol. Soc. Vol. 88, 508-521.
- MOORE, R.D., 1983; A comparison of the snowmelt energy budgets of two alpine basins; Arch. Geoph. Biocl. Serv. B. Vol. 33, 1-10.

- MOORE, R.D. and OWENS, I.F., 1984; Controls on advective snowmelt in a maritime alpine basin; J. Appl. Met. Vol. 23, 135-142.
- MUNN, R.E., 1966; Descriptive Micrometeorology; Academic Press.
- MUNRO, D.S.M., 1970; Problems in assessing glacier energy balances (unpublished); McMaster University, Hamilton, Ont.
- MUNRO, D.S. and YOUNG, G.J., 1982; An operational net short-wave radiation model for glacier basins; Water Resources Research, Vol. 18, No. 2, 220-230.
- NUNEZ, M., 1983; Estimation of solar radiation received on slopes in Tasmania; Pap. Proc. Royal Society Tasmania, Vol. 177, 153-159, Hobart, Tasmania.
- NUNEZ, M., DAVIES, J.A. and ROBINSON, P.J., 1971; Solar radiation and albedo at a Lake Ontario tower site; Third Report, No. HO. 81276, Dept. of Geography, McMaster University, Hamilton, Ont., 82 pages.
- NICHOLS, K.D., 1958; Soil formation on dolerite in Tasmania; In Dolerite: A symposium, University of Tasmania, Geology Dept. 204-209.
- NOBLE, M.G., 1981; Vegetation organisation along altitudinal gradients in Tasmania; Ph.D. Thesis, A.N.U., Canberra.
- NUNEZ, M., 1980; The calculation of solar and net radiation in mountainous terrain; J. Biogeog. Vol. 7, 173-186.
- O'NEILL, A.D.J., 1972; The energetics of shallow prairie snow packs; Ph.D. thesis, Univ. Sask., 197 pages.
- O'NEILL, A.D.J. and GRAY, D.M., 1973; Spatial and temporal variations of the albedo of prairie snowpack; The Role of Ice and Snow in Hydrology: Proc. Banff Symp. Sept. 1972, Unesco-WMO-IAHS Geneva-Budapest-Paris, Vol. 1, 176-178.
- OUTCALT, S.I., GOODWIN, C., WELLER, G. and BROWN, J., 1975; A digital computer simulation of the annual snow and soil thermal regimes at Barrow, Alaska; Cold Regions Research and Engineering Laboratory Research Rep. 331, Hanover, N.H., 18 pages.
- OWENS, I.F., MARCUS, M.G. and MOORE, R.D., 1984; Temporal variations of energy transfers over the lower part of the Franz Josef Glacier; 12th New Zealand Geography Conference, N.Z. Geog. Soc., Christchurch.
- PALTRIDGE, G.W., 1975; Net radiation over the surface of Australia; Search, Vol. 6, 37-39.

- PAITRIDGE, G.W. and PLATT, C.M.R., 1976; Radiative Processes in Meteorology and Climatology; Elsevier, Amsterdam.
- PINKARD, G.J., 1980; Land Systems of Tasmania, Region 4; Department of Agriculture, Tasmania.
- PRICE, A.G., 1977; Snowmelt runoff processes in a sub-arctic area; Climatology Research Series No. 10, McGill University, Montreal, 106 pages.
- PRICE, A.G. and DUNNE, T., 1976; Energy balance computations of snowmelt in a subarctic area; Water Resour. Res. 12, 686-694.
- PROWSE, T.D. and OWENS, I.F., 1982; Energy balance over melting snow, Craigieburn Range, New Zealand; J. Hydrol. Vol. 21, No. 2.
- ROSENBERG, N.J., 1974; Micrometeorology: The Biological Environment, Wiley, N.Y.
- SATTERLUND, D.R., 1979; An improved equation for estimating longwave radiation from the atmosphere; Water Resour. Res. Vol. 15, 1643-1650.
- SCHNEIDER, S.H. and GAL-CHEN, T., 1973; Numerical experiments in climatic stability; J. Geophys. Res. Vol. 78, 6182-6194.
- SELIGMAN, G., 1936; Snow Structure and Ski Fields; Macmillan, London.
- SELLERS, W.D., 1965; Physical Climatology, Univ. of Chicago, Chicago.
- SCHERTZER, W.M., 1975; A model for calculating daily totals of global solar radiation in cloudless and cloudy sky conditions; M.Sc. Thesis, McMaster University, Hamilton, Ont.
- SPORNS, U., 1976; Snow cover mapping in mountainous areas - Columbia River drainage above Mica Dam; Unpubl. Rep. B.C. Hydro., Vancouver, B.C.
- SUCKLING, P.W. and HAY, J.E., 1977; A cloud layer sunshine model for estimating direct diffuse and total radiation; Atmosphere, Vol. 15, 194-207.
- SUMMIT SUN, 1984; Snowfall in Perisher Valley; Summit Sun (August).
- SWINBANK, W.C., 1963; Longwave radiation from clear skies; Quart. J. Roy. Meteorol. Soc. Vol. 89, 339-348.
- SVERDRUP, H.U., 1936; The eddy conductivity of the air over a smooth snow field; Geofysiske Pub. Vol. 11, No. 7, Oslo.

TAYLOR, A., 1953; Snow Compaction; Snow Ice and Permafrost Research Establishment, Corps of Engineers, U.S. Army, Illinois.

TREIDL, R.A., 1970; A case study of warm air advection over a melting snow surface; Boundary Layer Meteorol. Vol. 1, 155-168.

U.S.A.C.E., 1956; Handbook of Snow Hydrology; U.S. Army Corps of Engineers, N. Pac. Div., Portland, Oregon.

WEISMAN, R.N., 1977; Snowmelt: a two dimensional turbulent diffusion model; Water Resour. Res. Vol. 13, No. 2.

YOSIDA, Z., 1972; Investigation on snow conditions for the XI Olympic Winter Games, Sapporo, Feb. 3-13; Scientific Study of Skiing in Japan, Soc. Ski. Sci., Hitachi, Tokyo, 113-126.

APPENDIX 1

CONSTANTS and SYMBOLS

Constants (1a)

Gravitational acceleration	9.81 m s^{-2}
Solar constant	1.353 kW m^{-2}
Stefan Boltzman constant	$5.67 \times 10^{-11} \text{ kW m}^{-2}\text{K}^{-4}$
Universal gas constant	$8.32 \times 10^3 \text{ J kg}^{-1}\text{mole}^{-1}\text{K}^{-1}$
Von Karman constant	0.4
Density of air	@ s.t.p.; 1.3 kg m^{-3} @ 85000 Pa & 0°C; 1.1 kg m^{-3}
Density of water	1000 kg m^{-3}
Latent heat for fusion	333.5 kJ kg^{-1}
Latent heat for sublimation	$333.5 + 2500 = 2833.5 \text{ kJ Kg}^{-1}$
Latent heat for vaporization	2500 kJ kg^{-1}
Specific heat of air	$1 \text{ kJ kg}^{-1}\text{K}^{-1}$
Specific heat of water	$4.2 \text{ kJ kg}^{-1}\text{K}^{-1}$
Specific heat of water vapour	$1.86 \text{ kJ kg}^{-1}\text{K}^{-1}$
Specific heat of ice	$2.115 + 0.00779T_i \text{ kJ kg}^{-1}\text{K}^{-1}$
Longwave emissivity for snow	0.99
Melt temperature of snow	0°C
Roughness parameter for snow	$2.5 \times 10^{-3} \text{ m}$ (Sverdrup, 1936)
Standard atmospheric pressure at sea level	$1.01325 \times 10^5 \text{ Pa}$
Vapour pressure over ice at 0°C	610 Pa
Thermal conductivity of soil	$1.2 \text{ W m}^{-1}\text{K}^{-1}$

LIST OF SYMBOLS (1b)

A_E	eddy diffusivity coefficient for water vapour
A_H	eddy diffusivity coefficient for air
A_M	eddy diffusivity coefficient for momentum
B	thermal quality of the fraction of ice in a unit mass of wet snow
B_r	Bowen ratio
C_h	high cloud cover
C_i	amount of cloud layer (i)
C_l	low cloud cover
C_m	medium cloud cover
C_p	specific heat of air at constant pressure
C_{pi}	specific heat of ice
C_{pl}	specific heat of water
C_{pv}	specific heat of water vapour
D	diffuse solar radiation received on a horizontal surface
D_c	diffuse solar radiation under cloudy conditions received on a horizontal surface
D'_c	diffuse solar radiation under cloudy conditions received on a sloping surface
D_E	bulk transfer coefficient for latent heat
D_H	bulk transfer coefficient for sensible heat
D_M	bulk transfer coefficient for momentum
D_o	diffuse solar radiation under cloudless conditions received on a horizontal surface
D'_o	diffuse solar radiation under cloudless conditions received on a sloping surface
D_r	solar radiation reflected from adjacent slopes
D_s	bulk transfer coefficient for momentum corrected for stability

H_1	sunrise on the study area
H_2	sunset on the study area
I	solar constant reduced by transmission through the atmosphere
I_0	solar constant
K^*	net solar or shortwave radiation
K_{\uparrow}	upward or outgoing solar radiation
K_{\downarrow}	downward or incoming solar radiation
$K_{\downarrow c}$	downward solar radiation under cloudy conditions received on a horizontal surface
$K'_{\downarrow c}$	downward solar radiation under cloudy conditions received on a sloping surface
$K_{\downarrow 0}$	downward solar radiation under cloudless conditions received on a horizontal surface
$K'_{\downarrow 0}$	downward solar radiation under cloudless conditions received on a sloping surface
K_z	radiation intensity at any depth in snow
L^*	net longwave radiation
L_{\uparrow}	upward or outgoing longwave radiation
L_{\downarrow}	downward or incoming longwave radiation
$L'_{\downarrow c}$	downward longwave radiation under cloudy conditions received on a sloping surface
L_d	diffusivity of water vapour in air
L_f	latent heat of fusion
L_v	latent heat of vaporization/condensation/sublimation
M	change in depth due to snowmelt
M_w	molecular weight of water
P_a	atmospheric pressure
P_0	standard atmospheric pressure at sea level
P_r	depth of rainfall
Q^*	net radiation
Q_E	latent heat (evaporation, condensation or sublimation)

Q_g	heat from the ground
Q_H	sensible heat
Q_i	heat from water phase changes within the snowpack
Q_M	heat or energy available for snowmelt
Q_R	heat from rain
R	universal gas constant
R_i	Richardson number
S	direct solar radiation received on a horizontal surface
S_c	direct solar radiation received under cloudy conditions on a horizontal surface
S'_c	direct solar radiation received under cloudy conditions on a sloping surface
S_o	direct solar radiation received under cloudless conditions on a horizontal surface
S'_o	direct solar radiation received under cloudless conditions on a sloping surface
T	temperature
T'	fluctuating component of the temperature ($\bar{T} - T$)
\bar{T}	mean temperature
T_a	air temperature (screen)
T_g	ground temperature
T_m	mean snow temperature
T_s	snow temperature
ΔT	change in temperature ($T_a - T_s$)
T	absolute temperature
VF	view factor
W_f	free water content of a unit mass of wet snow
X	zenith angle of the normal to the slope
Y	azimuth angle or aspect of the slope
Z	solar zenith angle

a, b, c	constants as defined in the text
d	depth of snow
e	vapour pressure
e_a	vapour pressure of air (screen)
e_s	vapour pressure over ice
Δe	change in vapour pressure ($e_a - e_s$)
f_s	fractional sunshine recorded on a suncard
g	gravitational acceleration
h	thermal conductivity of soil
k	Von Karman constant
m	optical air mass
n	fractional amount of cloud cover
n_e	observer estimate of cloud cover
p	atmospheric transmissivity
q	specific humidity
q'	fluctuating component of specific humidity
\bar{q}	mean specific humidity
q_a	specific humidity of air (screen)
q_s	specific humidity over ice
Δq	change in specific humidity ($q_a - q_s$)
t_i	transmission of cloud layer (i)
u	wind velocity
u'_N	fluctuating component of the wind normal to the surface
u^*	friction velocity
w	precipitable water vapour
z	height
z_o	roughness length

α	albedo of snow
α_b	albedo of the cloud base
α_n	albedo of the cloud top
γ	angle of incidence of the direct solar beam to the slope
∂	partial differential
Δ	'change in'
ϵ	surface emissivity
η	elevation angle of the horizon
θ	surface temperature
κ_m	molecular diffusivity of air
λ	wavelength
ν	10^{-6} metres
ν	kinematic viscosity
π	3.1426
ρ	density of snow
ρ_a	density of air
ρ_l	density of water
σ	Stefan Boltzman constant
τ	shearing stress or vertical momentum
ϕ	dimensionless parameter for turbulent exchange
ϕ_E	vapour pressure gradient
ϕ_m	temperature gradient
ϕ_m	vertical velocity
χ	cloud thickness to the mean path of light through the cloud
ψ	atmospheric exchange coefficient for:
ψ_{ch}	high cloud
ψ_{ci}	any cloud layer

ψ_{cl}	low cloud
ψ_{cm}	medium cloud
ψ_d	combined dust
ψ_{da}	absorption by dust
ψ_{ds}	scattering by dust
ψ_{rs}	Rayleigh scattering
ψ_{wa}	absorption in water vapour
ψ_{ws}	scattering by water vapour
Ω	cloud height and temperature coefficient
ω	solar azimuth angle

APPENDIX 2

DESCRIPTIVE DATA FOR BEN LOMOND

History (2a)

Ben Lomond was named by Colonel Patterson in 1804 and survey notes were found in Surveyor General Grimes' field note book of 1807 concerning the mountain. Nearly 100 years elapsed before further exploration took place. Between 1905 and 1906 Colonel W.V. Legge and his parties made several trips. Legges Tor was properly surveyed and in his report to the A.A.A.S. (1907) Legge gave a most detailed description of all the aspects of the physical geography of the mountain including flora and fauna. Many of the names of outstanding features were given by Legge in 1913.

Official recognition of the potential of the mountain for wilderness recreation came when it was gazetted as a National Park in 1947. Three years afterwards the government recommended the development of a ski resort on the site that is now developed. Details of the tow development on the ski-field are included in the appendix.

Two major studies have been made more recently about the mountain. The blockfield geomorphology was investigated by Caine (1968) whilst the report on altitudinal variation in vegetation was written by Noble (1981). Davies (1969) had covered the history and effect of glaciation in Tasmania and included comment on Ben Lomond.

To date there is no reticulated power and access along the unsealed road is subject to the weather and rockfall in the steeper sections on Jacobs Ladder. In the sixteen years since the road was completed to the plateau, the number of skiers using the mountain on any one day have grown from

50 to 1500 (Faulkner, 1984) prompting calls for better management studies and a more scientific approach to snow usage to maximise the potential of the ski area (B.L.S.A., 1981).

The road was finally constructed to the skifield area by members of the Northern Tasmanian Alpine Club in 1967.

Early meteorological observations were made as often as possible in the winter by Mr. W. Simpson, a member of the club. Records are kept by the National Parks and Wildlife ranger for the park as duty permits. However, no regular daily data was noted before 1981. Commercial development of the area commenced in 1970 and was still in progress in 1985.

TABLE A1

TOW SUMMARY (2b)

No.	Name	Owner	Built	Type	Length	Descent	Slope	Azimuth
1	Giblin	A.E.	1975	Poma	253m	58m	13°	292°T
2	Big Ben	NTAC	1967	Rope	375m	59m	9°	320°T
3	Fannies	A.E.	1973	T Bar	273m	61m	13°	328°T
4	Creek	A.E.	1979	Poma	256m	35m	8°	250°T
5	Beginners	A.E.	1973	Poma	269m	55m	12°	250°T
6	Thirty Second	NTAC	1964	Rope	386m	92m	14°	280°T
7	Summit	A.E.	1973	Poma	334m	87m	15°	285°T
0	Bill's	A.E.	1985	T Bar	250m	51m	12°	310°T

A summary of the ski tow characteristics for the Ben Lomond Ski Field for 1985.

Additional data: Tows 1,2 and 3 commence at 1490 -1500m altitude whilst tows 4 to 7 commence at approximately 1460m. All except tows 4 and 5 finish between 1550 and 1560m. Tows 4 and 5 finish at 1490 and 1518m respectively. In 1985 tows 2 and 6 were changed to a Poma type.

Sources: Northern Tasmanian Alpine Club (N.T.A.C.), Alpine Enterprises (A.E.) and Tasmap publication of Ben Lomond National Park.

Vegetation and Soils (2c)

Site and Sample (Noble, 1981)

At grid reference 8414-537029 a core of soil 81 cm in depth was taken. The site is within 1 kilometre of the skifield area to the north west of Legges Tor in an area known as the Land of Little Sticks.

Depth (cm) Description

0-11	Brown soil with thick mat of roots.
11-29	Brown soil.
29-81	Dark brown to black soil; clayey; numerous charcoal fragments with a distinct layer 3 mm thick at 35.5 cm; layer of small dolerite stones at 43 to 46 cm.
81-90	Dolerite stones and clay.
90	Dolerite bedrock.

The present vegetation at the site consists of species-rich shrublands and herbfields. The most common species in the immediate vicinity are:

WOODY

Baeckea gunniana
 Bellendena montana
 Coprosma nitida
 Epacris serpyllifolia
 Helichrysum backhousii
 Leucopagon hookeri
 Olearia algida

HERBACEOUS

Acaena novae-zelandiae
 Astelia alpina
 Cardamine neterophylla
 Carpha alpina
 Craspedia alpina
 Drosera arcturi
 empodisma minus

Olearia ledifolia

Olearia obcordata

Orites acicularis

Orites revoluta

Richea scoparia

Epilobium curtisiae

Euphrasia diemenica

Gentianella diemensis

Geranium potentilloides

Gnaphalium traversii

Lycopodium fastigiatum

Oreomyrrhis sessiliflora

Plantago tasmanica

Poa fawcettiae

Restio australia

Senecio pectinatus

APPENDIX 3

MODELLING NET RADIATION FOR MOUNTAINOUS TERRAIN

Modelling Net Radiation for Mountainous Terrain

In this study the daily energy balance was initially calculated for the horizontal surface at the meteorological station by applying (Equation 3):

$$Q_M = Q^* + Q_H + Q_E + Q_P .$$

An investigation of spatial variability of energy available for melt necessitated adjustments within the energy equation to allow for the complex topography of the ski field. The practises of Male and Gray (1981), Munro and Young (1982) and Hogg et al (1982) were pursued so that all the heat fluxes with the exception of net radiation were applied from the point measurement, without adjustment, across the ski field.

Net radiation was adjusted for slope and aspect, reduced sky view and shadowing through application of the model of Nunez (1980). The solar radiation incident on a horizontal surface was stated as (Equation 17):

$$K\downarrow_0 = I \cos Z + D_0 .$$

The solar constant ($1353 \text{ J m}^{-2}\text{s}^{-1}$) was adjusted for attenuation within the atmosphere by applying the transmission coefficients:

$$\psi_{wa} = 1 - 0.077 (wm)^{0.3}, \quad \text{McDonald, 1960}$$

$$\psi_{ws} = 1 - 0.0025 (wm), \quad \text{McDonald, 1960}$$

$$\begin{aligned} \psi_{rs} = & 0.972 - 0.8262 m + 0.0933 m^2 \\ & - 0.00095 m^3 + 0.0000437 m^4, \end{aligned} \quad \text{Houghton, 1954}$$

$$\psi_{da} = \psi_{ds} = 0.975^m,$$

$$\psi_d = \psi_{da} \psi_{ds} = (c)^m,$$

$$c = 0.95,$$

$$m = [\cos Z + 0.15 (93.885 - Z)^{-1.253}]^{-1}, \quad \text{Kasten, 1966}$$

$$\text{and } w = \text{precipitable water vapour.} \quad \text{List, 1968}$$

The direct solar beam received on a unit horizontal surface may now be described (Equation 19):

$$I = I_o \psi_{wa} \psi_{da} \psi_{ws} \psi_{rs} \psi_{ds}.$$

Nunez (1980) reported that Houghton (1954) assumed absorption occurred before scattering and that half of the latter was incident to the earth's surface allowing the diffuse solar radiation to be expressed by (Equation 20):

$$D_o = I \cos Z \psi_{wa} \psi_{da} [1 - \psi_{ws} \psi_{rs} \psi_{ds}] / 2.$$

The zenith angle of the direct solar beam to a horizontal surface was adjusted for slope and aspect so that the ensuing angle of incidence was (Equation 32):

$$\cos \gamma = \sin Z \cos \omega \sin X \cos Y + \sin Z \sin \omega \sin X \sin Y + \cos Z \cos Y.$$

The nature of the surrounding terrain and the increase in slope at various points on the ski field caused shadowing as the direct solar beam was obstructed. The calculation of shadow areas may be described by first observing Figure A1.

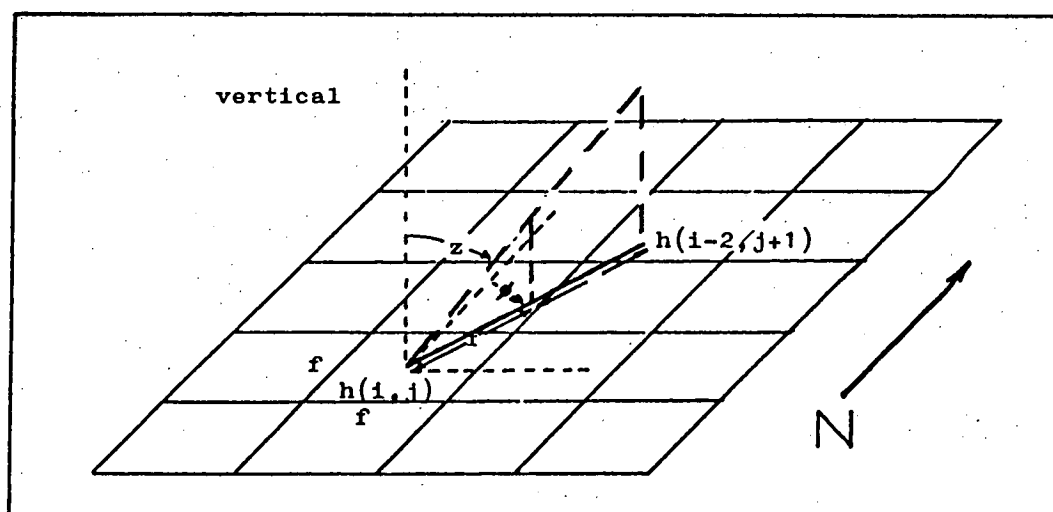


FIGURE A1. Schematic used in the calculation of shadow areas (Nunez, 1980)

The surface of the ground is segmented into a series of cells of specific area and altitude. The direct solar beam radiation of zenith angle (z) is assumed incident on the centre of a cell of side (f). The altitude or height of each cell is defined as $h(i, j)$ as illustrated in Figure A1. For each cell step, the height of the solar beam may be expressed as $nf/\sin Z$, where n is the number of cell steps. If the cell height is greater than the beam height, the solar beam is intercepted.

Nunez (1980) has written a programme tracing the solar beam and identifying cells that are intercepted as receiving the direct solar beam. Those that do not intercept the solar beam are identified as being in shadow. The author used cells of 50 m x 50 m in determining shadow areas.

Nunez (1980) assumed that diffuse radiation was isotropic so that any reduction of the sky view in turn reduced the diffuse radiation receipt. The sky view factor may be determined by taking a series of maximum angles subtended by the topography and averaging their projected radii.

Nunez (1980) suggested a hemispherical dome be projected over each cell. Four maximum elevation angles (η) are selected, determined by the topography and illustrated in Figure A2. As each angle representing the lowest solar beam to illuminate the cell cuts the hemispherical dome, a perpendicular is dropped. The distance from the foot of the perpendicular to the centre is the projected radius of each angle of elevation, which may be represented as $r_i = \cos \eta$.

The view factor reported by Nunez (1980) according to Davies,

Robinson and Nunez (1970) is the ratio of the area determined by the radii to the area of the circle representative of the cell (Figure A2.) and may be written:

$$VF = \frac{(r_1 + r_2 + r_3 + r_4) \pi / 4}{\pi}, \quad 88$$

$$= \frac{r_1 + r_2 + r_3 + r_4}{4}. \quad 89$$

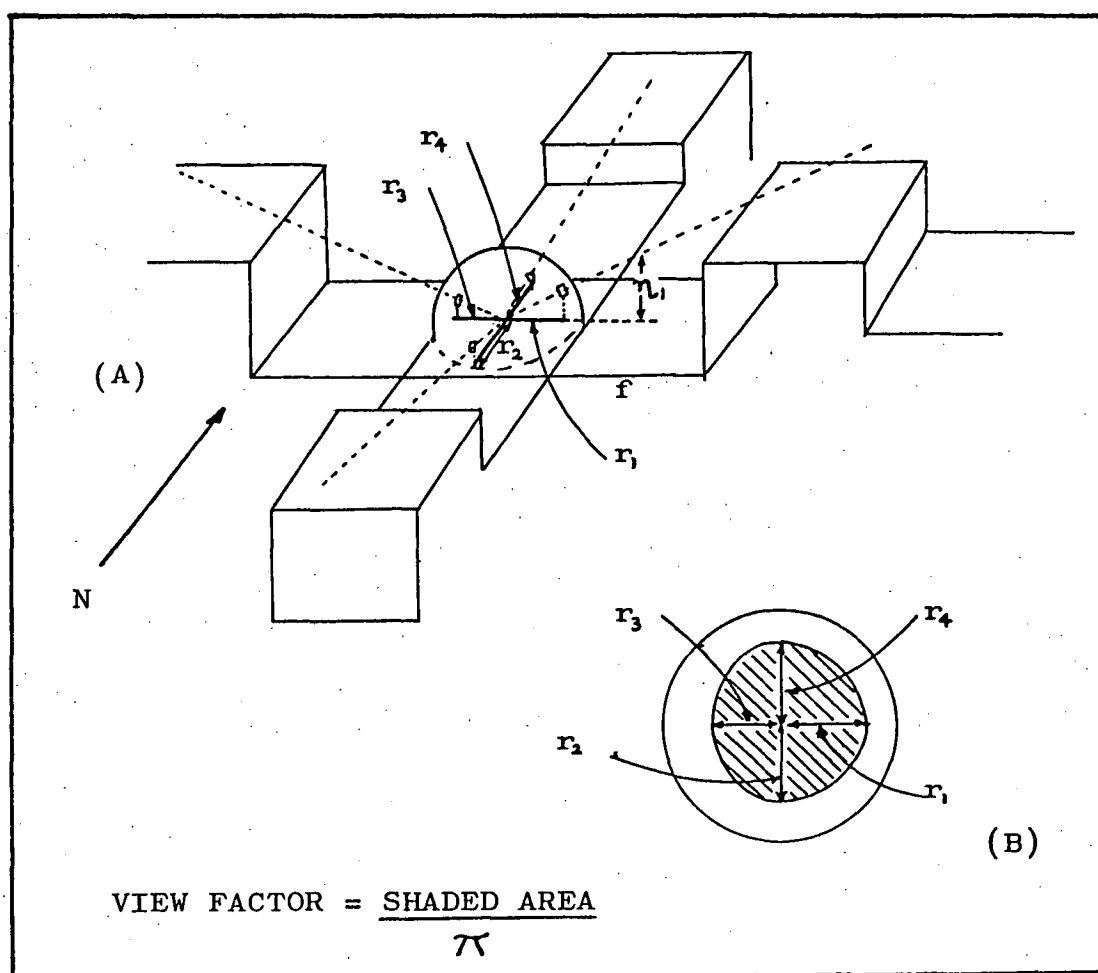


FIGURE A2. Schematic used in the calculation sky view factors. (Nunez, 1980)

Applying the view factor, diffuse radiation was described by (Equation 37):

$$D'_o = D_o \cdot VF + (1 - VF) Kt_o \alpha.$$

Now substituting Equations 32 and 37 in 17, the solar radiation incident received on a non horizontal surface under cloudless conditions was (Equation 38):

$$K\downarrow_o = I \cos \gamma + D_o' .$$

The global solar radiation incident on a horizontal surface under cloudy skies was (Equation 27):

$$K\downarrow_c = K\downarrow_o \psi_{cl} \psi_{cm} \psi_{ch}$$

where the transmission for each cloud layer i was described by Equation 28 (Haurwitz, 1948):

$$\psi_{ci} = 1 - (1 - t_i) C_i$$

$$\text{and } t_i = (1/K\downarrow_o) \exp (-bm) a/m \tag{90}$$

The values for a and b were as described below in Table A2.

TABLE A2. CLOUD TRANSMISSION CONSTANTS

	Cloud Type			
	Fog	Sc	Ac	C
$a \text{ (J m}^{-2} \text{ s}^{-1} \text{)}$	178.6	403	609	954
$b \text{ (dimensionless)}$	0.028	0.104	0.112	0.079

Values for a and b (after Haurwitz) used to evaluate cloud transmission.

Equation 27 was adjusted to allow for reflection between the lowest cloud base and the ground so that Equation 31 was:

$$K\downarrow_c = K\downarrow_o \psi_{cl} \psi_{cm} \psi_{ch} (1 + 0.5 \alpha C_l)$$

The direct radiation reaching the surface under cloudy conditions was written as:

$$I_c = I (1 - C_l)(1 - C_m)(1 - C_h) \cos Z \quad 91$$

so that the diffuse radiation became:

$$D_c = K\downarrow_c - I_c \quad 92$$

The solar radiation incident on a surface of arbitrary slope and aspect summarised in Chapter 4 was described by (Equation 39):

$$K'\downarrow_c = I(1 - C_l)(1 - C_m)(1 - C_h)\cos\gamma + D_c VF + K\downarrow_c \alpha (1 - VF)$$

whilst the reflected solar radiation component was (Equation 41):

$$K'\uparrow_c = \alpha K'\downarrow_c.$$

Net shortwave radiation became the difference between Equations 39 and 42:

$$K^* = K'\downarrow_c - K'\uparrow_c \quad 93$$

and net longwave radiation described by Equation 87 was:

$$L^* = [(5.31 \times 10^{-13} T_a^6 + 6.0n)VF + \epsilon\sigma\theta^4(1 - VF)] \\ - [\epsilon\sigma\theta^4 + L'_c (1 - \epsilon)]$$

The net all wave radiation now may be expressed as the sum of K^* and L^* :

$$Q^* = K^* + L^* \quad 94$$

APPENDIX 4

DATA ACQUISITION

The Calculation of the Free Water Content of Snow (4a)

Thermos Calorimetric Method:

1. Determine the calorimeter water equivalence.
2. Weigh the calorimeter empty.
3. Weigh the calorimeter and hot water.
4. Measure the temperature of the hot water.
5. Measure the temperature of the snow.
6. Weigh the calorimeter, hot water and snow sample.
7. Shake the mixture to ensure even cooling.
8. Measure the temperature of the mixture in equilibrium.
9. Calculate the free water content applying:

$$M_L = M_s - M_i, \quad 95$$

$$\text{where } M_i = \frac{\{(M_h + M_c)(T_h - T_e)\} - \{M_s(T_e - T_s)\}}{L_f + C_p}, \quad 96$$

and M_h - mass of hot water,

T_h - temperature of hot water,

M_s - mass of snow,

M_i - mass of ice,

M_L - mass of snow water,

T_e - temperature of mixture of equilibrium,

M_c - calorimeter water equivalence.

$$\text{so that } W_f = M_L / M_s \quad 97$$

There are two cases to consider:

1. When the temperature of the snow mass is zero or greater,
2. When the temperature of the snow mass is less than zero.

In case 2. the energy required to raise the temperature of the ice in the snow mass to 0°C must be allowed for before the snow water mass can be calculated.

The Calculation of Vapour Pressure (4b)

Campbell Scientific (1980) write a programme using temperature and relative humidity against saturation vapour pressure expressed:

$$e_a = \%RH/100 * e_{sa} \quad 98$$

where

e_a - vapour pressure (P_a)

e_{sa} - saturation vapour pressure (P_a)

%RH - percent relative humidity

The saturation vapour pressure is derived from an approximating polynomial by Lowe (1976) applicable to a range $\pm 50^\circ\text{C}$ for water and -50°C to 0°C for ice. The water reference polynomial is designed to utilize the minimum amount of time with an error of less than 1%.

$$e_{sa} = a_0 + T_a(a_1 + T_a(a_2 + T_a(a_3 + T_a(a_4 + T_a(a_5 + a_6 T_a)))))) \quad 99$$

where

e_{sa} - saturation vapour pressure (P_a)

T_a - temperature in $^\circ\text{C}$ (or K)

a_i - ($i = 1, 2, \dots, 6$) the numerical coefficients for each term of the polynomial.

The numerical coefficients for the water reference formula using $^\circ\text{C}$ temperatures are:

$$a_0 = 6.107799961$$

$$a_1 = 4.4365186521 \times 10^{-1}$$

$$a_2 = 1.428945805 \times 10^{-2}$$

$$a_3 = 2.650648471 \times 10^{-4}$$

$$a_4 = 3.031240396 \times 10^{-6}$$

$$a_5 = 2.034080948 \times 10^{-8}$$

$$a_6 = 6.136820929 \times 10^{-1}$$

CR21 PROGRAMME TABLES (4b)

Input Programme Table (4)

TABLE A3

Sensor Number	Range (E.U.)	Output (E.U.)	Input Program	Program Number	Multiplier (EU/IU)	Offset (E.U.)
1	<1.3	kW m ²	mV	2	0.1513	0
2	<1.3	kW m ²	mV	2	0.1526	
3	0-360	°T	DC Exc & volts	3	360	0
4	-35-47	°C	DC Exc temp	7	1	0
5	15-97	%	AC Exc Rel Hum	8	1	0
6	±1.7	kW m ²	mV	2	0.1887	0
7						
8	1-45	m s ⁻¹	pulse counts	6	0.0800	0.4770
9		mm	pulse counts	6	1	0

(No.) Sensor Description and Calibration

1. Silicon Pyranometer - 6.6 mV kW⁻¹m² (K ↑)
2. Silicon Pyranometer - 6.55 mV kW⁻¹m² (K ↓)
3. Potentiometer Wind Vane
4. Thermistor CS1 model 201 for Air Temperature (and Relative Humidity)
5. Thermistor CS1 model 201 for Relative Humidity (and Air Temperature)
6. Fritschen type 3030 Net Radiometer - 5.3 mV kW⁻¹m² (Q^W)
7. -
8. Wind Speed Contact Anemometer
9. Tipping Bucket Rain Gauge (1 tip per mm)

CR21 Output Programme Table (1)

Output Time Interval (minutes) : 60

TABLE A4

Output I.D.No.	Output Program	Parameter 1 (Input)	Parameter 2 (Input)	Description
4	51	6	0	Av. (Q^*)
5	66	2	1	Av. (K^*)
6	51	4	0	Av. Air Temperature
7	51	5	0	Av. Relative Humidity
8	51	3	0	Av. Wind Direction
9	51	8	0	Av. Wind Speed
10	71	4	5	Av. Vapour Pressure
	0	1	0	

CR21 Output Programme Table (2)

Output Time Interval (minutes) : 360

TABLE A5

Output I.D.No.	Output Program	Parameter 1 (Input)	Parameter 2 (Input)	Description
2	51	4	0	Av. Air Temperature
3	51	5	0	Av. Relative Humidity
4	51	3	0	Av. Wind Direction
5	51	8	0	Av. Wind Speed

CR21 Output Programme Table (3)

Output Time Interval (minutes) : 1440

TABLE A6

Output I.D.No.	Output Program	Parameter 1 (Input)	Parameter 2 (Input)	Description
2 & 3	53	4	1	Maximise Air Temp.
4 & 5	54	4	1	Minimise Air Temp.
6	51	4	0	Av. Air Temperature
7	66	2	1	Av. K^*
8	51	3	0	Av. Wind Direction
9	52	2	9	Total Precipitation
10	1	6	0	Av. Q^*

Table 1 outputs on the hour (E.S.T.)

Table 2 outputs at 0600, 1200, 1800 and 2400 (E.S.T.)

Table 3 outputs at 2400 (E.S.T.)

The Julian Day is registered in output table 1., I.D. No.2.

 Q^* - Net radiation $K \uparrow$ - Outgoing shortwave radiation $K \downarrow$ - Incoming shortwave radiation K^* - Net shortwave radiation